AN ALTERNATIVE DIAGNOSTIC METHOD USING MICRONEEDLES FOR SAMPLING THE IMMUNE SYSTEM *IN SITU*

by
Anasuya Mandal

B. Tech., Chemical Engineering
Indian Institute of Technology Bombay, India (2011)
M.S. Chemical Engineering Practice
Massachusetts Institute of Technology, Cambridge, USA (2014)

Submitted to the Department of Chemical Engineering
in partial fulfillment of the requirements for the degree of
Doctor of Philosophy
at the
MASSACHUSETTS INSTITUTE OF TECHNOLOGY
May 2017
[June 2017]

© 2017 Massachusetts Institute of Technology. All rights reserved.

Signature Redacted

Signature of Author.....
Department of Chemical Engineering
Friday, May 19, 2017

Signature Redacted

Certified by: .....
Paula Hammond
David H. Koch Professor, Department of Chemical Engineering
Thesis Supervisor

Signature Redacted

Certified by: .....
Darrell J. Irvine
Professor of Materials Science and Engineering and Biological Engineering
Thesis Supervisor

Signature Redacted

Accepted by.....
Daniel Blankschtein
Herman P. Meissner '29 Professor of Chemical Engineering
Chairman, Committee for Graduate Students

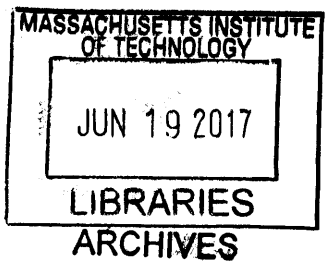

Members of Thesis Committee

Paula T. Hammond
Professor of Chemical Engineering
Massachusetts Institute of Technology
Thesis Advisor

Darrell J. Irvine
Professor of Biological Engineering and Materials Science & Engineering
Massachusetts Institute of Technology
Thesis Advisor

J. Christopher Love
Professor of Chemical Engineering
Massachusetts Institute of Technology

Michael F. Rubner
Professor of Polymer Material Science and Engineering
Massachusetts Institute of Technology

ALTERNATIVE DIAGNOSTIC METHODS FOR SAMPLING THE IMMUNE SYSTEM *IN SITU*

by

Anasuya Mandal

Abstract

Current protocols for immune system monitoring involve the collection of cells from blood or cerebrospinal fluid. However, since major populations of immune cells reside within tissues, these invasively-obtained body fluid samples are, at best, indirect indicators of the status of the immune system. Direct tissue sampling through biopsies is difficult to incorporate into long-term, repetitive, longitudinal immune monitoring. Whereas delayed-type hypersensitivity tests (e.g., Mantoux tuberculin test) query the presence of antigen-specific cells in the skin, but do not provide information about the phenotype and functional characteristics of responding immune cells.

Here we present a technology that addresses several of these challenges simultaneously, with the synergistic goals of providing enhanced diagnostic methods for sampling and analyzing the function of the immune system, and providing a greater insight into the status of the immune system than state-of-the-art assays. We designed hydrogel-coated, immune-monitoring, sampling microneedles that are capable of sampling non-recirculating immune cell populations present in the skin and permitting the quantification of biomarkers present in collected dermal interstitial fluid, thus enabling the parallel monitoring of both cellular and humoral immune responses.

We focused, first, on optimizing the materials for fabricating sampling microneedles with the requisite properties of mechanical integrity and robustness, reproducible fabrication, effective skin penetration, ability to include bioactive cell-signaling molecules in the MN sampling platform and a compartment within the platform for sample collection and retention. Next, we utilized two animal models: an immunization model in which mice were vaccinated with model antigen ovalbumin, and an infection model in which mice were infected, via tail-skin scarification, with vaccinia-virus expressing SIVgag. We established that including adjuvants and antigen as cargo in lipid nanocapsules embedded in the hydrogel coating of the microneedles elicit the recruitment and sampling of not only antigen-specific cells, but also non-recirculating tissue resident memory cells. In both models, we demonstrated that even at long times post antigen exposure, sampling microneedles consistently recruited for higher proportions of antigen-specific cells than those present in blood. Finally, we also showed that the dermal interstitial fluid collected via sampling microneedles, could be reliably quantified for biomarkers such as antigen-specific IgG.

The technology of sampling microneedles allows *ex vivo* analysis of cells retrieved directly from the local tissue environment and enables the investigation of antigen-specific cells for diagnostic purposes as well as answering spatio-temporal questions related to immunology in local tissue environments. This simple, painless and minimally-invasive sampling approach should facilitate longitudinal monitoring of antigen-specific immune cell populations in the skin relevant for a variety of infectious and autoimmune diseases, and aid the process of vaccine design.

Thesis Supervisor: Paula T. Hammond
Title: David H Koch Professor of Chemical Engineering

Thesis Supervisor: Darrell J. Irvine
Title: Professor of Biological Engineering and Materials Science and Engineering

For Ma & Baba

Acknowledgments

Six years ago, there is no way I could have predicted the twists and turns this journey would bring to my life. But as they say, hindsight is 20/20 and as I wrap up this phase of scholastic endeavors, I am grateful to have the opportunity to thank the many, many people who have helped me connect the dots along the way – scientifically, professionally and personally. I would like to express my sincere and heartfelt gratitude to the following people:

To my thesis advisors: Prof. Paula Hammond – for giving me the opportunity and having the confidence in me to take stab at this difficult project. Thank you for your kindness, constant encouragement and infectious enthusiasm, for the brief asides on 'science and language' and for showing me how collaborations can take science so much farther, with the synergies of combined expertise and effort. The sense of effortless class and warmth you radiate is a quality that I shall always strive toward. Prof. Darrell Irvine – I am deeply thankful to have received your guidance and mentorship. Thank you for all the scores of hours that we brainstormed for new ideas and directions, when I came in to meet you with nothing having worked in the prior two weeks. I left your office feeling elated each time, with a smile on my face, my head held high and with a sense of renewed purpose. Some of my most cherished moments from these years have been discussing raw data with you and planning beforehand to preempt your insightful questions. Our interactions have shaped the way I approach and think about science and for that, I am indebted. Thank you for your caring, for pushing me to persevere and answer the 'why,' the 'how' and the 'what if' questions. Thank you for your dedication towards all of us in the lab and our scientific pursuits.

To my thesis committee: Prof. Chris Love, thank you for your motivation, facilitating our collaboration and your discerning and detailed technical comments. Prof. Rubner, thank you for the undying optimism and encouragement, for always asking about 'the big picture,' and for your materials related questions and technical expertise.

To my lab mates and lab alumni: I have been fortunate to be part of two big families in the Hammond and Irvine labs. Archana, this thesis would not have been possible without you and your infectious 'let's make your plan, write up the list and do this' and 'this just *has* to work' attitude. Almost all of the work that comprises this thesis happened after your advent into the lab. For all the scientific teaching and advice, the numerous iterations and discussions of experiment lists and for being my sounding board always – thank you, thank you, thank you! I will thoroughly miss the catching up over microneedle applications and necropsies. Pete, for your guidance and mentorship and for teaching me about the 'art' of microneedles. Stepping into your shoes was a difficult ask and I benefited greatly from those initial months of learning from you. Talar, Mari, Greg – for your advice over experimental protocols and procedures. Kavya – for teaching me the scarification technique and working with vaccinia virus. Sudha – for your unparalleled expertise and relentless assistance in all things microscopy. Nitasha and Eric – for your advice in my chemistry-related undertakings. Kelly – for promptly providing all of the ova vaccine for my mice, whenever I needed. Wuhbet and Heikyung– for all the help with the mice and troubleshooting protocols. Julio

– for your help with the SEM imaging of the 'Cappadocia' MNs. Melissa – for teaching me about ELISAs and to bleed mice 'like a pro.' Mohi – for listening and brainstorming with me in the initial phases of this project. Mila – for the amazing introductory crash course in immunology and for your continued advice over the years. Liz – for the AFM characterization of the alginate gels. Those AFMs essentially laid the foundation of this thesis. Andrew, Erik, Lawrence, Santi, Brett – for asking the perceptive questions that are crucial to research. Jenny – for your inquisitiveness and for your hard work. Li, Sabrina, Jake, Lauren, Mehdi, Nicole, David, Prabhani, Samantha, Samin, Steven, Stephen, Yana, Yiran, Jouha – all for your help, advice, our conversations and fun memories. Alex, Andrew, Llian, Chris, Nikki – for helping to make the lab such a fun and vibrant place!

To my collaborators: Todd and Lionel, for being so industrious and eager to help me Seqwell and MuSIC. It was an absolute pleasure to work with both of you.

Technical assistance at the core facilities: Glenn Paradis and Mike Jennings (flow cytometry), Scott Malstrom (*in vivo* imaging), Bill DiNatale (SEM).

To the lab managers and amazing administrative assistants: Mark (for running the lab so seamlessly), Val, Mariann, Liz, Erin and Xiuyun – all of you make life so much easier. Thank you for all your help!

To members of the Course-X community: Suzanne, Fran, Joel, Sydney, Sharece, Eileen and 'New-Zanne' – the student office does such a wonderful job in making the department so lively, warm and welcoming. My 'split-session' practice school group: Prof. Claude Lupis and Prof. Bob Fisher, for your careful guidance; Helen, Karthik, Chris, Sakul, Nate, Sean, Alex, Jicong – for enjoyable times and cherished memories. Prof. Kris Prather – thank you for your counsel. Kristen, Garrett, Ankur, Connor, Lisa Guay, Natasha, Kevin, Lisa Volpatti, Mark Keibler, Mike – being part of the GSAB and REFS-X with all of you have been some of the most valued experiences at MIT. Siva, Sagar, Sayalee, Connie and Carl – for all the advice and guidance.

To members of the HST (GEMS) community: Prof. Edelman – for giving me chance to pursue this brilliant program. Adam, Becky, Jenny, Amanda and Rachit – for your camaraderie and discussions. My preceptorship hosting team – Dr. Pomahac, Ericka, Sotirios, Nicco, Thet Su, Lisa Quinn, Catherine, Grace, Lisa, Ramon, Bill, Ashley, and David – for allowing me to witness the incredible ways you all touch the lives of patients. Prof. Shiv Pillai – for the finest pedagogy I've ever experienced and for teaching us about the remarkable workings of the immune system. The Lymphocyte Rap is one of my guilty pleasures.

To colleagues and mentors at MIT: Libby Mahaffy – your teachings about conflict management and the 'yes and's will forever be etched in my brain; for learnings in compassion, empathy and emotional vocabulary. The International Students Office – for being so, so kind and supportive. The Fall 2016 6.928 group: Prof. Niño, Nada, Andrew Dykhuis, Andrew David, Elizabeth, Jenny,

Eugene, Matt, Stephanie, Emily, Nil, and Filiz – for your diverse opinions, outlooks and exchanges in one of the best courses I've taken at MIT. To Amar, Wenda, Anthony, Gabrielle, Arvind, and Chris – for sticking through and helping me get better at tackling cases. To the drivers of the Tech shuttles and Saferide shuttles – for making those experimental time points in the wee hours just a little bit easier to get to.

To Sai, Chiraag, Nikhil, Priya, Mehul, Atulya, Rutu, Deeksha, Rahul, Ananth, Diviya, Hari, Annalisa and Manish, thank you for all the laughter and fun.

To my funding sources: the Institute for Soldier Nanotechnologies, the Koch Institute and the Alkermes Fellowship – for supporting my time and work here at MIT.

To 'my crew' – I owe you my sanity. Thank you all for being my sounding boards, all across the world, patiently listening to my rants; for our quirky discussions, for your empathy and kindness, and, for celebrating my triumphs and commiserating with me. Tejal – for our laughter and never-ending chats that brought welcome respite to low-spirited days; Yash – for your candor, your zeal and, recently, our impromptu 'coffees'; Prashant – for all the 6am crib sessions and health talk; Nishant – for your thoughtfulness and our candid dialogues; Antariksh – for inspiring me to always look out for the next creative, eccentric thing to do; Lishi – for your compassion; Sriram – for the esoteric anecdotes and all the addictive hot pot; Sood – for your caring; and Priyanka – for all the fun in our artsy and gastronomy-related endeavors. Dr. Anjana Rajan – your carefully chosen words have helped me navigate some difficult times, and for our conversations, I shall be forever thankful.

To my family: my parents – for always believing in me, for constantly supporting my various, often disjoint, efforts; for pushing me to aim high and work hard; for inspiring me to pursue 'biology'. I am who I am because of you and your sacrifices. I hope to continue to make you proud of me. To Kasturi and Sid – for being the closest thing to home here in Boston.

And finally, to Vishnu – for your unwavering support, for being my biggest cheerleader, for always being the familiar face in the crowd, for proofreading all my drafts, for giving me strength when I didn't have any, for encouraging me to be enterprising, for practicing difficult conversations with me, for holding my hand on the slippery and difficult terrains of hikes and life alike, for our many adventures, and for so much more. I am wonderfully lucky to have and share my life with you. Thank you for your love.

CONTENTS

LIST OF FIGURES

LIST OF ABBREVIATIONS

APC	Antigen Presenting Cell
DTH	Delayed-Type Hypersensitivity
ICMV	Inter-bilayer Crosslinked Multi-lamellar Vesicle
ISF	Interstitial Fluid
MN	Microneedle
MuSIC	Multispectral Imaging Cytometry
OVA	Ovalbumin
PLLA	Poly-L-lactide
PLLy	Poly-L-lysine
TLR	Toll-Like Receptor
T_{RM}	Resident Memory T cell

Chapter One

INTRODUCTION

1.1 The Immune System and Immune Response

Our body is under constant attack from various elements present in its environment – microbial pathogens, viruses, and various chemical and physical factors. The body's immune system, comprising many biological structures and processes, plays a crucial role in defending and protecting the body against disease. The immune system has two main subsystems: the innate and the adaptive immune systems. Components of the innate immune system are present at barrier tissues such as the skin, gut, lungs, and other organs with mucosal linings that face continuous insults from the environment. They mainly protect against infection, in a non-specific manner of response, via cell mediated and humoral components. The innate immune system has no immunological memory and each exposure to pathogen leads to an immediate maximal response. It consists of the complement system and innate leukocytes such as natural killer cells, mast cells, eosinophils, basophils, phagocytic cells including macrophages, neutrophils, and dendritic cells, which identify and eliminate pathogens that might cause infection. The adaptive immune system, on the other hand, acts in slower manner, taking between 24-72 hours to mount a specific, tailored response against a particular antigen. It consists mainly of B cells and T cells that interact to provide and form antigen-specific responses, which, after their initial formation, retain the ability to mount tailored responses due to their immunological memory for the specific antigen.

The lymphatic system, which is part of the circulatory system, consists of lymphatic organs and a vast network of lymphatic vessels that form the roads using which immune cells are transported. Primary or central lymphoid organs (thymus and bone marrow) are the creation sites of lymphocytes and early, immature progenitor cells. Immature naïve T cells undergo maturation in the thymus where those cells that are unable to differentiate "self" from "non-self" antigens undergo apoptosis. Secondary or peripheral lymphoid organs, including lymph nodes and the spleen, mainly consist of mature naïve lymphocytes, and are the sites at which an adaptive immune response is initiated via lymphocyte activation by antigen presentation. Non-lymphoid or

peripheral tissues such as skin and intestine have previously been considered only as passive-barrier layers. However, in recent years, it has been shown that antigen-specific memory cells specifically home to and reside in peripheral tissue to confer long lasting immunity, for many years, at the most probable sites of invasion.[1–4] To better understand the formation of and importance of these memory cells in peripheral tissues, we will now outline the timeline of the immune response.

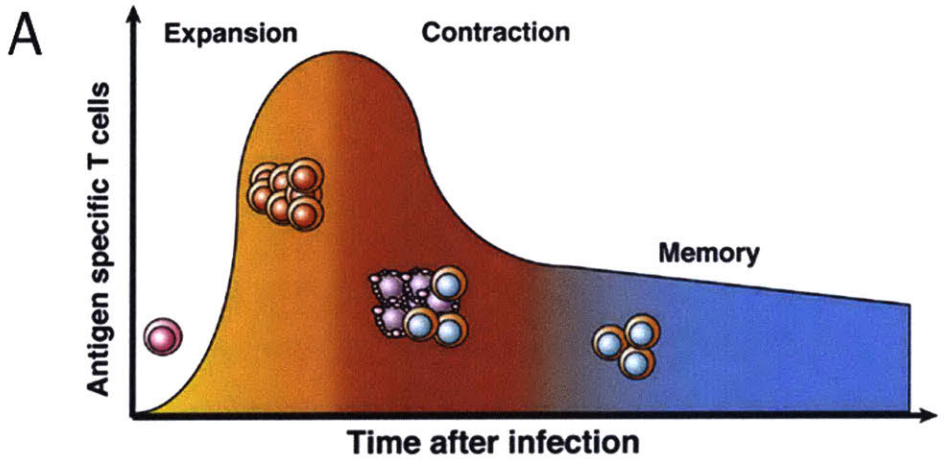

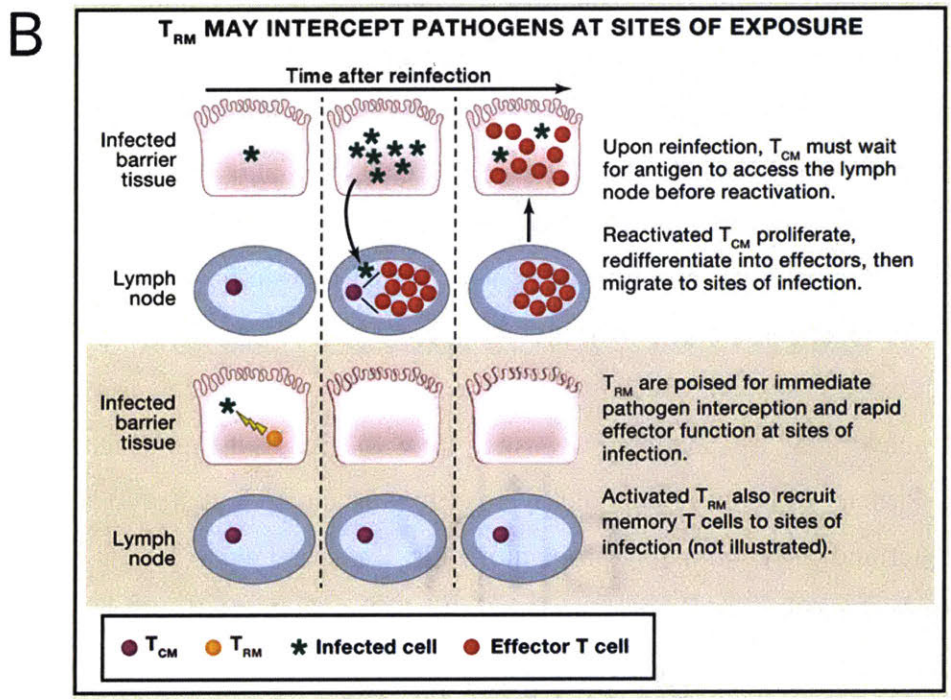

Figure 1-1: Memory cells and their role in an immune response. (A) Naïve T cells are activated by pathologic infections and differentiate into effector or killer T cells. Activated T cells clonally expand in response to particular antigens (expansion phase). After pathogen clearance, high proportions of the expanded antigen-specific T cells undergo apoptosis (contraction phase). Some population of the surviving antigen-specific T cells is maintained as memory T cells (memory phase). Adapted from [5]. (B) Function of T_{RM}s in the event of pathogen exposure. Adapted from [6].

An immune response is mounted upon pathogen or antigen encounter, most likely at the site of entry, which may be a skin wound, lesion, or breakage in the continuity of a barrier tissue. Epithelial barrier cells and resident innate immune cells express pattern-recognition receptors that recognize specific pathogen components and can trigger downstream activation cascades. Activation of dendritic cells through the activation of toll-like receptors (TLRs) expressed on innate cells results in the increased production of pro-inflammatory cytokines, antimicrobial peptides, increased nitric oxide synthesis, enhanced bacterial killing and increased antigen presentation.[7,8] Antigen presenting cells (APCs) pick up antigens and which traffic to draining lymph nodes where mature, naïve T cells are encountered. As shown in **Figure 1-1**, this leads to clonal expansion, affinity maturation, recirculation of the activated effector lymphocytes to the site of infection or pathogen encounter.[9,10] This effector population contracts after the resolution of the infection to a stable memory population of intermediate frequency[11–17] in the form of recirculating central memory T cells (T_{CM}) and effector memory T cells (T_{EM}) which are excluded from many epithelial surfaces. However, some of these memory cells reside in peripheral tissues as terminally differentiated cytotoxic resident memory T cells (T_{RM}s), poised for immediate attack and interception of their specific cognate antigen, upon re-exposure.[18] In the next Section we shall specifically discuss the role of the skin in the immunological context.

1.2 Skin as an Immune Organ

The skin in a human adult comprises around 20 billion memory T cells, nearly twice the number of T cells in circulation.[19,20] Though it is the largest and most exposed interface of the body with the environment, until recently, the skin was thought to serve as a passive barrier between the host and an environment that presents constant challenges in the form of microbial pathogens, chemical and physical intrusions, and radiation. The skin, in fact, presents the first line of defense against many such pathogenic encounters and, in recent years, has been greatly appreciated for its central role in defending the body.[21]

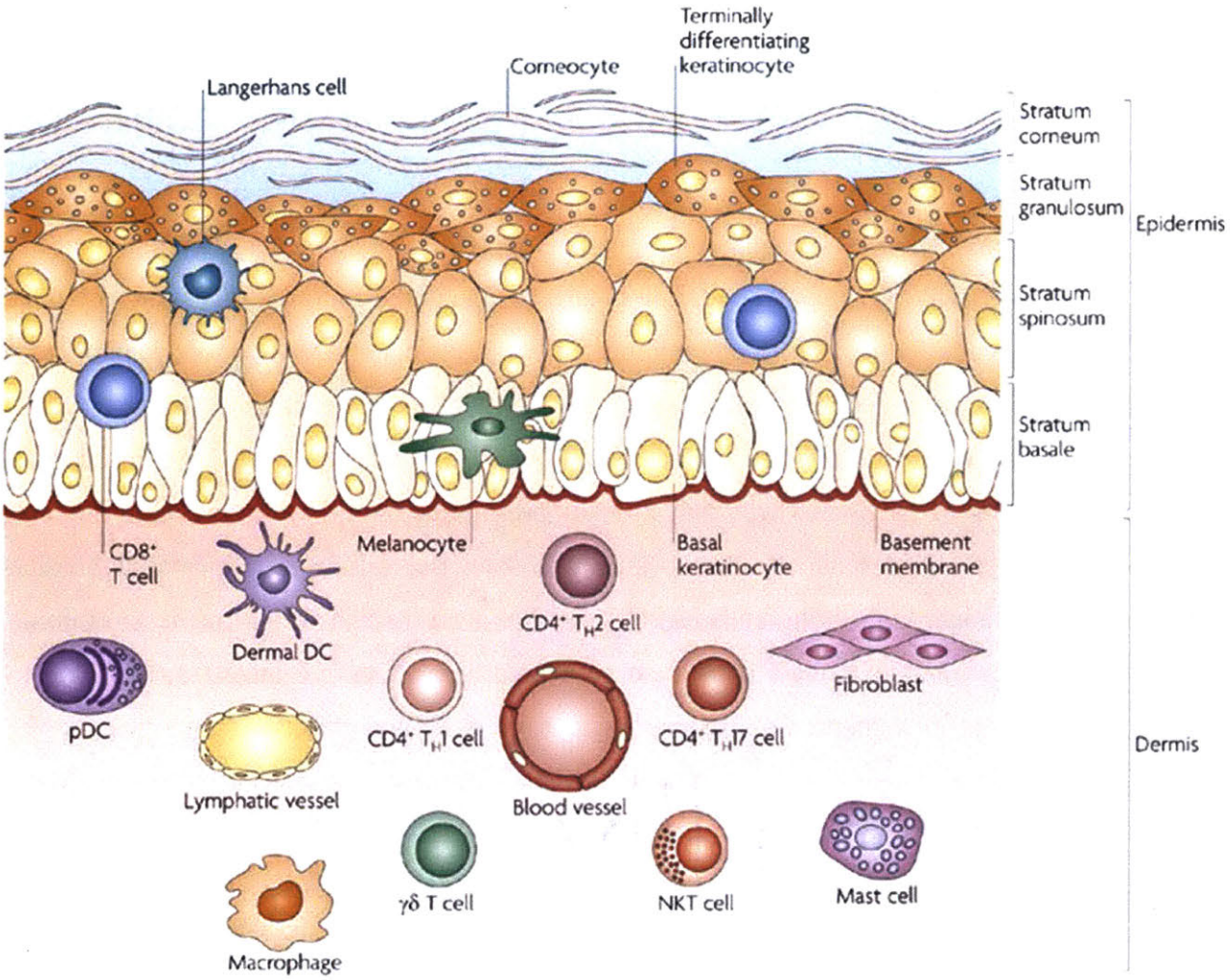

Figure 1-2: Anatomy of the skin and immune cells found in the skin. Adapted from[22].

Human skin has two main compartments: the epidermis and the dermis (**Figure 1-2**), both of which feature many players of the innate and adaptive immune system. The epidermis consists of the stratum basale, the bottommost layer of the epidermis, which is a perennially differentiating single layer of keratinocytes. As these keratinocytes differentiate, they move up the epidermis, changing morphology and function in the stratum spinosum and the stratum granulosum until they reach the very top layer of the stratum corneum. Dead keratinocytes are packed in a brick-and-mortar like structure to form the outermost layer of the epidermis, protecting the body from toxic agents and dehydration.[23] Melanocytes, skin-resident APCs (Langerhans cells), and cytotoxic CD8+ T cells can be found in the epidermis. The thickness of the stratum corneum varies between 10-30 μm and the epidermis varies between 50-110 μm, depending upon the body site and

pigmentation.[24] The dermis is composed of collagen and elastic tissue, and consists of many specialized cells, especially dendritic cell subsets including dermal DCs and plasmacytoid DCs, T cell subsets including CD4+ T helper 1 (T_H1), T_H2 and T_H17 cells, γδ T cells and natural killer T cells , macrophages, mast cells and fibroblasts. The dermis also features blood capillaries, lymphatic vessels and nerves. The dermis is between 1.5 – 4 mm thick.

Because of the heavy presence of immunological components, the skin presents an attractive and easily accessible immunological site for the delivery of vaccines,[25] as has been explored in our research groups in the recent past.[26,27] In conjunction, so vital is the immunological role of the skin in the maintenance of homeostasis that for patients receiving immunosuppressive therapy after organ transplantation or as a treatment for genetic and acquired immunodeficiency disorders, there is a marked increase in the severity and frequency of cutaneous malignancies and infections.[28,29]

1.3 The Need for a Novel Immune Monitoring Method

The methods used to access to fluid compartments of the body today for the purposes of diagnosis and monitoring fall into three categories: (i) invasive (in which a break in the skin is created, or there is contact with mucosa, or other internal body cavities beyond a natural or artificial body orifice, such as via traditional phlebotomy using venipuncture), (ii) minimally-invasive (featuring minimal damage of tissues at the site of entry of instrument(s), such as saliva swabs obtained from the inner lining of the cheek) and, (iii) non-invasive (in which no skin-break or mucosal-contact occurs, such as urine collection).

The field of immune monitoring is mainly dominated by analysis of blood draws, a practice that has been reported for millennia[30], in which systemically circulating blood is drawn from a vein, typically in the arm. In recent decades, immune monitoring by flow cytometry on peripherally sampled blood has become the standard method for immunophenotyping.[31,32]

However, systemically circulating blood does not feature the many important immune cell populations, as discussed previously, which preferentially reside in peripheral tissues including the skin, the gut and other mucosal linings. One widely used method to query the skin is via delayed-type hypersensitivity (DTH) tests[33,34] such as the Mantoux test[35] and allergen patch tests,[36,37] which offer qualitative read outs related to the immune response towards a particular antigen. For

example, in the case of the tuberculin Mantoux test, the tuberculin antigen is initially injected into the dermis and the skin is monitored for the next 2-3 days for the development of an induration, which classifies as a mounted immune response. It has been shown that the cells that respond to these injected stimuli are both central memory and effector memory cells which traffic to the site of antigen deposition, as well as skin-resident antigen-specific T cells.[38] However, these methods remain qualitative and fail to offer quantitative information about the phenotypical and functional aspects of the cell infiltrate. There exist invasive methods of sampling and accessing non-recirculating immune cell populations from lymph nodes[39] or from skin[40] but these are apparatus intensive and require special training for use. Additionally, in the contexts of (i) immunosuppression given to patients with genetic and acquired immunodeficiency disorders, and (ii) organ transplants and, (iii) vaccine development, assessing the immune status of the skin or related peripheral organs, which are not queried by blood draws, in a minimally invasive manner, is an unsolved problem.

We shall now proceed to highlight some specific needs in the medical field that would benefit from a sampling method capable of accessing immune cell populations not found in systemic circulation.

1.3.1 Case Study on Immune Monitoring in Organ Transplantation

Solid organ transplantation, despite continued improvement in its clinical management, still faces challenges due to infectious complications.[41] Since patients who have undergone organ transplants, are on a strict immunosuppression regimen, they are not only susceptible to infections due to the lowered efficacy of their own immune system but are also at the risk of potentially rejecting the organ. Both of these factors require these individuals to be frequently monitored, especially for the status of their immune system. To illustrate this need further, we consider the case of skin-based allotransplants and the niche and new field of vascularized composite allotransplantation,[42–44] in which multiple tissues are transferred from donor to recipient as a single functional unit. In the specific case of face transplants,[45] patients are continually monitored via invasive punch biopsies at the graft margin to test for transplant rejection periodically. These biopsies are analyzed via histological staining, a method that is impractical and cumbersome, and creates a lot of waste in the process of obtaining the biopsy (**Figure 1-3**). In the specific case of skin allograft transplants, histological analysis of biopsies betrayed the role of donor and recipient

T cells in the graft.[46] For many of these patients, a biopsy implies travel to a specific medical facility and often, for patients not living in the area, travel days.

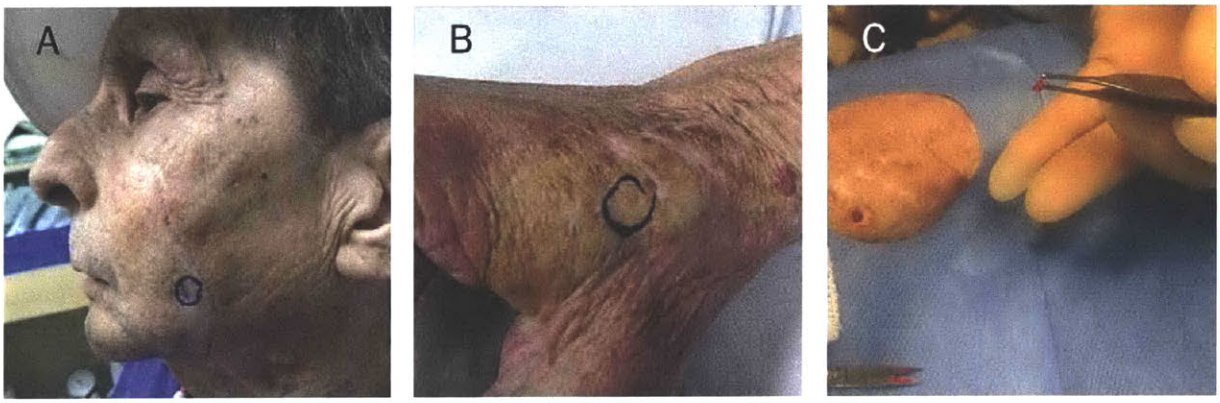

Figure 1-3: Immune monitoring in vascularized composite allotransplantation. Areas marked out for punch biopsy using blue ink on the allografted facial tissue (A) and sentinel hand flap (B). Biopsied tissue is seen on the tip of the tweezer (C). The biopsy cavity (3mm diameter, 7-8 mm deep) is closed via suture.

While non-invasive methods of monitoring using imaging have been explored,[47] skin samples obtained via biopsies offer a wealth of information about the functional, phenotypical, and morphological makeup of the tissue. Thus, there is an opportunity here for a good compromise between non-invasive imaging methods and invasive biopsy methods: a minimally invasive method to 'micro-biopsy' the skin to access immune cell populations and be able to characterize them via high throughput methods.

1.3.2 Case Study on Systemic Lupus Erythematosus (SLE)

Systemic Lupus Erythematosus, commonly known as Lupus or SLE, is a collection of auto-immune diseases in which the immune system becomes hyperactive and attacks healthy tissue. Lupus affects an estimated 5 billion people worldwide and presents as pain and inflammation in joints, skin, kidneys, blood cells, brain, heart and lungs.[48,49] Lupus has no cure but only treatment upon diagnosis. A classic hallmark of lupus and other similar autoimmune diseases such as rheumatoid arthritis and ulcerative colitis, is that these can periodically flare up and then improve. Flares are treated by regulating the dose of medication for these patients. They cannot currently be detected and the current standard of medical care includes annual, or monthly (as deemed

necessary based on severity of disease presentation) blood work to test for antinuclear antibodies (ANA), BILAG, FBC, ESR, CRP, urea, creatinine, electrolytes, dsDNA titer and complement C3/C4 levels, and urine, liver and kidney function tests.[50] These tests require trained professional to be administered and for blood to be drawn. They are time and resource intensive both, on the care provider's side, as well as the patient side. In addition, these tests do no help to predict flares but only to record the levels of analytes of interest during the given immune status of the patient. In recent years, there have been some efforts to identify biomarkers, present in blood, to predict the onset of a flare in a patient. Candidate biomarkers include anti-C1q antibodies, anti-nucleosome antibodies and complement C4d (erythrocyte bound) found in serum or peripheral blood and MCP-1, neutrophil gelatinase-associated lipocalin, transferrin, hepcidin and tumor growth factor β (TGFβ) found in urine, to name a few.[51–54]

So far, most of these efforts have been confined to the analysis of blood, which is cumbersome to rely on, as discussed above. There have been some reports of the implications of the cellular immune response in the skin for lupus varieties: specifically, the lack of presence of regulatory T cells in skin lesions of patients with cutaneous lupus erythematosus.[55] Such cellular immunological implications, derived from skin in such autoimmune diseases shows promise in improving the lives of patients with these diseases since skin has the possibility being sampled minimally-invasively, as we shall discuss in Chapter 4. The gap that lies in the monitoring of such long-term autoimmune diseases, can be closed by enabling diagnosis and sampling for flare detection at home, by the patient, via a minimally invasive method for sample collection.

1.4 Microneedle-Based Systems

MN-based systems consist of an array of projections, upto a millimeter in length, and are used by the field mainly for transdermal delivery of proteins, drugs and vaccines.[56,57] MNs can penetrate the stratum corneum and access the viable dermis. However, they do not reach the nerve endings or the capillaries. Consequently, MNs provide a painless and minimally invasive method to access the immunologically rich reservoir that is present in the epidermis and dermis of the skin (**Figure 1-4**). These qualities make MNs appealing for administering drugs and vaccines in children[58,59] and in patients where compliance because of pain may present an issue. Chapter 2 provides a more detailed background on MNs.

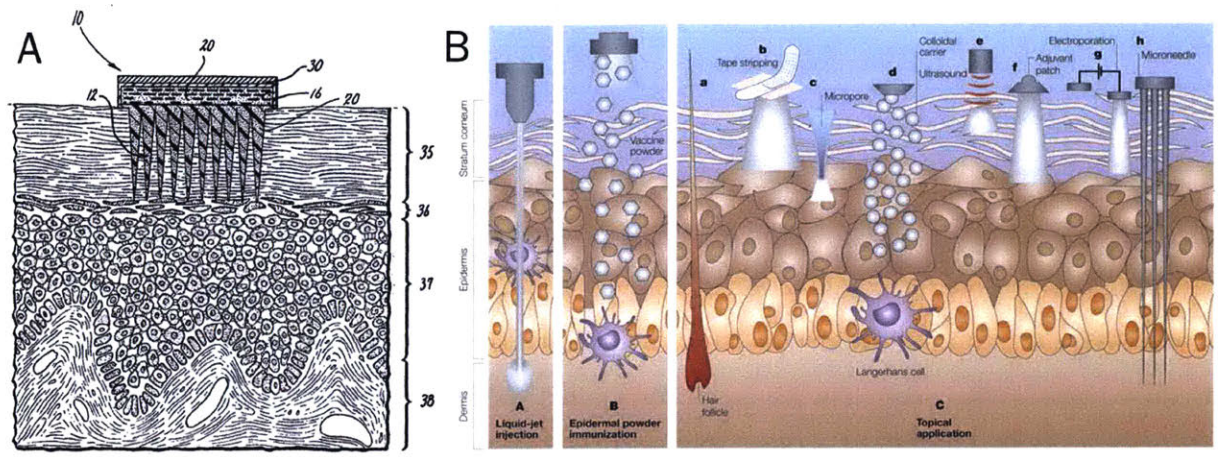

Figure 1-4: Schematic of MNs and their interaction with the dermis and epidermis. (A) Schematic showing the earliest rendition of MNs, piercing the stratum corneum to deliver drugs into the skin transdermally, adapted from [60] (B) Schematic showing MNs "h" entering the viable dermis, as compared to other transdermal delivery methods, adapted from [61].

While there have been some efforst to sample and quantify analytes using MNs, they have been limited mainly to small molecules and proteins.[62–69] Thus, in this thesis we consider the use of MNs for the purpose of immune monitoring – to access immune cell populations that are currently difficult to reach, or are obtained only via invasive means.

1.5 Scope and Outline of Thesis

In this thesis, we designed immune-monitoring sampling MNs that are capable of sampling non-recirculating immune cell populations present in the skin as well as biomarkers present in collected dermal interstitial fluid (ISF).

Chapter 2 describes our efforts to fabricate sampling MNs with the requisite properties of mechanical integrity and robustness, reproducible fabrication, effective skin penetration, ability to include bioactive cell-signaling molecules in the MN sampling platform and a compartment within the platform for sample collection and retention. We optimized the physical and chemical properties of the alginate-based hydrogel used to coat the surface of the MNs, the time of application as well as the dose of chemoattractants CCL21 and CXCL10 as cell-signaling molecules to be included inside the sampling MNs platform. The sampling MN platform described

in this Chapter forms the basis of the sampling MNs used in the subsequent chapters to query specific immune cells and biomarkers from dermal ISF.

Chapter 3 expands upon our most significant body of work, providing initial proof that sampling MNs, including adjuvants and antigen as cargo in lipid vesicles called ICMVs, elicit the recruitment and sampling of not only antigen-specific cells, but also non-recirculating skin-T_{RM}s. Here we first optimized the combination of adjuvants used to enhance the recruitment of cells into the sampling MNs and showed in a DTH test scenario, in an animal model featuring mice immunized with model antigen ovalbumin (OVA), that sampling MNs were comparable to blood, as body fluid compartments to sample similar proportions of CD8+ cells that were antigen specific. We then characterized the time of application and dose of antigen required to signal for the recruitment of antigen-specific T_{RM}s. We finally showed the similar results in a second mouse model featuring mice infected with vaccinia-SIVgag virus, via a tail-skin scarification method. We also compared frequencies of antigen-specific cells obtained from peripheral blood draws and from sampling MNs, at long times post antigen exposure in both animal models. Finally, with the help of the MuSIC technology, we characterized the phenotype of the sampling MN infiltrate to explore the mechanistic steps required in cell recruitment into the sampling MNs.

Chapter 4 explores the possibility of using sampling MNs to access dermal ISF and hence, the ability to sample for and detect biomarkers found in dermal ISF. We first quantified the volume of dermal ISF we obtained with sampling MNs and proceeded to quantify the levels of immunoglobulin G as well as antigen-specific IgG in the OVA-immunized mouse model.

Chapter 5 provides an overall summary and conclusions of this thesis as well as possible future directions. The Appendix details several key methods and protocols that were developed for this work.

Chapter Two

OPTIMIZATION OF MATERIALS FOR CELL AND INTERSTITIAL FLUID SAMPLING USING CHEMOATTRACTANTS

2.1 Introduction

Though microneedles (MNs) were first proposed during the 1970s[60] the tools and techniques to manipulate micron-sized features were not fully utilizable and cost-effective. With the advent of microfabrication technologies in the early 1990s[56,70], MNs have primarily been used for the transdermal delivery of various active agents—primarily drugs and vaccines. In a recent advance from our group, DeMuth et al[71] showed the disruptions in the *stratum corneum* caused by the insertion of poly-L-lactide MNs to be about 100 μm in diameter. While the nanometer to few micrometer-sized disruptions created by early MNs were adequate to permit the transport and delivery of small drugs and macromolecules like insulin[72,73], we hypothesized that 'holes' as big as 100 μm could allow the transport, and hence, sampling of cells, in addition to biomarkers that might be dissolved in interstitial fluid (ISF).[62,74,75] This represents a significant advance in the realm of diagnostics and sampling where, hitherto, MNs have only been used in the form of hollow conduits connected to an external pump for ISF extraction.[76] Furthermore, MN insertion sites have been shown to heal effectively in 1-2 days post MN insertion, with little scarring, erythema or inflammation.[77] While there have been some reports of sampling capillary blood[78] using MNs, the MNs used in our research group are designed not to penetrate the skin to reach the nerve endings and the capillaries, but only the viable dermis to assist a painless and immunologically potent MN application or sampling.

In this chapter, we report on a MN system capable of sampling both cells and ISF from the skin. Specifically, we will describe: (i) their mechanical integrity and robustness, (ii) their reproducible fabrication, (iii) the effectiveness of their skin penetration, (iv) the compartment within this platform to contain cell-recruiting signals, (v) a fabrication process amenable to the

inclusion of bio-active molecules, and (vi) a compartment within this sampling platform for cells and ISF to be collected, and retained upon collection.

Our first efforts focused on the fabrication of porous MNs, using materials that could provide both the requisite rigidity, mechanical integrity, and other mechanical properties needed to pierce the *stratum corneum*, as well as a porous structure to serve as a cell and ISF retention matrix. These, however, proved to be difficult to reproducibly fabricate, and could not consistently penetrate murine ear skin effectively.

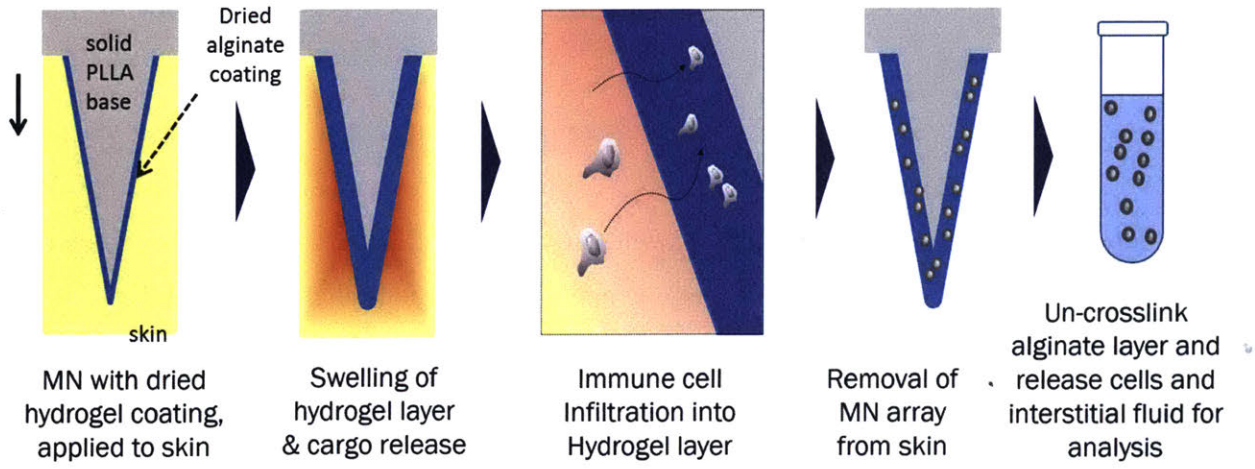

Figure 2-1: Schematic of working of sampling MNs for cell and ISF sampling.

We then took advantage of the reproducible *stratum corneum* penetrating ability of the solid polymer PLLA MNs previously used in our research group.[27,71,79] By layering ionically crosslink-able alginate gels[80–82] on top of these MNs, it was possible to recreate a porous scaffold that could serve as an effective cell and biomarker retention matrix (**Figure 2-1**). Our decision to pursue this material for sampling MNs was strengthened by the FDA's designation of Alginate as a GRAS (Generally Recognized As Safe[83]) material. Alginates are also capable of swelling *in vivo*[84], increasing the volume available for the capture and retention of cells and ISF within the sampling MNs. We subsequently investigated the optimal molecular weight and cross-linking density, which provided the most favorable conditions for cell recruitment.

To signal for immune cell recruitment for the purpose of sampling, we considered the incorporation of chemoattractants or chemokines (chemotactic cytokines) into the alginate matrix,

which would facilitate cell movement and trafficking into the MNs via chemotaxis.[85–89] Our research group has previously shown that chemoattractant-loaded gels and microspheres can be used to signal for immune cell recruitment and enrichment *in vivo*.[90–92] We chose to investigate the use of pro-inflammatory chemokines CCL21 and CXCL10 in the alginate layer of our sampling MNs. CCL21 attracts activated dendritic and central memory T cells whereas CXCL10 is natively secreted by various cell types in response to IFN-γ like monocytes, endothelial cells and fibroblasts.[85] We employed subcutaneous gel injection models to optimize the dose of chemoattractant and recruitment time necessary for the maximal recruitment of cells. We then translated these conditions to the sampling platform by layering the alginate onto the solid PLLA MNs and characterizing its swelling, and porosity, and the MN's insertion efficacy, and cell recruitment ability.

The work described in this chapter informs the design of the working version of the sampling MNs platform that is used in the subsequent chapters of this thesis.

2.2 Materials and Methods

2.2.1 Materials and Animals

Poly-L-lactide (Resomer L207S) was purchased from Evonik Industries AG (Essen, Germany). SLM20 (MW 75-150 kDa, > 50% manuronic acid content, apparent viscosity 20-99 mPa·s, < 100 EU/g endotoxin, pH 5.5-8.5) and SLG100 (MW 200-300 kDa, > 60% manuronic acid content, apparent viscosity 100-300 mPa·s, < 100 EU/g endotoxin, pH 5.5-8.5) sterile ultrapure alginates were purchased from Pronova (FMC Biopolymer/Novamatrix, Sandvika, Norway). Polycaprolactone (440744), calcium chloride dehydrate, polymethylmethacrylate microparticles (74161 -10ML-F) and sucrose were purchased from Sigma-Aldrich. Polystyrene microparticles were purchased from Polybead® Polysciences Inc. Wild type C57BL/6 mice (stock #: 000664) and wild type BALB/c (stock #: 000651) were purchased from Jackson Labs. Animals were cared for in the USDA-inspected MIT Animal Facility under federal, state, local, and NIH guidelines for animal care.

2.2.2 Preparation of Porous Microneedles

PDMS molds (Sylgard 184, Dow Corning) machined using laser ablation (Clark-MXR, CPA-2010 micromachining system) to create patterns of micron-scale surface-cavities. We selected molds

containing square pyramidal cavities, approximately 550 μm in height and 250 μm in width at the base. Porous MNs were prepared by melt-molding a polyester matrix around polystyrene or poly(methyl methacrylate) microspheres used as porogens. 45 μm diam. microparticles based on polystyrene (Polybead® Polysciences Inc. 07314-5) or polymethylmethacrylate (Sigma 74161 -10ML-F) were diluted to 2 w/vol % concentration by adding 20 μL of stock solution to 70% ethanol in water. 100 μL of 2% PS beads were added to the center of the PDMS mold and centrifuged in 6 well plates at 2000rpm for 10 minutes. After removal from centrifuge, the surface of the molds was wiped with a damp Kim wipe to remove remaining PMMA beads from the surface of the mold. 150 mg of PLLA (Resomer L-207S) or 150 mg of PCL (polycaprolactone, Sigma 440744) was added to each MN mold and placed in an oven at 150°C, under vacuum (-25mm Hg) for 30 minutes. The oven was set to 200°C and incubated for an hour while the physical appearance of polymer was closely monitored. After the vacuum in the oven was released, the MNs were kept at 200°C for 10-15 minutes until all bubbles disappeared. The MNs were then cooled at -20°C for > 30 minutes prior to demolding. At this stage, the MNs were characterized using optical microscopy.

In order to leach the porogen microparticles, the MN array was placed in a scintillation vial containing approximately 5 mL of toluene or xylene, with the needles facing up, for 15 minutes. After removal from solvent, the MNs were placed on a Kim wipe to remove excess solvent and then gently dried with compressed air. Finally, the MNs were characterized using optical microscopy and tested for ear tissue penetration.

2.2.3 Trypan Blue Test for Microneedle Insertion

Mice were euthanized using CO_2, and after confirmation of death, murine ears were dissected with scissors and mounted on double-sided adhesive tape, with their dorsal sides facing up, on a glass slide. Approximately 50 μL of PBS was used to hydrate the ears for ~10 minutes at room temperature. The MN array was pressed to the ear with a thumb, held stable with fingers and applied with slowly increasing pressure, for one minute. Subsequently, 40 μL of Trypan Blue dye as obtained from manufacturer was spread on the area of application and incubated for 10 minutes. The murine ear tissue was then pat-dried using a Kim wipe and imaged with an optical microscope.

2.2.4 Alginate Swelling Studies

100 μL each of 1 wt %, 2 wt % or 3 wt % solutions of SLM20 or SLG100 (Pronova) in PBS were mixed with 6.25μL of $CaCl_2$ of 5 wt %, 10 wt %, 20 wt % or 30 wt % in inserts of a 24-

well Transwell plate. $3x10^5$ alginate microspheres prepared according to Wang et al's protocol[91] were added to promote uniform gelling, in addition to the $CaCl_2$ solution, relevant samples. The mixture was immediately mixed via pipette after the addition of the $CaCl_2$ solution. The plate was then incubated for 15 minutes at 37°C, and 100 μL of PBS was added to each sample and allowed to swell for 24 hours at 37°C. After 24 hours, excess PBS was removed and their wet weight was noted. The samples were then lyophilized and their dry weight was noted. The ratio of wet and dry weights was determined to be the swelling ratio.

2.2.5 Atomic Force Microscopy of Alginate Gels

Samples for AFM were prepared in a manner similar to that used for the swelling experiments, described above, in Transwell plates, and allowed to swell for ~ 24 hours in PBS at 37°C. The bottom membrane of the Transwell chambers was cut out and samples were pushed out onto glass slides with flat surface up. MFP-3D-Bio (Asylum Research) AFM at the MIT Center for Materials Science and Engineering in force mode was used, under 'submerged liquid conditions' to record the elastic modulus of the wet gels.

2.2.6 Subcutaneous Gel Injection Studies

The backs of 8-12 week old C57BL/6 or balb/c mice were shaved ~24 hours before gel injection. For gel injection, 200 μL of 1 wt % SLM20 or SLG100 (Pronova) in PBS, including chemoattractants when relevant, was prepared in a 27 ½ G needle syringe and syringe with 31 G needle was filled with 25 μL of $CaCl_2$ solution of desired concentration. Using the 27 ½ G needle, the skin on the dorsal flank was pulled up to create the area where the subcutaneous gel was administered. The 31 G needle was inserted into the pulled-up skin and the alginate and calcium chloride solution were subsequently co-injected at the site. The area was rubbed lightly for uniform gelling.

For retrieval and processing, gels were harvested from euthanized mice and immersed in 200 μL RPMI in 24-well plates. Gels were mashed with the back of a plunger of syringe. 980 μL RPMI and 20 μL Liberase (Roche) at 5mg/mL were added and incubated for 20 minutes at 200 rpm, 37°C on an incubating mini-shaker. 1 mL of alginate lyase (1 mg/mL) containing 0.02% EDTA was added to solution after the gel was broken down via pipetting. After 15 minutes of incubation at 150 rpm, 37°C, gels were washed with PBS while passing the solution through a 40μm cell strainer into a 50 mL Falcon tube. Volume was made up to 10mL and centrifuged at

1500 rpm (700 g) for 5 minutes to pellet. Supernatant was discarded and cell pellet was resuspended in RPMI for cell counting using a hemocytometer or processed forward for flow cytometry.

2.2.7 Preparation of Sampling (Alginate Coated) Microneedles

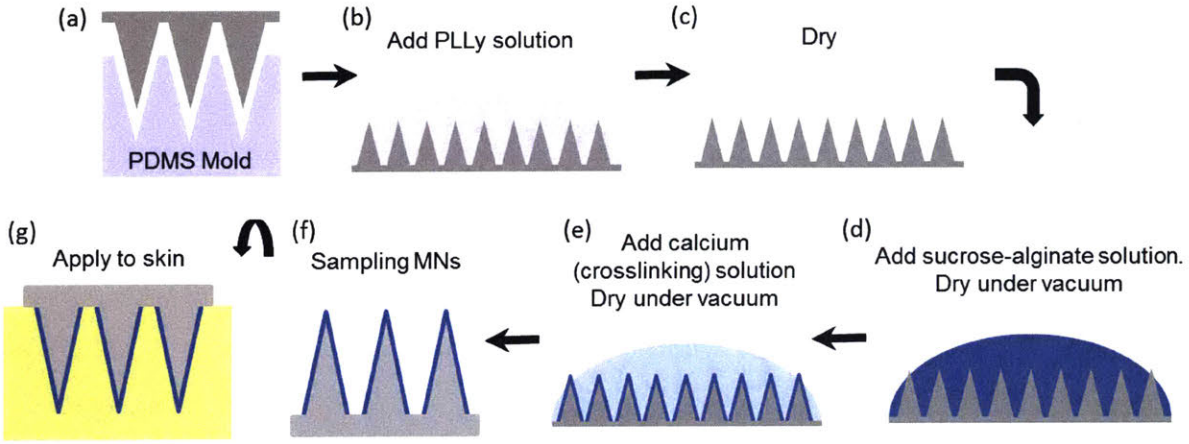

Figure 2-2 Schematic of method of fabrication of sampling (alginate coated) MNs. (a) MNs were fabricated by melt-molding poly-L-Lactide into PDMS molds (b) PLLy was added for 30 minutes, removed and (c) dried. (d) Sucrose-alginate solution was added and dried under vacuum. (e) Calcium solution was added and dried under vacuum. (f) The resulting sampling MNs were stored under vacuum before (g) application to skin.

Poly-L-lactide (PLLA) MNs were melt-molded into PDMS molds (with cavities of square cross section, pyramidal, ~550 μm height and 250 μm base) by adding 150mg of PLLA (Resomer L-207S) to the PDMS molds, incubating at 150°C for 30 minutes under vacuum (-25mm Hg) and then melting at 200°C for one hour until melted and free of internal bubbles. Molds were kept at -20°C for at least 30 minutes, prior to careful demolding.

To create the alginate coating, MNs were exposed to poly-L-lysine (PLLy, Sigma P4832) by pipetting 100 μL of PLLy solution on each MN array and incubated at room temperature for 30 minutes. The PLLy solution was removed and the MNs were allowed to dry at room temperature for 2 hours. The alginate layer was fabricated by pipetting 60μL of sucrose-alginate solution (35 μL SLG100 from Pronova 0.01 g/L in milliQ water + 25 μL of 5.625% sucrose from Sigma dissolved in milliQ water) onto each MN array and subsequently drying the MNs under vacuum (-25 mm Hg) for > 2 hours at 25°C. To include a 'cargo' in the alginate layer, 'cargos' were added

to the sucrose-alginate mix prior to deposition on the MN, keeping the total volume ≤ 75 μL. The alginate layer was crosslinked by adding 20 μL of 0.5 wt % $CaCl_2$ in milliQ water, made up to 50 μL (for ease of pipetting and covering entire MN array with solution) with milliQ water on top of the MN array with dried alginate. To include a 'cargo' in this crosslinking layer, the 'cargo' was dissolved with 20 μL of 0.5 wt % calcium and diluted with milliQ water up to 50 μL.

2.2.8 Crosslinking of Alginate Coated Microneedles

For sintered MNs, the alginate-sucrose formulation described above was dried under vacuum at room temperature onto the PLLA MN surface for 4 hours. Dried alginate coated MNs were placed in an oven that was preheated to 100°C, for 45 minutes, under vacuum. After they were allowed to cool to room temperature, a solution containing calcium for crosslinking and CCL21 (2 μg) was pipetted on the MNs.

For MNs containing microspheres (MS), $5x10^4$ alginate microspheres, prepared according to a previously established protocol[91], were spiked into the alginate-sucrose solution, before drying under vacuum. Crosslinking solution containing 0.5 wt % calcium chloride and 2μg CCL21, made up to 50 μL with milliQ was pipetted onto the MN array and allowed to dry under vacuum.

For MNs containing 'sintered MS', MNs were processed in a manner similar to the protocol for the 'sintered MNs' described above except that the alginate-sucrose formulation was also spiked with $5x10^4$ alginate microspheres before drying and placing in the oven.

2.3 Results and Discussion

2.3.1 Porous Microneedles Insertion *In Vivo*

A key technical challenge for the fabrication of cell-sampling MNs was to create a porous MN structure that will allow cell collection while maintaining sufficient mechanical integrity for skin insertion/retrieval. We first attempted to create MNs capable of sampling cells and ISF involved by exploring methods to create porous, interconnected networks within solid poly-L-lactide (PLLA), poly-lactide-*co*-glycolide (PLGA), or polycaprolactone (PCL) MNs which were formed via melting granules or powder forms of these polymers into PDMS molds, previously produced via laser ablation. Sacrificial microspheres made of polystyrene (PS) or polymethylmethacrylate (PMMA) were embedded into the solid polymers. As shown in **Figure 2-3A&B**, PMMA microspheres were deposited into a poly(dimethyl siloxane) rubber mold. The

matrix of the MNs was then deposited by melting the solvent-resistant biodegradable polymer to fill the mold cavities around the porogen microspheres (**Figure 2-3C**). The PMMA or PS porogens were subsequently dissolved away by immersing the MN arrays in either of ethyl acetate, DMF or acetic acid– good solvents for PS and PMMA but poor solvents for the polyester matrices– resulting in porous MNs (**Figure 2-3D**).

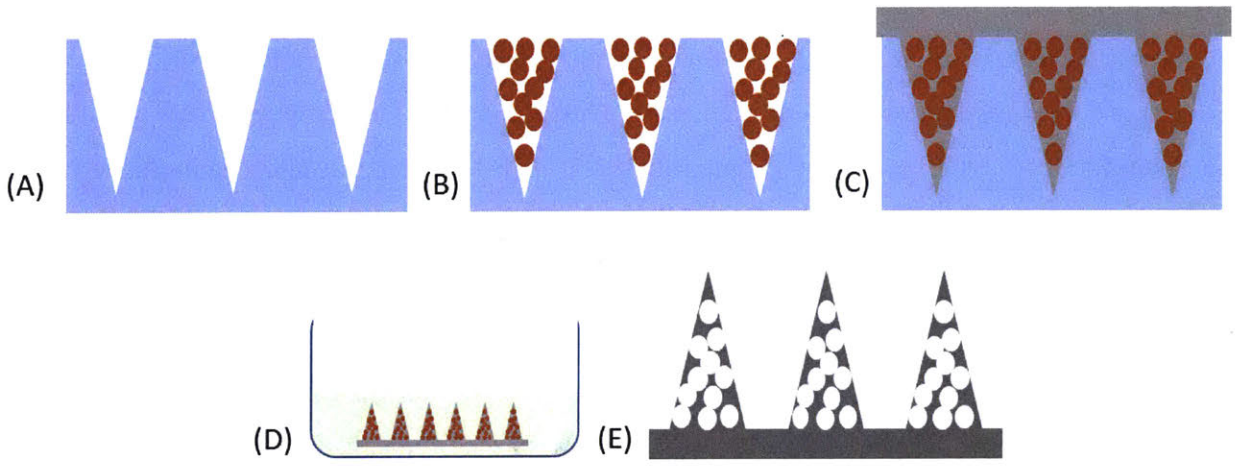

Figure 2-3 Schematic of fabrication of porous MNs. Microspheres are centrifuged into PDMS molds (A) & (B). PLLA is melt-cased into PDMS mold (C) and de-molded MNs are leached via immersion in ethyl acetate (D), producing porous MNs (E).

To characterize the reproducibility of production of these MNs, their mechanical integrity, and robustness, MNs were imaged with an optical microscope at all steps of fabrication as well as before and after tests of insertion into murine ear tissue. We found that these porous MNs did not have the required mechanical integrity to penetrate the *stratum corneum*, and showed extensive buckling/fracture when applied to untreated murine skin as shown in **Figure 2-4** and **Figure 2-5**. Porous MNs made using polycaprolactone showed poor results upon testing for skin insertion as confirmed by Trypan blue staining (**Figure 2-4A**) even though they showed excellent pore formation upon exposure to solvent (**Figure 2-4B**). The MNs were observed to be excessively bent (**Figure 2-4C**) when imaged with an optical microscope which caused dispersed bruising and cell death on the surface of the ear. Although they showed good formation of tips, prior to leaching, and de-molded well (**Figure 2-4D**) PLLA MNs started dissolving upon exposure to DMF for 15

minutes, leaving behind brittle and incomplete MNs which were very fragile (**Figure 2-4E**). These MNs were not tested further for skin insertion.

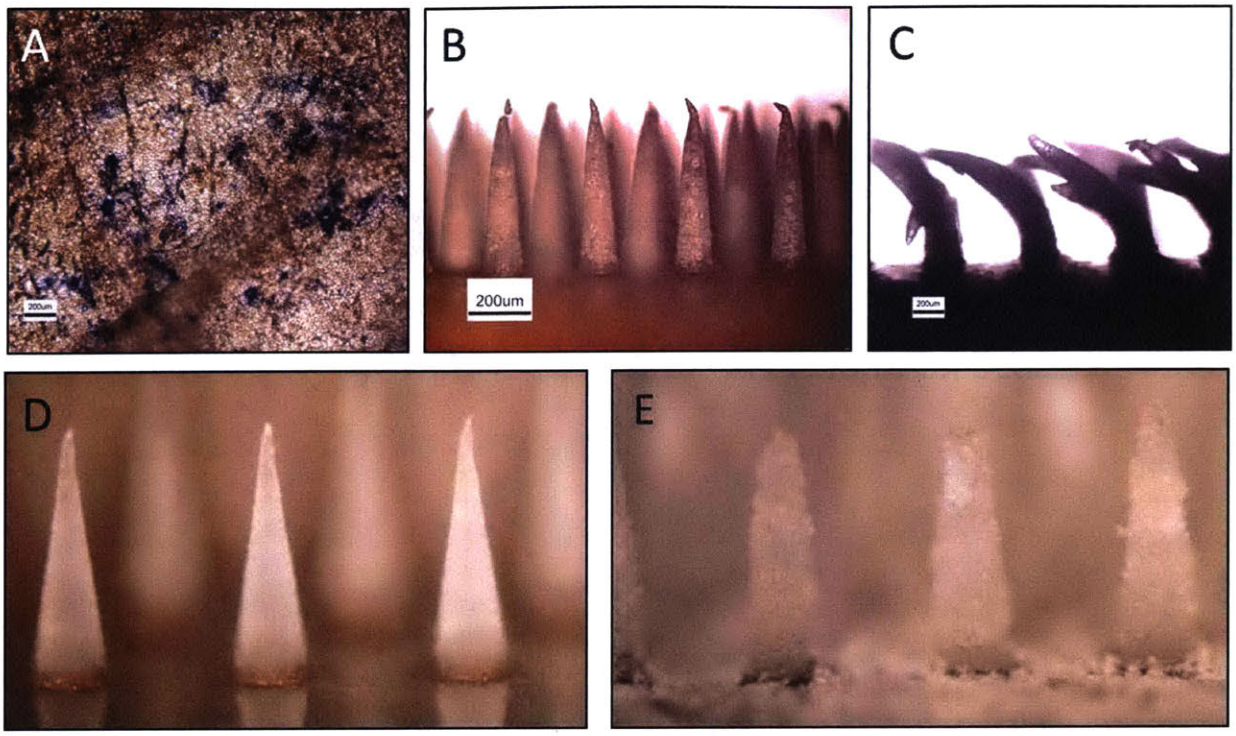

Figure 2-4 Porous MNs perform poorly upon insertion into murine ear skin. Murine ear skin stained with Trpan Blue after insertion test (A) with porous PCL MNs viewed via optical micrography before (B) after insertion test (C). Conical PLLA MNs before (D) and after leaching (E) with DMF.

Since DMF proved to be too strong a solvent for the preferential leaching of PLLA, we attempted to leach PLLA MNs containing PMMA beads with ethyl acetate and acetic acid. Although leaching with ethyl acetate resulted in the formation of pores having access to the surface of the MNs (**Figure 2-5A**), this pattern was not seen on all MNs in the array casting doubts on the reproducibility of this fabrication method. Leaching with acetic acid for 15 minutes also created porous MNs, as seen in **Figure 2-5B**; however, this caused some of the MNs to break away when exposed to compressed air for drying. Shorter solvent exposure times (5 minutes and 10 minutes) were found to produce a higher number of intact MN arrays but reduced the preferential dissolution of the sacrificial porogens.

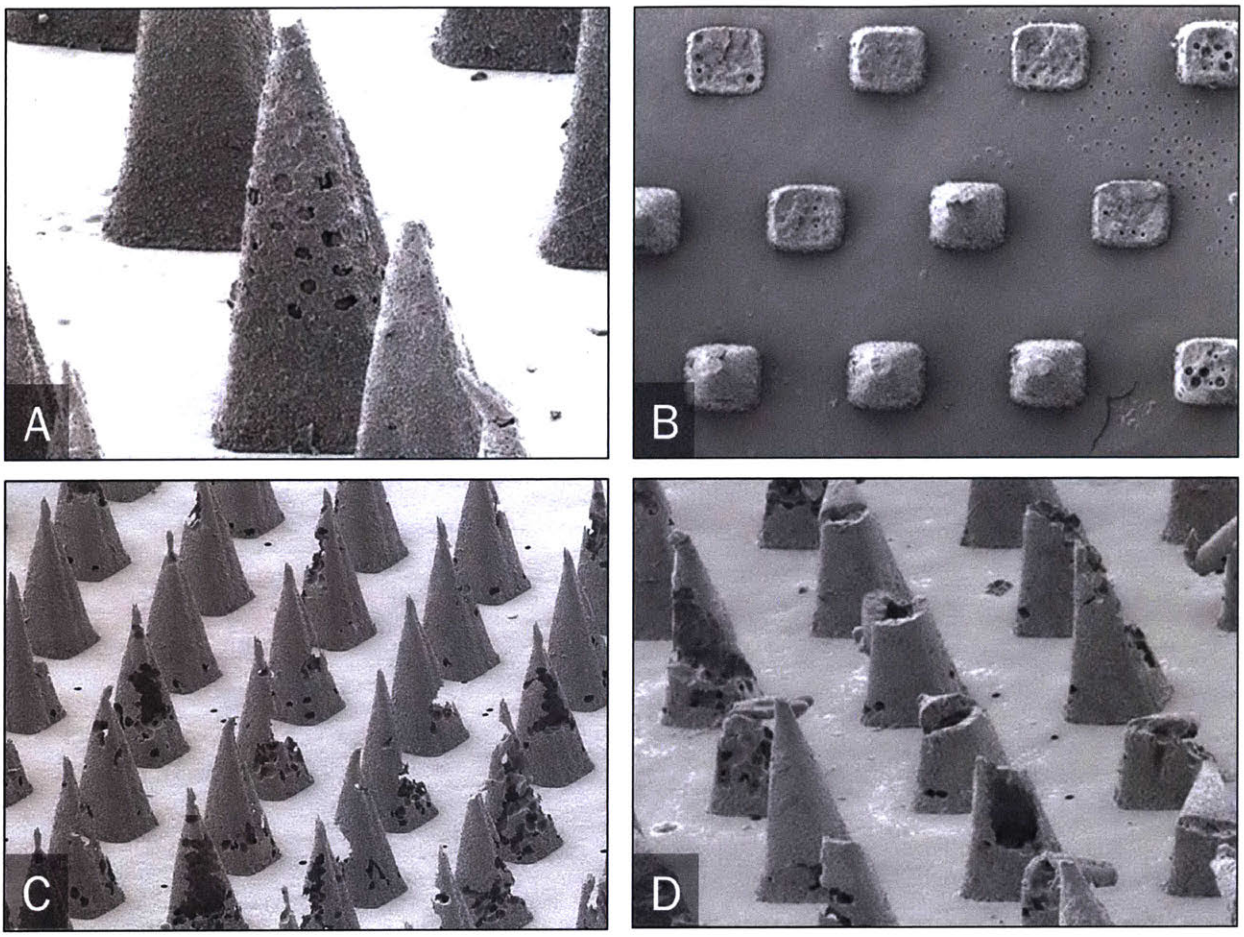

Figure 2-5: Porous MNs pre and post insertion into murine skin, as viewed by scanning electron microscopy. PLLA with PMMA beads leached with ethyl acetate (A) and acetic acid (B). PLLA MNs with polystyrene microspheres after leaching with ethyl acetate (C) and after insertion into mouse ear tissue (D). Scale bar: the distance between the centers of the bases of adjacent micorneedles is 500μm.

Next, we tried polystyrene (PS) microbeads as porogens. Leaching with ethyl acetate produced more drastic results: Many MNs in an array were partially excavated due to the dissolution of porogens and interstitial PLLA though regions of contiguous PLLA were resistant and consistent tip formation was observed (**Figure 2-5C**). Post insertion into murine ear tissue for 10 minutes, as expected, many of these tips were broken (**Figure 2-5D**) which rendered them unfit in terms of mechanical integrity and robustness.

Our next strategy to solve this challenge was based on the generation of "protected" porous MNs, using a glassy sugar matrix as a protective coating to provide mechanical strength to porous

MNs during skin insertion. To this end, the porous microprojections were strengthened by vacuum drying an aqueous sucrose solution over the MN array, forming an initially hard sugar-glass coating that fills the MN pores, which would rapidly dissolve on application of the array to the skin (**Figure 2-6A&B**). We hypothesized that this instantly-dissolving support layer (**Figure 2-6C**) would also be ideal for stably entrapping stimulatory/chemoattractant compounds that can recruit immune cells into the MN cavities on skin penetration (**Figure 2-6D**).

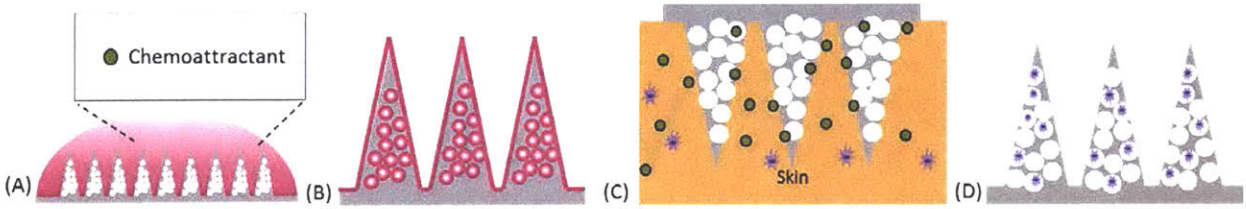

Figure 2-6: Fabrication of chemokine loaded sugar-glass-reinforced porous MNs. (A) Sucrose solution with chemoattractants is dried overnight on porous MN array, yielding (B) sugar-glass-reinforced porous MNs, (C) Skin application, dissolution of sucrose layer, release of chemoattractant cargo, and chemotaxis of cells into porous MNs, followed by (D) Porous MN array containing collected cells removed from skin.

The morphology of porous MNs at each stage of the fabrication process is highlighted in the optical micrographs shown in **Figure 2-7A-C**. Initial testing on murine skin showed that sucrose-reinforced porous MNs provided consistent penetration of the skin of C57Bl/6 mice (revealed by Trypan blue staining of skin post-MN application, **Figure 2-7D**). This staining pattern was identical to the pattern obtained when murine ear tissue is penetrated with non-porous solid PLLA MNs, suggesting effective stratum corneum penetration. PMMA microspheres of three sizes were tested as porogens in the MN arrays– 30 μm, 40 μm and 50 μm diameter. MNs templated with 50 μm microspheres showed the most reproducible penetration of murine skin and mechanical integrity. SEM images in **Figure 2-7E-F** show that there are openings with ~10 μm diameter on the exterior surface of the MNs and an interconnected network inside post skin application, confirming that pores remain open even following application to the skin. However, MNs were not intact after penetration tests as many of the microprojections would be left behind in the skin and the array consisted of broken MNs (**Figure 2-7H, I, J**). This defeated the purpose of fabricating MNs which would be able to sample for cells and micro-biopsy the skin, if the needles which collected the sample were left behind in the skin itself.

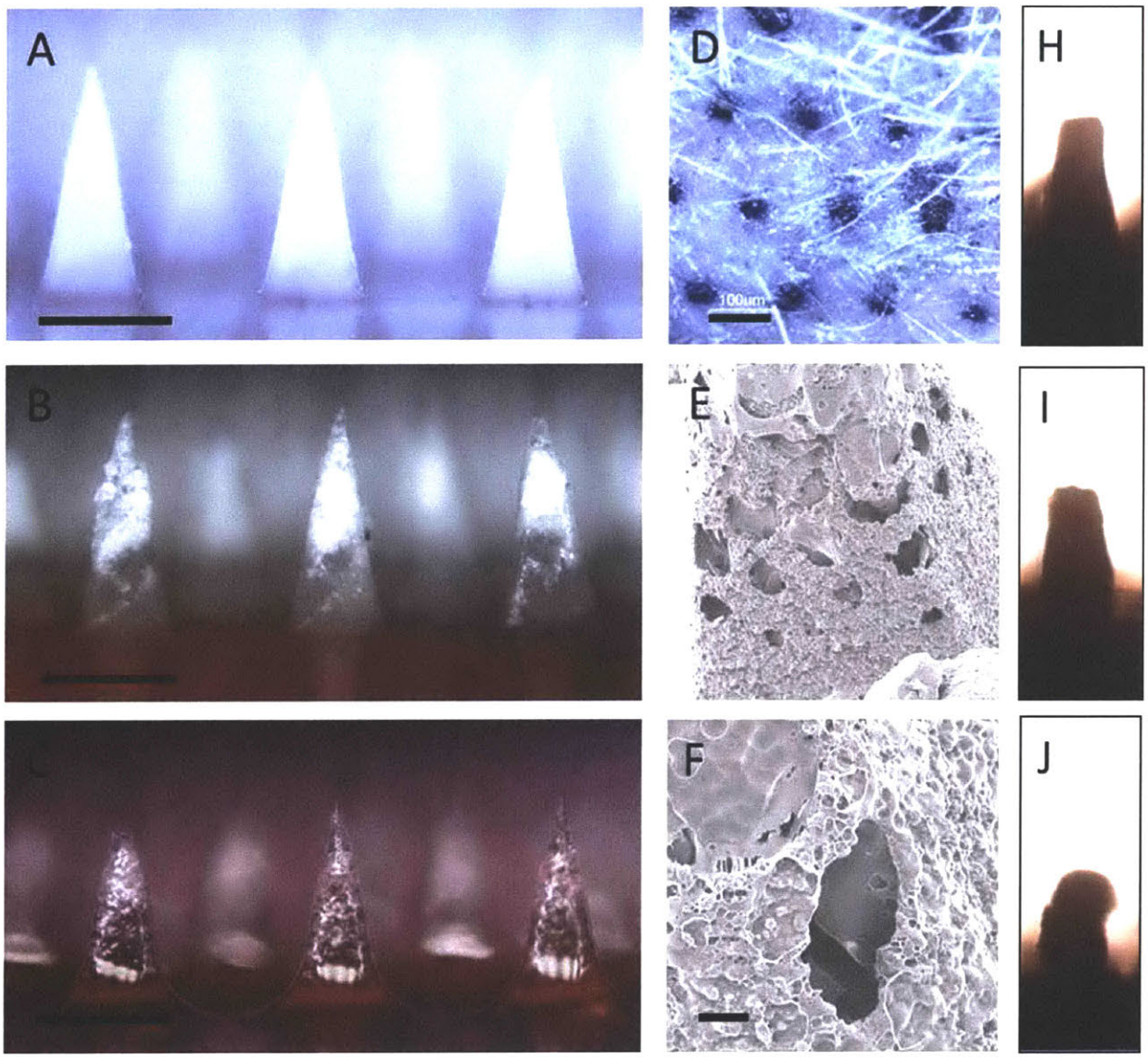

Figure 2-7: Sucrose-glass reinforced porous MNs do not provide reproducible results for interconnected porous networks and mechanical integrity. Brightfield images of as-fabricated solid MNs prior to PMMA porogen etching (A), after porogen dissolution (B), and after sucrose over-coating (C). (D) Optical micrograph of trypan blue-stained murine skin following application of sucrose-reinforced MNs revealing the pattern of *stratum corneum* penetration following MN patch application. Scale bars for (A)-(D) are 100 μm. (E, F) SEM images of porous MNs prior to sucrose coating showing pores on exterior MN surfaces. Scale bars are 10 μm. (H, I, J). Optical micrographs of MNs post murine-skin insertion test. Each MN at the base is 250μm wide.

Thus, we discarded this approach of creating inter-connected porous networks within the solid biodegradable polymer MN tip matrix, since the presence of the pores themselves weakened the penetrating ability of the MNs.

2.3.2 Choice of Alginate

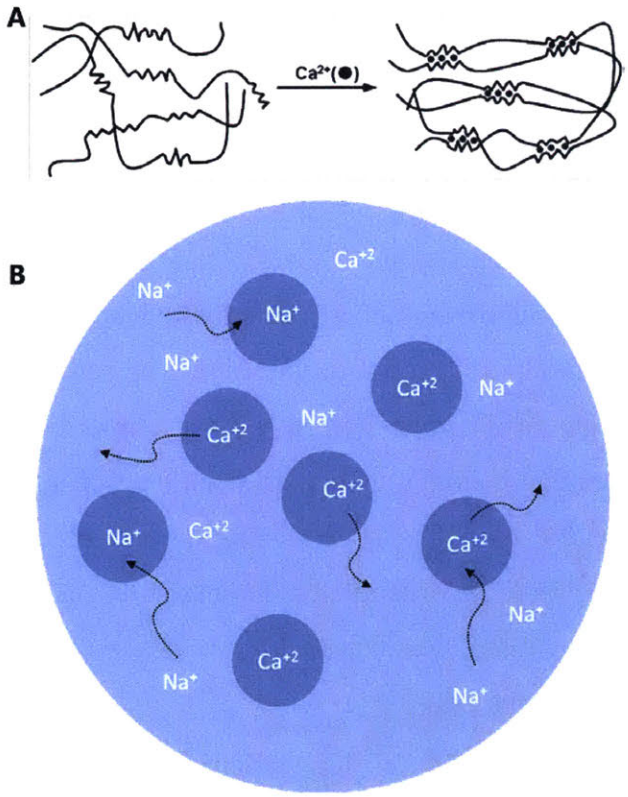

Figure 2-8: Crosslinking of alginate with calcium ions. (A) Calcium ionically crosslinks alginic acid chains[93] (B) Strategy for internal crosslinking of hydrogel layer with alginate microspheres acting as calcium reservoirs to crosslink the surrounding alginate chains.

We chose to take advantage of the *stratum corneum* breaching ability of the solid PLLA MNs—the primary reason of using MN—and considered coating a layer that could serve as a retention matrix for the micro-biopsy sample. We selected alginate, a natural polysaccharide block copolymer containing two carboxylic acid units (guluronic and mannuronic acid), for the cell retention matrix because of several of its useful physical properties. In the presence of divalent cations such as calcium, alginate forms an ionically-crosslinked physical hydrogel that has been proven to be biocompatible and safe for biomedical applications.[90,93,94] We have previously shown

that leukocytes can efficiently infiltrate alginate gels *in vivo*.[90,93] Sucrose was included in the gel coating layer as a porogen that would increase the porosity of the swollen matrix *in vivo* without sacrificing mechanical integrity of the coating layer during initial penetration of the *stratum corneum.* In addition, the process of coating the solid MNs allowed the possibility of inclusion of bio-active molecules without degradation or denaturation (because of exposure of the high temperatures at which the solid MNs are initially melt-cast).

In order to recruit cells of interest into the hydrogel-coated MN platform, it was imperative that the alginate coating remain intact on the MN surface during insertion and removal from the skin. This requirement has two aspects: (i) an optimal degree of internal crosslinking of the hydrogel layer to promote mechanical integrity, while retaining porosity to allow cell migration and recruitment and (ii) adherence of the hydrogel coating to the MN surface to avoid loss of the hydrogel layer upon application to skin. Alginate hydrogels can be ionically crosslinked by the addition of divalent cations like calcium and zinc. However, addition of salts like $CaCl_2$ which are highly soluble in aqueous media to an alginate coating can lead to instantaneous crosslinking of the alginate surface, leaving behind a non-crosslinked interior. As an alternative, in preliminary experiments we tested the use of alginate microspheres[91] embedded within the (initially un-crosslinked) alginate matrix to serve as calcium reservoirs that can ion-exchange with monovalent ions from the surrounding matrix, leading to calcium transfer to the surrounding matrix and gel crosslinking internally (**Figure 2-8**).

We first tested alginates of varying compositions and strengths of crosslinking. These samples were created by using two forms of commercially available alginate (SLM20 and SLG100, from Pronova) and different concentrations of crosslinking solution (calcium chloride in water). The two alginates differ in content of mannuronic and guluronic acid (higher content of which promotes stiffer, more crosslinked hydrogels)[95,96]. SLM20 consists of 50% mannnuronic acid units and SLG100 consists of 60% guluronic acid units. They also differ in molecular weights: 75000 – 220000 g/mol range for SLM20 and 200000 – 300000 g/mol range for SLG100. As expected, SLG100 is also more viscous (100-300 mPa·s as compared to 20-99 mPa·s for SLM20). We hypothesized that SLG100 would be easier to handle because of its increased stiffness and would also be more cell-friendly and biocompatible.[97]

One of the first attributes of these hydrogels to be tested was their swelling behavior. In order to perform as a cell-retention matrix, we required the dried alginate to swell as much as

possible with the intake of ISF when applied to skin. This behavior was tested by generating alginate gels from 100 μL of 1 w/w%, 2 w/w% or 3 w/w% solutions of the alginates in PBS in Transwell plates that could be gelled by the addition of calcium chloride solution, as indicated in **Figure 2-9**. For the samples that included alginate microspheres, the microspheres were mixed in along with the alginate before addition of calcium chloride solution.

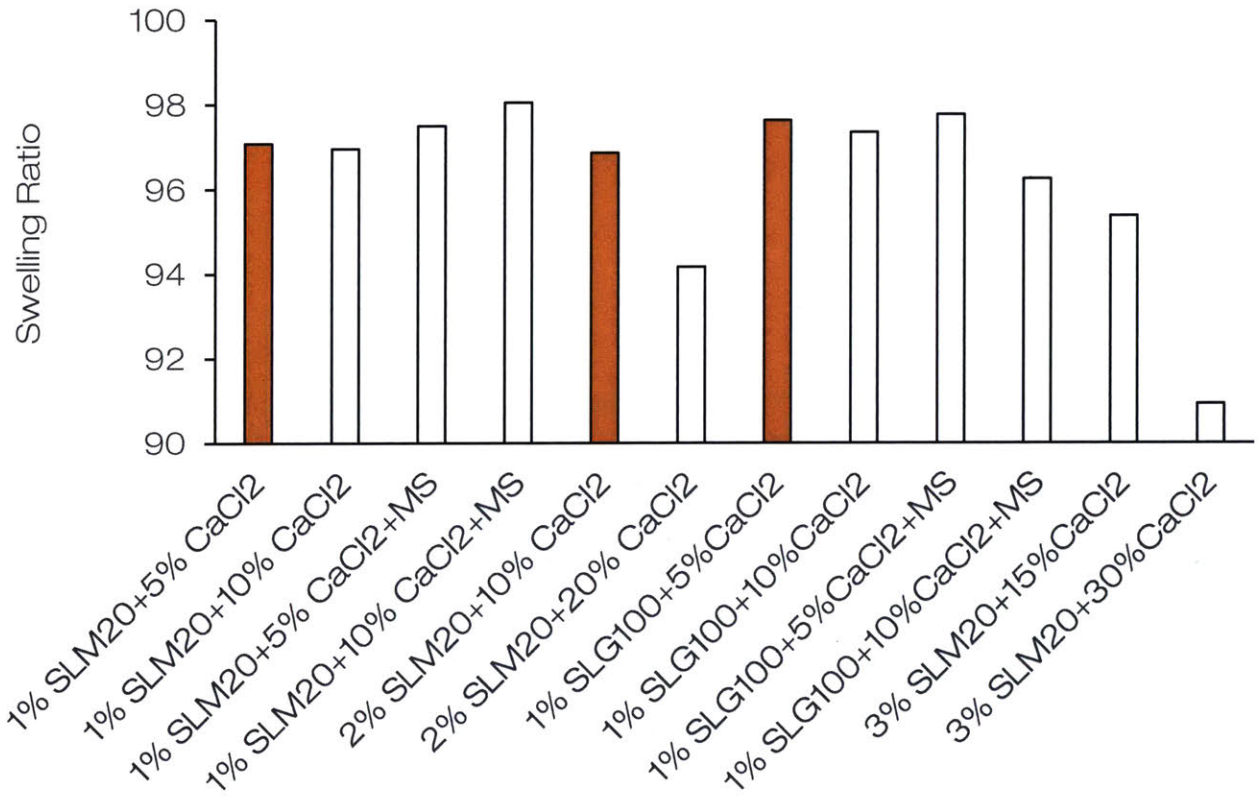

Figure 2-9: Choice of alginate via study of swelling behavior. Difference in wet (swollen state) weight to dry weight, as a percentage of the dry weight giving the swelling ratio for different compositions of alginate (concentration in w/w% in PBS) and strength of crosslinking via calcium chloride (concentration in w/w% in water).

For the higher concentrations of calcium chloride solution, gels were formed almost instantly, resulting in non-uniform crosslinking, as evidenced by slicing the gels using a razor blade which revealed a liquid, non-gelled center and a thicker periphery indicating gelation only at the surface. For the gels that were crosslinked more mildly (especially the ones indicated by the solid orange bars in **Figure 2-9**), the slower gelation allowed for the mechanical mixing of the

calcium chloride solution with the alginate solution and promoted more uniform gelling. After gelation, and swelling in PBS for 24 hours at 37°C, the wet weight of the gels was noted. The swelling ratio shown in **Figure 2-9**, was calculated as the ratio of this wet weight to the dry weight (after lyophilization of alginate gels).

All formulations of the gels showed greater than a 90% increase in weight when swollen in PBS, as compared to their dry weight, and those gels crosslinked with less than 15 w/w% $CaCl_2$ showed swelling ratios of greater than 95%.

Based on these observations, and incorporating the ease of formulation and handling of the gels, we chose the gels indicated by solid orange bars in **Figure 2-9** for further characterization. Specifically, we examined their stiffness, mechanical integrity, and cell recruitment and retention properties.

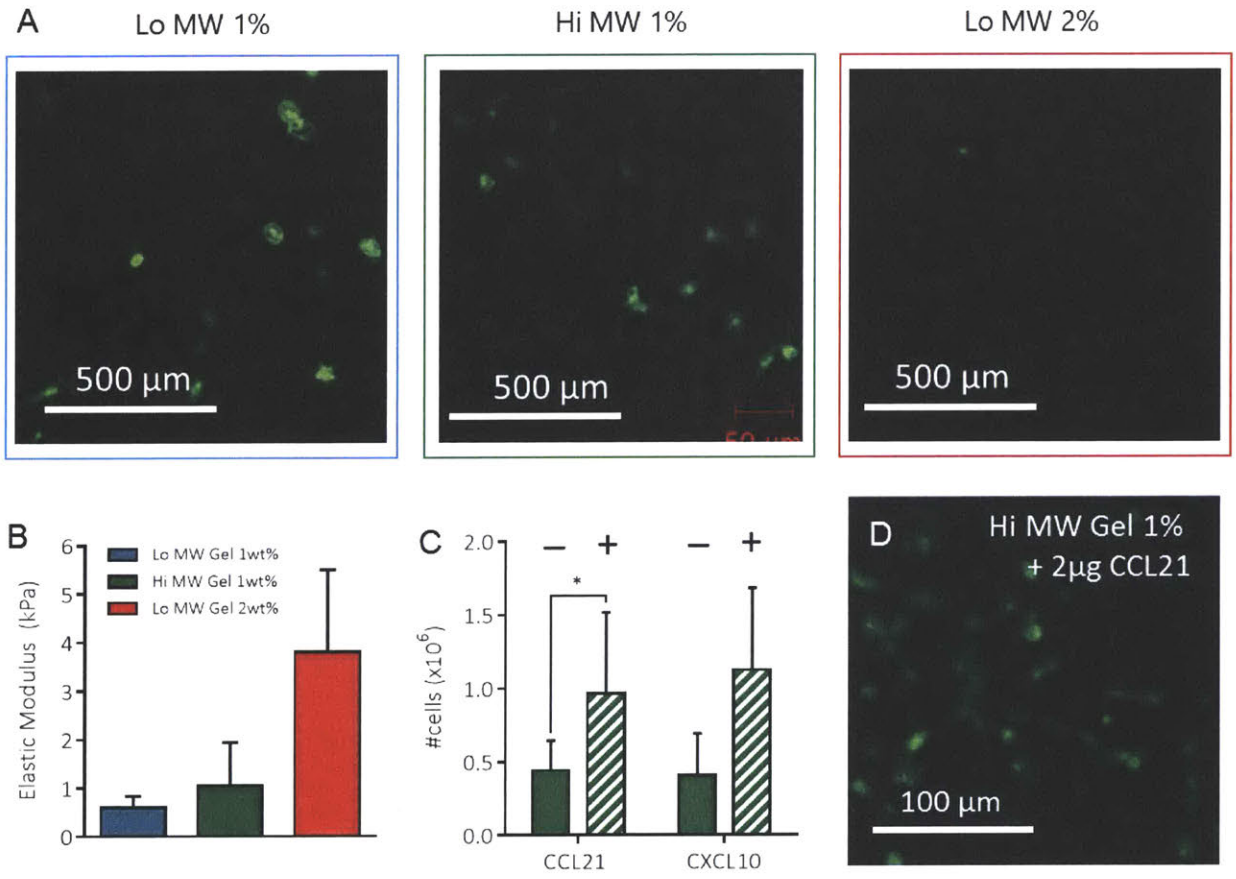

Figure 2-10: Optimization of alginate coating composition. (A) Basal infiltration of cells nto gels of low (75,000 g/mol) and high (200,000 g/mol) molecular weight (without adjuvants or

chemoattractants added), at 1% and 2% w/w of gel when subcutaneously injected under the dorsal flanks of EFGP mice. (B) Elastic modulus of the same gels as measured by AFM. (C) Comparison of number of cells infiltrated into gel using high MW gel 1%, with (hatched bars) and without (solid bars) the presence of chemoattractants CCL21 and CXCL10, using the subcutaneous gel injection model. (D) Confocal micrographs showing infiltration of cells with the presence of chemoattractant CCL21.

We employed a subcutaneous injection model to assess the relative utility of different gel compositions to support immune cell recruitment into alginate matrices. In this model, alginate gels were injected into the dorsal flanks of eGFP-transgenic mice (where GFP is expressed by all nucleated cells). The animals were euthanized at 24 hours and the gels were retrieved and imaged using confocal microscopy. We found that basal cell infiltration into gels lacking chemoattractant was comparable for Hi MW gels composed of 1 wt % alginate and for low MW gels composted of 1 wt % alginate (**Figure 2-10B**). The Lo MW 2 wt % gel showed minimal to no cell recruitment and so we focused on the Hi MW 1 wt % composition for chemoattractant tests since it was higher in stiffness and easier to manipulate and handle. We also used atomic force microscopy to quantify the elastic modulus of the resulting series of alginate coatings, and showed that, as expected, the elastic modulus increased with polymer concentration and alginate molecular weight, though all of the tested compositions had moduli in the 1-4 kPa range (**Figure 2-10B**). Gels were tested with or without two different chemoattractants for leukocytes embedded in the matrix, CCL21 and CXCL10 and shown in (**Figure 2-10C**), approximately $0.5x10^6$ cells infiltrated these gels in 24 hours. This population could be doubled by including either CCL21 or CXCL10 to chemoattract cells to the matrix. As shown in the confocal micrographs of (**Figure 2-10D**), cells recruited by gels releasing chemokine were present throughout the alginate matrix.

Based on these *in vivo* results, we focused on 1 % w/w high molecular weight alginate as the gel matrix for further studies on the MN platform.

2.3.3 Effect of Chemoattractant Dosing and Time on Cell Recruitment

Using the subcutaneous gel injection model employed above to rapidly explore key variables important to cell recruitment into alginate matrices, we next proceeded to identify the optimal (a) duration to allow cell infiltration and (b) chemoattractant dose for maximal cell recruitment *in vivo*. We first tested immune cell recruitment by CCL21 and CXCL10 embedded within alginate gels at a dose of 2 μg/mg alginate. Alginate gels with embedded chemoattractants

were injected subcutaneously, and at the designated time-point, gels were harvested, digested using alginate lyase and collagenase, and the recovered cells were stained with antibodies and analyzed using flow cytometry. Based on prior studies of DTH tests, we hypothesized that we would observe maximal recruitment at 48-72 hours. Consistent with this expectation, we observed a general trend of increased recruitment of immune cells over time for most cell subsets analyzed, for both CCL21- and CXCL10-releasing gels (**Figure 2-11A-B**). At 48 hours, we observed up to 1.5% $CD4^+$ T cells (of total recruited live cells) in gels containing 4 μg of CCL21 while for gels containing 4 μg of CXCL10, $CD4^+$ T cells made up ~3% of total recruited live cells. This trend held true for both total and memory $CD4^+$ cells, and similar recruitment was observed for $CD8^+$ T-cells when CXCL10 was employed. In all cases, CXCL10 recruited more cells than CCL21-containing gels. The rest of the infiltrate was composed majorly of macrophages and other cells of myeloid origin, as indicated by the presence CD11b and CD11c cell surface markers. (data not shown)

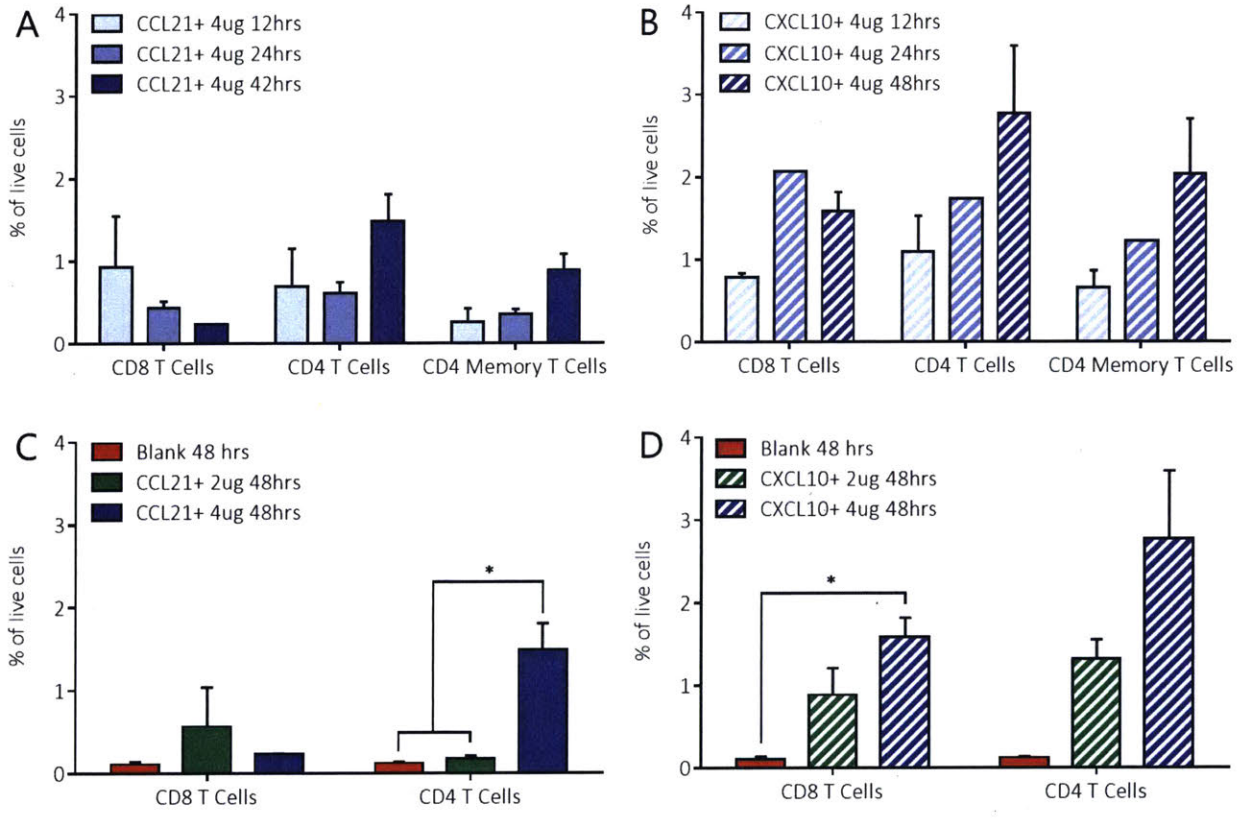

Figure 2-11: Effect of chemoattractant dosing and time on cell recruitemnt (A) and (B) show the effect of time on infiltration of CD8, CD4 and Memory CD4 T cells and CD44+ memory cells at 4 μg of CCL21 and CXCL10. 1% High molecular weight gels were injected subcutaneously

into the dorsal flanks of C57BL/6 mice. Gels were retrieved at indicated times and analyzed using flow cytometry. (C) and (D) show the effect of dose of chemoattractants CCL21 and CXCL10 on gels retrieved at 48 hours.

To answer our second question about the optimal chemoattractant dosing for cell recruitment, we compared three levels of dosing – blank gels, 2 μg and 4 μg of both CCL21 and CXCL10. From previous studies, it had been observed that two doses of CCL21, at 2μg each, 4 hours apart have been able to recruit increased numbers of $CD4^+$ and $CD8^+$ T-cells to injected skin regions and to draining lymph nodes, persisting for up to 4 days after the initial injection.[98,99] In our studies, we observed that higher chemoattractant dosing recruited more T-cells at 48 hours, with CXCL10 again recruiting more cells than CCL21 (**Figure 2-11C-D**).

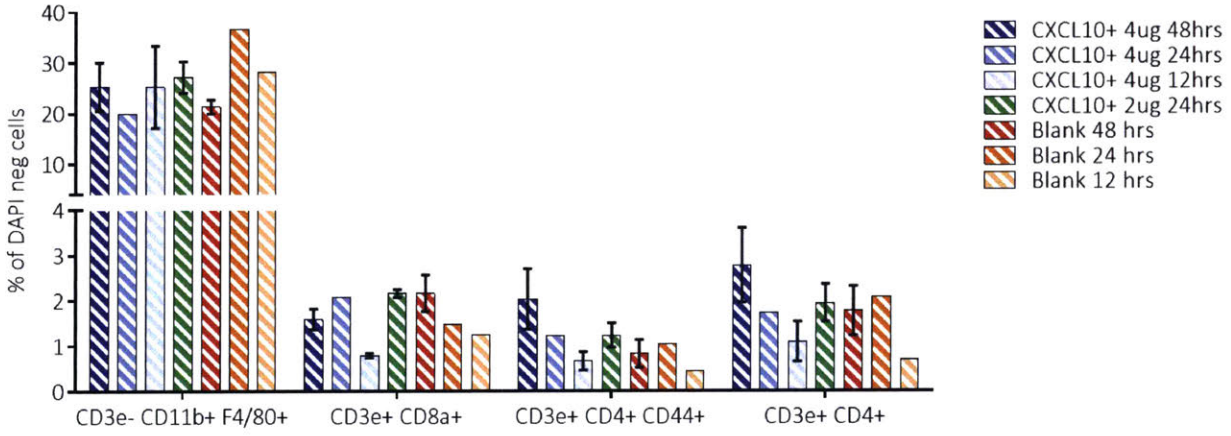

Figure 2-12: Subcutaneously injected gels majorly comprise of macrophages. Phenotypical analysis of cell infiltrate using flow cytometry of alginate gels (1mg, SLG100) when injected underneath the dorsal flank of C57BL6 mice with (varying doses) or without CXCL10 ("blank") for 12, 24 or 48 hours.

However, as expected, the cells that were both the first to arrive into the gels, and the majority of the cell population within the infiltrate, were CD11b+F4/80+ macrophages. Irrespective of the dose of included CXCL10 or the duration for which the gel was injected subcutaneously underneath the skin, macrophages consistently accounted for more than a third of the cell infiltrates, as quantified and phenotyped by flow cytometry (**Figure 2-12**). Macrophages were also the dominant population when the chemokine included is CCL21, irrespective of dose of CCL21 included (data not shown). The ubiquitous presence of macrophages, can be explained

by considering the implantation of the alginate gel as a foreign body and it is well known that macrophages are the main players in a foreign body reaction.[100]

2.3.4 Persistence of Alginate on MN Application to Skin

There are two important attributes of the cell-retention matrix (the alginate-hydrogel) formed on the MN surface: it must (i) stay adhered to surface upon removal from skin and (ii) facilitate release into skin of chemoattractants added to the alginate coating. Thus, ideally, if we were to track the fraction of alginate retained on the MN surface, it should stay as close to the initial amount as possible and the fraction of chemoattractant should decrease with time and be as close to zero as possible upon removal. We initially performed studies with the low molecular weight variety of alginate surface. The alginate and chemoattractant were both fluorescently labeled (in the 647 channel and 555 channel respectively), and the MNs coated with these fluorescently labeled components were applied to the shaved dorsal flanks of C57Bl/6 mice. In all of these studies, the chemoattractant was included in the calcium crosslinking solution of the formulated MN. MNs were imaged before and after, at different durations of MN application via IVIS (**Figure 2-13A**). As expected, the fraction of CCL21 on the MN surface decreased in an exponential manner (similar to a first order release via diffusion) which was favorable (**Figure 2-13B**). However, since the alginate was inadequately adhered to the MN surface, the fluorescent signal from the alginate was also lost indicating loss of alginate itself from the MN surface.

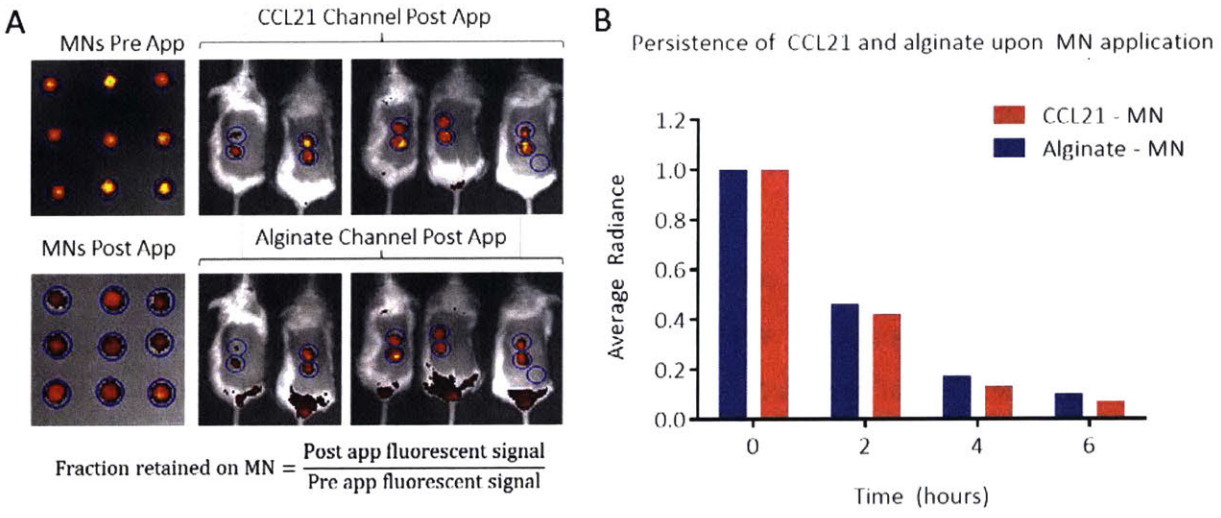

Figure 2-13: Fraction of CCL21 and alginate present on the surface of MN at various times post application to mouse flank skin as measured by IVIS (A) before (pre) and after application (post app) and quantified (B), by normalizing to initial radiance.

To counter this, and to promote adherence between the MN surface and the hydrogel, we tested the impact adsorption of a layer of a strong positive polyelectrolyte, PLLy (molecular weight 150,000 – 300,000 g/mol), prior to the alginate/sucrose deposition. Our initial tests of alginate-coated MNs applied to mouse skin showed that the alginate gel tended to be sloughed around the base of MNs following application/removal, rather than remaining coated along the full MN shafts. By contrast, the inclusion of the PLLy base layer enabled retention of the hydrogel layer along the shafts of each MN project following 10 hours of application on mouse skin.

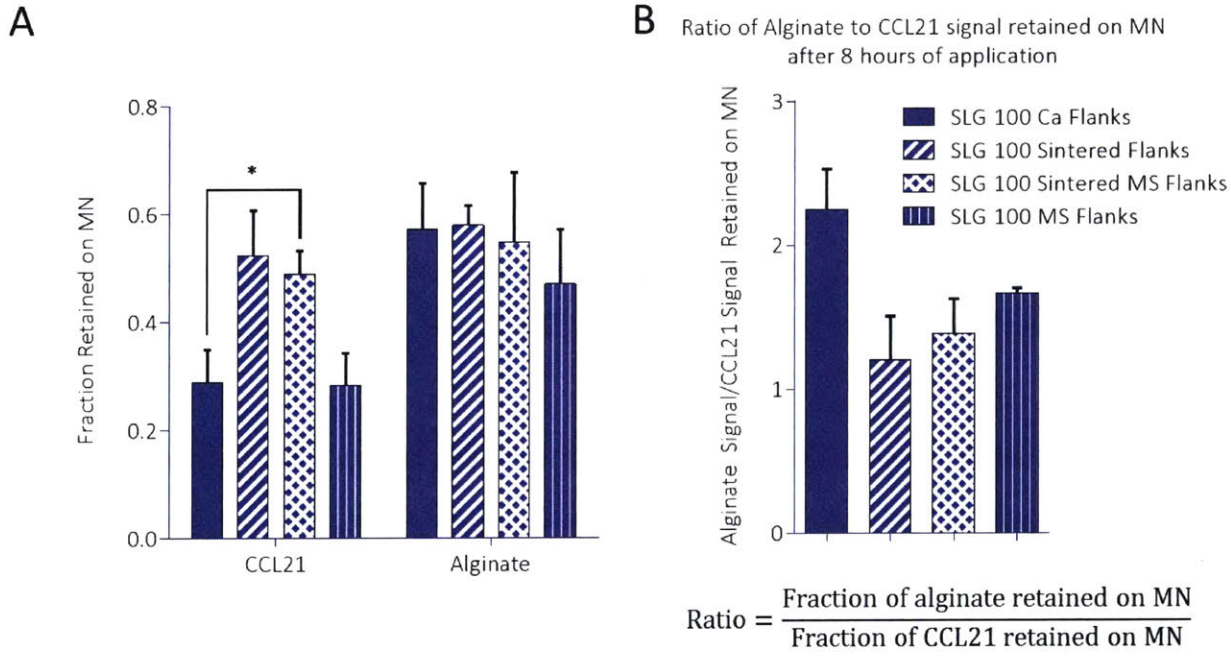

Figure 2-14: Various methods of crosslinking the alginate to confer heightened persistence of alginate layer upon application to skin. (A) Fraction of radiance as detected by IVIS on MN surface for CCL21 and alginate after 8 hours of application, as compared to initial radiance pre-application to skin. (B) Ratio of alginate to CCL21 signal retained on MN surface post 8 hours of application to skin.

With the adherence issue resolved, we sought to optimize the crosslinking strategy for the alginate coating itself, to ensure that the coating was uniformly crosslinked throughout its

thickness, we tested varying the format of calcium ion inclusion in the alginate layer, now testing with the high molecular weight SLG100 that formed stiffer gels. All of these formulations were tested via application to the shaved dorsal flanks of C57BL6 mice, for a duration of 7-8 hours. MNs were imaged via IVIS to quantify the amount of fluorescent alginate present on the MN surface pre- and post-application. We explored the possibility of including alginate microspheres (which contain calcium ions) to promote uniform crosslinking in the alginate layer (as shown in **Figure 2-8B**) as well as sintering the alginate layer before addition of bio-active chemoattractants. With the inclusion of the pre-coat of PLLy on the MN surface, up to about 60% of the alginate was retained for alginate coated MNs simply crosslinked using calcium, and none of the treatments were significantly different for alginate retention on the MN surfaces (**Figure 2-14**). However, since the alginate coating should also ideally allow maximally free diffusion of chemoattractant cargo out of the alginate coating, calcium-crosslinked alginate coated MNs performed the best, showing least amount of fluorescently labeled CCL21 retained on the MN surface after 7-8 hours of application. This can be explained by considering that the inclusion of microspheres adds further tortuosity in the diffusion path of the chemoattractant molecules out of the alginate.

Based on these results, all further studies were done using SLG100 as the cell retention matrix, a pre-coat layer of PLLy to increase adherence of the alginate layer onto the PLLA MN surface, and using 20 μL of a 0.5 w/w % of calcium chloride to re-hydrate and crosslink the alginate layer.

2.3.5 Sampling Microneedle Characterization, Insertion and Sampling *In Vivo*

Building on the previous results, we now had a finalized 'alginate coated sampling MN array' (henceforth referred as 'sampling MNs') fabrication protocol, as elaborated in **Section 2.2.7**. Briefly, solid polymer MNs molded from PLLA were coated with a solution of alginate and sucrose, which was dried under vacuum. This process yielded a thin layer of the polysaccharide and sucrose sugar glass conformally deposited on the MN array (**Figure 2-2**). As shown in **Figure 2-15A**, dried alginate/sucrose layers formed uniform conformal coatings over the PLA MN arrays. Dried alginate/sucrose films containing cargo showed an average thickness of ~22μm when deposited on flat silicon substrate and analyzed via profilometry (**Figure 2-15B**). Inclusion of calcium and cargo, as expected, caused the films to be about 4μm thicker than non-crosslinked alginate films deposited on silicon substrates. Upon application to skin, the sucrose leaches out to leave behind microscopic pores in the gel layer to allow cells to efficiently enter the alginate matrix

in vivo (**Figure 2-15C**). On application to the skin of C57Bl/6 mice for 10 mins these sampling MNs showed effective penetration as visualized by staining the skin with Trypan blue post-insertion (**Figure 2-15D**). Once inserted into murine skin, the alginate coating swells with ISF and forms a soft gel crosslinked via endogenous Ca^{++} and Mg^{++} in the tissue fluid. This is illustrated by the optical micrographs of the dry and swollen gel layers pre- and post- skin-application respectively (**Figure 2-15E-F**).

In summary, this fabrication process fulfilled all the properties required for a device amenable to sampling for cells and ISF. This allowed us to embark upon the most telling experiment yet—to check if these sampling MNs would indeed be able to recruit and sample for cells from the skin of mouse ear tissue.

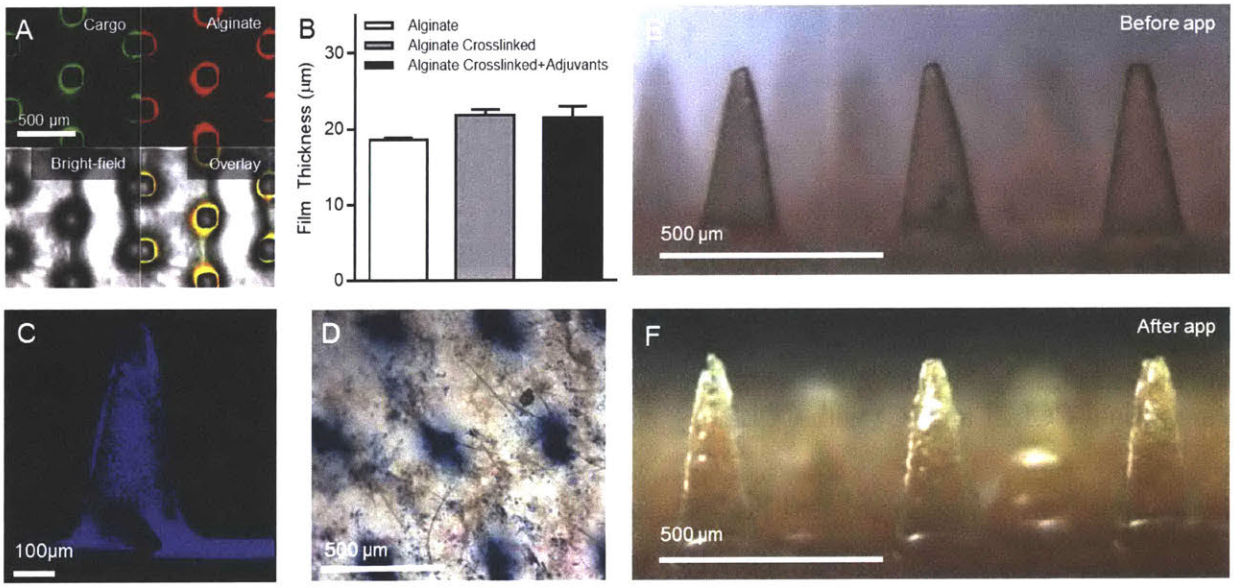

Figure 2-15: Morphological characterization of alginate coated sampling MNs. (A) Confocal micrograph showing conformal coating of MNs (shown in top view) and co-localized cargo (green) and alginate (red) on MN surface. (B) Thickness and roughness of dried alginate films via profilometry on silicon substrate. (C) Confocal micrograph showing porous nature of alginate coating on the surface of a single MN. (D) Trypan blue stain of mouse ear tissue showing effective penetration of MNs. (E) and (F): Optical micrographs showing cell-sampling MNs before and after application to C57BL6 mouse ears.

To this end, we formulated (i) alginate coated PLLA MNs, that would serve as a background for fluorescence since they would not be applied to the eGFP mouse ear, (ii) sampling MNs without chemoattractant and (iii) sampling MNs containing 2 µg of CCL21 in the alginate

coating. These MNs were applied to the ears of EGFP mice for 24 hours and analyzed via confocal microscopy. EGFP mice express the green fluorescent protein in all nucleated cells. Thus, the presence of fluorescent signal could be attributed to cells sampled from the EGFP mice. We hypothesized, based on our data from subcutaneous gels injection studies, that sampling MNs containing chemoattractant should recruit highest numbers of cells. This hypothesis was validated when we observed the maximum fluorescent signal emanating from the CCL21-containing sampling MNs (**Figure 2-16**).

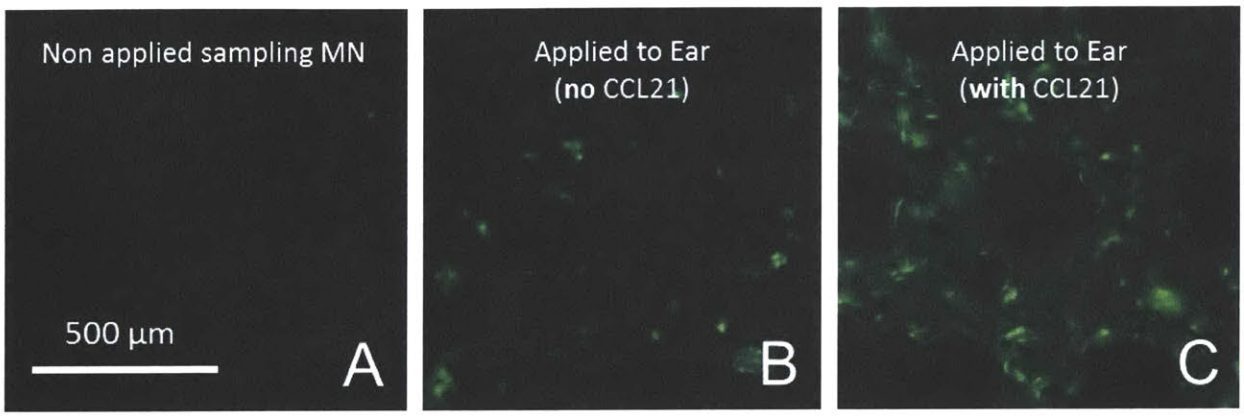

Figure 2-16: CCL21 containing sampling MNs show recruitment of cells upon application to murine ear skin. (A) Non-applied sampling MN, (B) alginate coated MN applied to EGFP mouse eear without CCL21 and (C) with CCL21.

However, we observed that the inclusion of chemoattractants in sampling MNs caused irritation and inflammation of the mouse ear tissue and, in some cases, scar tissue formation and necrosis of the ear tissue as well. Thus, in our future endeavors, we focused on including milder, non-inflammatory cell-signaling molecules. This work is described in Chapter 3.

2.4 Conclusions

In this chapter we explored two approaches of fabricating a MN based platform capable of sampling for cells and ISF from tissue *in situ.* The first approach—fabricating porous MNs—was unsuccessful because the porous nature of the entire polymer matrix compromised their mechanical integrity and rendered these MNs incapable of consistently penetrating the skin of murine ears.

Our second approach consisted of coating the solid surface of a PLLA MN array with a hydrogel (alginate) that would be initially dry, be able to contain bioactive cargo to signal for the recruitment of cells, and provide a retention matrix for recruited cells to adhere to before removal. These sampling MNs exhibited all of the properties desired for our cell and ISF sampling MNs: (i) mechanical integrity and robustness, (ii) reproducible fabrication (iii) effective skin penetration, (iv) a compartment within platform to contain cell-recruiting signals, (v) a fabrication process amenable to the inclusion of bio-active molecules, and, (vi) a compartment within the sampling platform for cells and ISF to be collected, and retained upon collection.

In the following chapters we will apply these sampling MNs to test for the recruitment of immune cell populations that are not found in found in blood. Specifically, we will demonstrate the applicability of this sampling platform for providing information about the immune status at a level that is inaccessibly to currently available sample collection methods and assays.

Chapter Three

ADJUVANT AND ANTIGEN TOGETHER ELICIT RECRUITMENT OF ANTIGEN-SPECIFIC CELLS AND RESIDENT MEMORY T CELLS

3.1 Introduction

Microneedles (MNs) are micrometer to millimeter long projections,[101,102] which when applied to the surface of the skin, are capable of penetrating the *stratum corneum*[103] and painlessly[59] reaching the viable epidermis or dermis. In chapter 2, we elaborated on a strategy of adapting MNs, which are predominantly used for transdermal delivery of proteins[104–106], drugs[107,108] and vaccines,[109–114] to a diagnostic and sample collection context, as shown in **Figure 2-1**.. We explored the use of pro-inflammatory chemoattractants (CXCL10 and CCL21) to attract cells into these sampling MNs and proved the efficacy of utilizing sampling MNs to attract and collect cells from the mouse ear skin.

We observed that the inclusion of chemoattractants in sampling MNs caused irritation and inflammation of the mouse ear tissue and, in some cases, scar tissue formation and necrosis of the ear tissue as well. Thus, in this chapter, in addition to chemoattractants, we explore the use of adjuvants[115,116] as agents of cell recruitment as shown in the schematic in **Figure 3-1**. Adjuvants (from Latin, *adjuvare* meaning 'to help') were first described[117] as "substances used in combination with a specific antigen that produced a more robust immune response than the antigen alone". Based on previous work done in the Irvine laboratory[79], we explored the use of TLR3 agonist polyI:C (a potent double-stranded RNA adjuvant for stimulating anti-viral responses)[118,119] as well as TLR1/2 agonist Pam_3Cys,[8] a synthetic lipopeptide, known to elicit antigen-specific IgG responses stronger than conventional adjuvants like alum.[120]

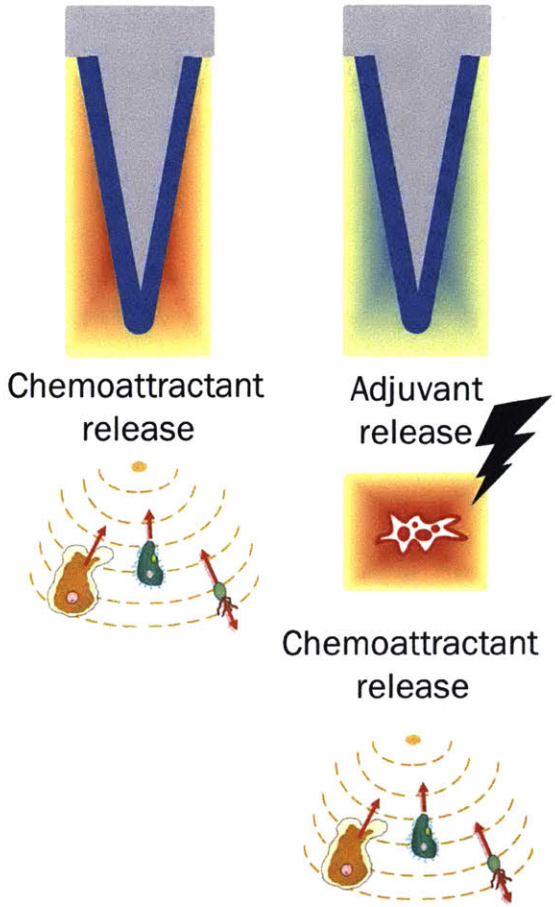

Figure 3-1: Schematic showing the hypothesized difference in mechanism of cell recruitment via chemoattractants and adjuvants, when released from sampling MNs. Chemoattractants create a gradient that cells respond to and migrate towards regions with higher concentrations of chemoattractant. Adjuvants often agonize nearby cells, often being TLR agonists themselves, and cause the distressed cell to release chemoattractants which causes other cells of interest to migrate towards the region of chemoattractant production.

In order to demonstrate the applicability and efficacy of sampling MNs as a platform for 'micro-biopsy', in this chapter we wished to answer to two main questions: whether sampling MNs were capable of collecting (i) antigen-specific immune cells and (ii) immune cell populations that cannot be accessed via peripheral blood.

To answer the first question, we adapted a DTH based test[34,35] which involves injecting an antigenic preparation into the dermis. Upon prior exposure and presence of previously sensitized antigen specific memory T cells, an induration accompanied by erythema is observed over the next 24-72 hours– in the classic DTH assay, this redness in the skin at the site of injection provides a qualitative indication of the presence of a memory T cell response to the injected antigen. The

cytokines and chemokines released by antigen-specific memory T cells localized at the site of injection act upon polymorphonuclear cells, macrophages and other lymphocytes[33,121] resulting in the classic DTH reaction. Interestingly, less than 1% of the infiltrate in a DTH response is comprised of antigen-specific T cells.[122]

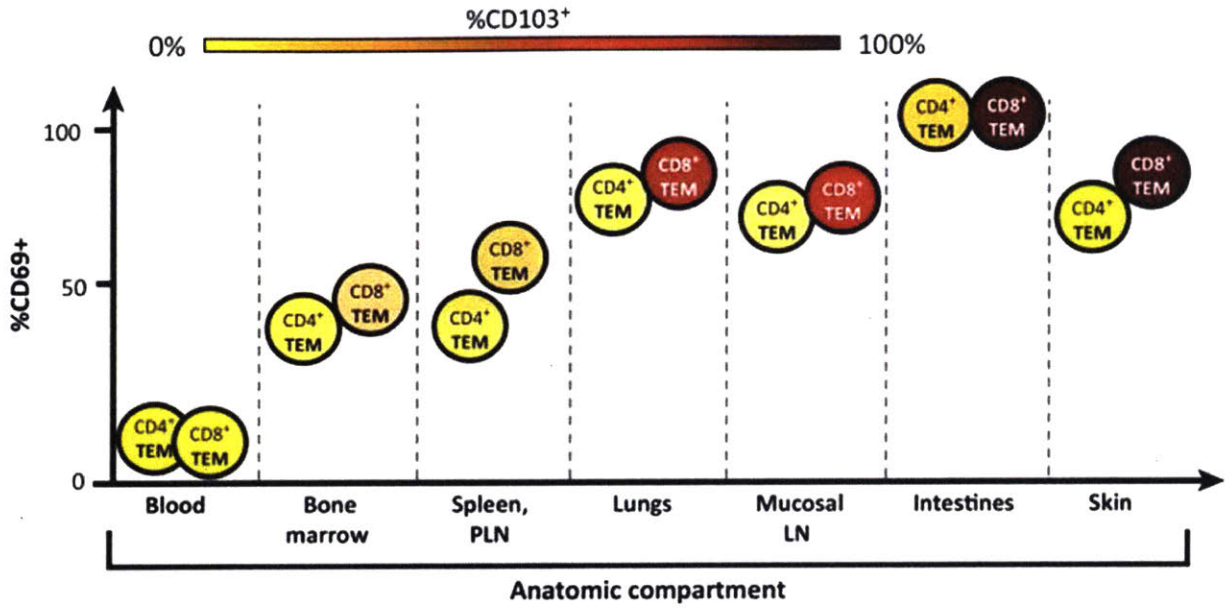

Figure 3-2: Variegation of T_{RM} phenotypes in different tissue sites. Expression of the T_{RM} markers CD69 and CD103 on CD4+ and CD8+ T_{EM} (effector memory T cell) populations in tissue sites (indicated on horizontal axis) is depicted by proportion of CD69+ based on position on the vertical axis, and proportion of CD103+, indicated by colored shading of each cell type (ranging from yellow = 0% to deep red/brown = 100%). CD69 is absent on circulating cells and is progressively upregulated on T_{EM} with the highest expression levels seen in mucosal sites. CD103 expression is highest in CD8+ T_{EM} in mucosal tissue sites and mucosal-draining lymph nodes with variable expression by CD8+ T_{EM} in other tissues, and CD4+ T_{EM} exhibit low or negligible CD103 expression. Adapted from [123].

To answer the second question, we investigated the recruitment of an important immune cell population that is absent from systemic circulation. Resident memory T cells (T_{RM}s)[3,19,21,124–127] are terminally differentiated T cells that reside specifically in peripheral tissues such as the skin, gut, mucosal linings and other barrier tissues[1]. They are cytotoxic CD8+ T-cells that are poised for immediate interception and killing of infected cells upon re-exposure to their target antigen.[128] Thus, they can be thought of as a frontline checkpoint for a successful immunization regimen.[123,129] These T_{RM}s are characterized by the expression of CD69 and CD103 as shown in **Figure 3-2**.

CD69 is an activation marker that is increasingly expressed on the surface of T cells, as they circulate from primary, to secondary to finally, non-lymphoid organs.[123,130] CD103 is an integrin mediating lymphocyte retention in non-lymphoid tissues such as the mucosal surfaces in lung and gut, and in skin.[4]

Since these cells are not accessible by standard peripheral blood draws because they do not circulate, it should be noted that the T_{RM} literature in humans is based on organ biopsies and tissue samples obtained, most frequently, from deceased individuals[130–132] or rarely, from invasive biopsies. In mouse models, animals are sacrificed and their organs are then digested to study cell counts and phenotypes. Given that MNs penetrate through to the viable dermis when applied to skin, and can, hence, access the immune surveillance reservoir[61] of the skin, we only needed to include the necessary cell signaling components to include in the sampling device, if any, to be able to collect these T_{RM}s. Sampling MNs can, thus, have important applications towards vaccine design. Thus, we considered utilizing sampling MNs for accessing these important immune cell populations in a minimally-invasive manner.

3.2 Materials and Methods

3.2.1 Materials and Animals

Poly-L-lactide (Resomer L207S) was purchased from Evonik Industries AG (Essen, Germany). SLM20 and SLG100 sterile ultrapure alginates were purchased from Pronova (FMC Biopolymer/Novamatrix, Sandvika, Norway). Calcium chloride dehydrate and sucrose were purchased from Sigma-Aldrich. R848, polyI:C and Pam3Cys were purchased from InvivoGen. Murine-IP10 (CXCL10) was purchased from PeproTech.

DOPC (1,2-Dioleoyl-sn-Glycero-3-Phosphocholine) and MPB (1,2-dioleoyl-sn-glycero-3-phosphoethanolamine-N-[4-(p-maleimidophenyl) butyramide) were purchased from Avanti Polar Lipids (Alabaster, AL). DTT (dithiothreitol) was purchased from Sigma-Aldrich. Chromatographically purified endotoxin-free ovalbumin (OVA) was purchased from Worthington (Lakewood, NJ).AL11 peptide (AAVKNWMTQTL) was synthesized by GenScript Corp. For CpG, solid phase DNA synthesis and 5' lipophilic conjugation were carried out as previously described using an ABI 394 synthesizer.[133] The sequence used was murine ODN class B sequence 1826 with two guanine spacers: 5' diacyl lipid -*G*G*T*C*C*A*T*G*A*C*G*T*T*C*C*T*G*A*C*G*T*T- 3.'

Following cleavage and deprotection, oligos were purified via RP-HPLC and quantified using UV-VIS. Note that * indicates phosphorothioate linkage.

Wild type C57BL/6 mice (stock #: 000664) were purchased from Jackson Labs. Evaluation of antigen specific CD8 T cells and T_{RM}s were done by staining with SIINFEKL/H-2Kb peptide–MHC tetramer (iTAg Tetramer/PE - H-2K^b OVA (SIINFEKL), from MBL) or SIVgag tetramer (iTAg Tetramer/PE - H-2D^b SIV GAG (AAVKNWMTQTL) from MBL), anti-CD45, anti-CD8a, anti-CD3e, anti-CD11b, anti-CD11c, anti-CD103 (BD Biosciences) and CFSE Cell Trace (Thermo Fisher Scientific C34554). Fc block from eBioscience (14-0161-86) was used to prevent non-specific binding.

3.2.2 Intradermal Injection of Adjuvant Based Studies

5μg of each adjuvant (R848, polyI:C and Pam3Cys) was injected intra-dermally in the dorsal auricular ear skin of 8-12 week old C57BL6 mice. Each injection was made up to 14μL in PBS and injections were administered 48 hours before the mice were euthanized and ear tissue resected and processed for phenotyping.

3.2.3 Ear Tissue Digestion

Adapting a previously established protocol for our needs,[134] the surface of the ear was cleaned for hairs using a blunt razor blade. The dorsal and ventral surface of the ear tissue were split mechanically using tweezers and immersed in RPMI containing liberase (Roche), collagenase, HEPES buffer and DNAase for 1.5 hours at 37°C on a shaking incubator at 200 rpm. The digested ear tissue was mashed using the back of a syringe plunger and passed through a 40 μm cell strainer. After pelleting the cell suspension, the samples were stained with anti-mouse antibodies (CD45, CD8a, CD11b, CD11c, DAPI) and analyzed via flow cytometry.

3.2.4 Synthesis of ICMVs

Interbilayer-crosslinked multilamellar vesicles (ICMVs) were synthesized as described previously.[135] Briefly, dried films of 1.26 μmol of lipids (DOPC:MPB at 1:1 mol ratio) and 5 μg of Pam3Cys were rehydrated in 20 mM bis-tris propane at pH 7.0 with 20 μg OVA or 20 μg AL11 peptide for 1 h with vortexing every 10 min and sonicated in alternating power cycles of 6 and 3Win 30 s intervals for 5 min on ice (Misonix Microson XL probe tip sonicator, Farmingdale, NY, USA). DTT and $CaCl_2$ were then sequentially added, immediately one after the other, at final concentrations of 3 and 40 mM, respectively, and incubated for 1 h at 37°C to form ICMVs. The

particles were recovered by centrifugation, washed twice, re-suspended in millQ water, and stored at 4°C until usage. In some experiments, ICMVs were prepared including a lipophilic tracer, DiD, at 0.1 molar % concentration with respect to lipids, and 20 μg of Alexa Fluor 555-conjugated OVA was used to hydrate the lipid films.

3.2.5 Immunizations

Groups of 8-12 week old C57BL6 mice were immunized using a prime-boost regimen: animals were primed on day 0 and boosted on day 14 with 10 μg OVA and 1.24 nmol CpG (in soluble form) suspended in PBS, via injections administered subcutaneously at the base of the tail.

3.2.6 Sampling MN Preparation

MN synthesis is described in detail in Chapter 2 and in the Appendix. Briefly, poly-L-lactide was melt-molded into PDMS molds to form MN arrays. MN arrays were exposed to poly-L-lysine for 30 mins and dried at room temperature and atmospheric pressure. Alginate-sucrose solution was then pipetted onto the 1 cm^2 MN arrays and dried under vacuum for 2 hours at room temperature. Calcium chloride solution containing polyI:C and ICMVs encapsulating Pam3Cys (and OVA or AL11 peptide) was pipetted onto MN arrays and dried under vacuum at room temperature for > 8 hours. MN arrays were stored under vacuum at room temperature until use.

3.2.7 OVA-specific IgG titer ELISA

Serum total IgG titers were determined as previously described.[136] Briefly, 96-well plates were coated with OVA and blocked with bovine serum albumin, then incubated with serially diluted serum and detected with HRP-labeled anti-mouse IgG (Bio-Rad), followed by development and measurement of optical absorbance at 450 nm. Antibody titer is reported as reciprocal serum dilution at an absorbance of 0.3.

3.2.8 Tail Skin Scarification with Vaccinia-SIVgag Virus

C57BL6 mice were anesthetized and tail skin area, 1 cm from the base of the tail, was wiped clean with 70% ethanol. 5 μL of diluted virus in PBS (total dose of either $2x10^5$ PFU, $1x10^6$ PFU or $2x10^6$ PFU) was applied to the cleaned tail skin and scratched gently 25 times with a 27 ½ gauge needle. Mice were monitored 3-4 times per week for lesion size, swelling size (measured with Vernier calipers) and body weight.

3.2.9 Characterization of Samples from Sampling MNs

Blood was processed via ACK lysis to lyse the red blood cells and enrich for leukocytes. Hair on the surface of ear tissue was first removed using a blunt razor blade. The dorsal and ventral surface of the ear skin were then mechanically separated before being subjected to enzymatic digestion using a combination of collagenase and DNase to break down the cartilaginous tissue.

Sampling MNs were applied to the dorsal surface of the C57BL6 mouse ears for 12 or 24 hours, secured using a combination of waterproof tapes. MNs were retrieved from anesthetized mice and the recovered cell suspension was retrieved from the gel coating via immersion in PBS containing 1% BSA and 100 mM EDTA for 30 minutes at 37°C while shaking at 150 rpm, washing the surface of the MN and pelleting via centrifugation. At relevant time points, blood was collected via retro-orbital bleeding, into EDTA and red blood cells were lysed using ACK lysis buffer. Samples were stained with anti-mouse antibodies (CD3e, CD8a, CD69 and CD103) as well as antigen-specific MHC tetramers (SIINFEKL or AL11). For CFSE staining, pelleted samples were resuspended in 100 μL of 0.36 μM solution of CFSE (Cell Trace, Thermofisher) for 5 minutes, at room temperature in the dark and quenched using 150 μL of RPMI containing 10% FBS for 15 minutes, washed and pelleted and analyzed via flow cytometry.

3.2.10 MuSIC (Multispectral Imaging Cytometry)

For the fabrication of the nanowell arrays, existing silicon masters mounted in metal molds were used (Love Lab, MIT). Poly(dimethylsiloxane) (PDMS) (Dow Corning) (10:1 ratio of base to catalyst) was injected through the input port of the molds, and cured at 80°C for 4 hours. The molds were then opened to obtain nanowell arrays containing 83,490 cubic wells (50 μm). Prior to use, the nanowell arrays were oxygen plasma treated for 2 minutes and immediately immersed in 100% fetal bovine serum at 50°C both to preserve the hydrophilicity resulting from plasma treatment, and to coat the array non-specifically with protein to improve cell viability. Prior to cell loading, nanowell arrays were rinsed with media.

Cells were stained as described in **Section 3.2.9** with a cocktail of anti-mouse antibodies (CD8α PE/Cy7, CD19 BV711, MHCII PerCP710, CD11b BV655, CD11c PE/Cy5, CD3e PerCP, CD45 BV605, Sytox Green and CD103 BV421.) from Biolegend. After staining, cells were loaded onto a nanowell array, with loading governed by a rough Poisson distribution. The loaded nanowell arrays were then imaged with an epifluorescence microscope (Zeiss) with filter wheels at the relevant excitation and emission wavelengths. Compensation was performed with agarose beads

(Agarose Beads Technologies) in 100mM sodium carbonate. Each antibody was incubated with a separate aliquot of beads and imaged in all the fluorescent channels of interest. The percentage of spillover from other channels into a given channel was calculated from the fluorescence data and then used to compensate the acquired cell fluorescence data.

Cells were identified from the obtained fluorescent images with Enumerator, an in-house image analysis software (Love Lab, MIT). For each nanowell array, a spreadsheet containing cell information including nanowell IDs, fluorescent intensities in each channel, and cell sizes, was generated. This data was then further analyzed and gated using Matchbox, an in-house MATLAB-based single-cell analysis software (Love Lab, MIT).

3.2.11 Statistical Analysis

Data sets were analyzed using two-tailed nonparametric Mann-Whitney test, one or two-way analysis of variance tests, followed by Tukey's HSD test for multiple comparisons with Prism (GraphPad Software, San Diego, CA). p-values less than 0.05 were considered statistically significant. All values are reported as mean ± s.e.m.

3.3 Results and Discussion

3.3.1 Confirmation of APC Hypothesis via MuSIC

Thus far, we have established a strategy to fabricate hydrogel-coated MNs capable of sampling ISF and recruiting cells from the skin via the delivery of immunostimulatory agents – **Figure 3-3** outlines the overall system design. Briefly, melt-molded polylactide MN arrays were coated with an alginate hydrogel layer that contains antigen/immunostimulator-loaded lipid nanoparticles (ICMVs). We hypothesized that upon application to skin, the adjuvant released from the hydrogel coating would APCs (**Figure 3-3** step (1)), which would internalize the ICMV nanocapsules present within the gel (step (2)). ICMV nanocapsules would get taken up by the recruited APCs, triggering their activation (step (3)), and these activated APCs would then act as active recruiting agents within the coating, releasing a collection of chemoattractant signals and cytokines that further recruit T-cells and other leukocytes to the sampling gel. We have previously shown that ICMV nanocapsules efficiently promote antigen presentation by APCs.[135,137] T-cells specific for antigens delivered in the ICMV capsules would recognize the antigens presented to them by the activated APCs in the gel coating, leading to their arrest and retention in the hydrogel

layer (steps (4), (5)). Upon removal from the skin, the hydrogel layer is digested to release recruited cells (step (6)), which can then be analyzed for phenotype, surface markers, cytology, etc.

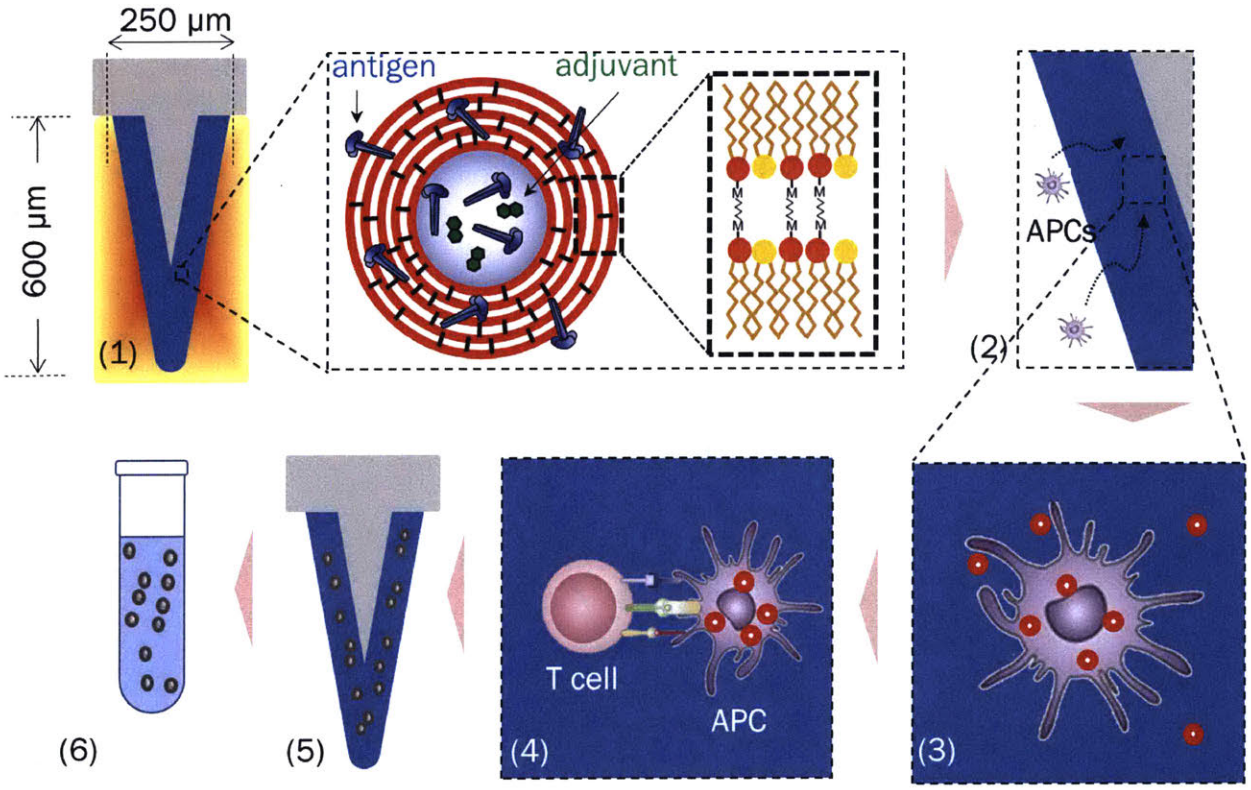

Figure 3-3: Schematic of Sampling MN platform. Hydrogel-coated MNs contain immunostimulatory ICMV nanocapsules (red). Upon application to skin, the hydrogel layer swells and releases chemoattractant. (2) APCs home into the gel layer from surrounding tissue, (3) Take up ICMVs and are thus stimulated to (4) recruit antigen-specific T cells into the gel. (5) The platform is removed from skin, and (6) the gel is digested to retrieve collected cells and ISF for further analysis.

In this section, we validate our hypothesis by showing that all of these steps indeed occur and demonstrate that we can successfully sample for cells, from the skin, via sampling MNs that have been applied to the surface of the skin.

Using cell-suspensions derived from the processing of sampling MNs applied to mouse ear skin for phenotypic analysis via flow cytometry presented hurdles is challenging because flow cytometry machines ideally perform well with cell events in excess of 10,000 cells.[138,139] In our

most studied model of the OVA-immunized mice, being able to retrieve 10,000 live cells was often a tough ask when the cell-suspensions were derived from a single sampling MN array.

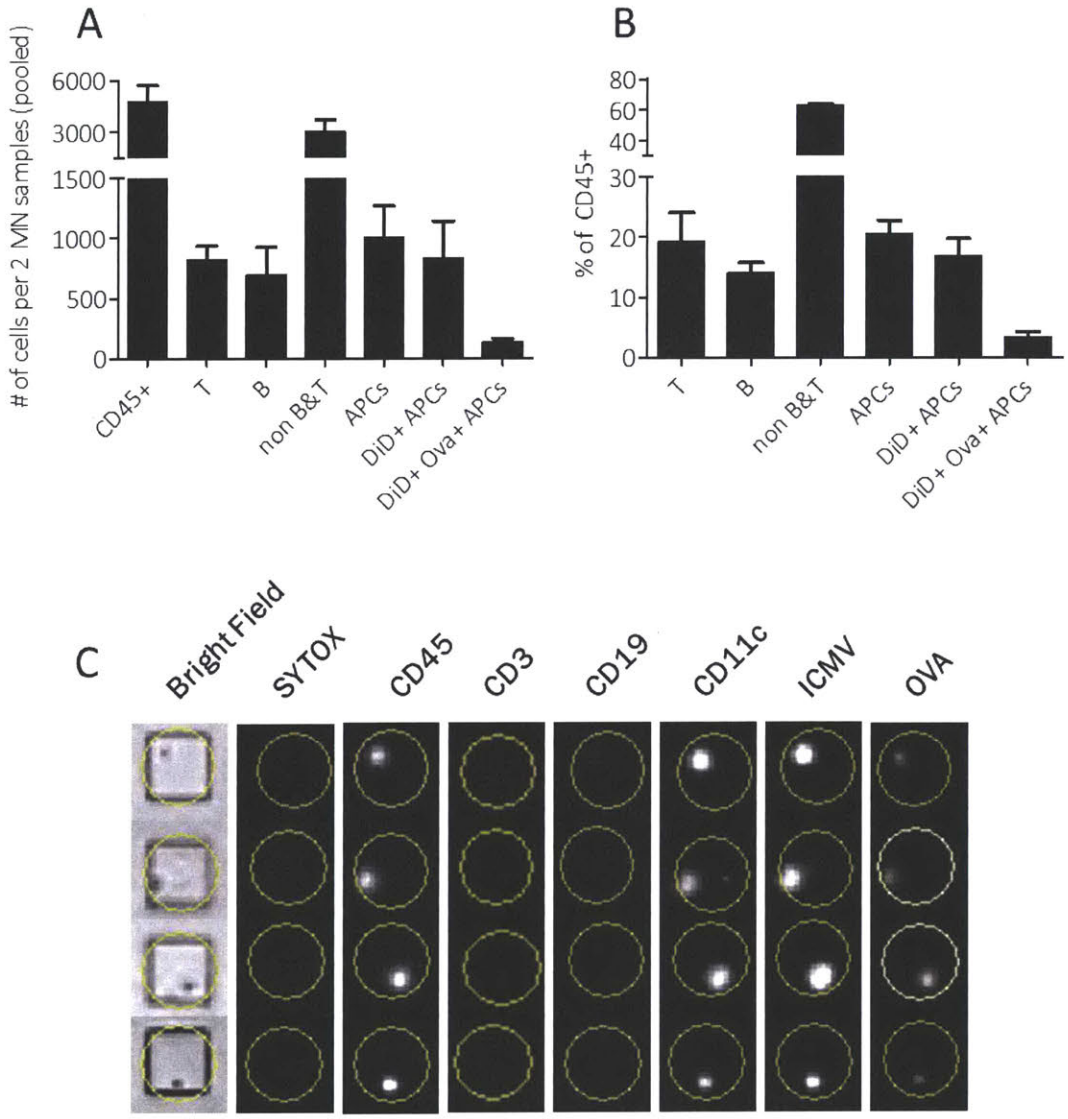

Figure 3-4: Characterization of MN infiltrate and confirmation of APC hypothesis via MuSIC. Groups of OVA-immunized mice (n=3/group) were sampled with sampling MNs containing 5 μg of polyI:C, and 2 μg OVA-Alexa Fluor555 and 5 μg Pam3Cys inside ICMVs containing DiD, for 24 hours, followed by retrieval, antibody stanining and phenotypic analysis via MuSIC. Cell numbers (A) as a proportion of CD45+ immune cells (B) recruited into sampling MNs applied for 24 hours onto OVA-immunized mice. (C) Micrographs showing overlay of fluorescent channels for live/dead dye Sytox, CD45, CD3, CD19, CD11c, DiD (ICMV) and OVA-Alexa Fluor 555, showing the presence of antigen presenting cells containing ICMVs. The edges of each well are 50 μm.

In order to prove that APCs interacted with the ICMVs that were embedded within the alginate coating of the sampling MNs (**Figure 3-4**), we wished to achieve deep phenotyping of the cell suspension we obtained from the sampling MNs. We synthesized ICMVs which encapsulated fluorescent OVA (Alexa Fluor 555 conjugate) and included DiD, a fluorescent lipophilic tracer dye which would be embedded in the lipid bilayers of the ICMVs. These ICMVs were included in the alginate coating (in the crosslinking layer) of the sampling MNs. MNs were applied for 24 hours on the ears of C57BL6 mice that had been immunized with OVA 24 weeks prior. The cell suspension obtained was analyzed using nanowell arrays and MuSIC[140], a technology developed by Love and coworkers at MIT, which allows for comprehensive phenotyping of scarce cells, especially those obtained from tissues directly for which conventional flow-based phenotypic methods present challenges.

MuSIC is an image-based cytometry methodology that increases the number of measurable surface markers from four to sixteen. The method uses combinatorial combinations of excitation and emission filters on a basic epifluorescent microscope to create sixteen unique spectral channels that match spectra of commercially available fluorophores. Custom software automatically identifies cells within images of the nanowell arrays and deconvolutes the intensity of each fluorophore on each cell using a spectral spillover matrix generated by imaging beads bound uniquely to each fluorophore.

We found that on average, we obtained about 5000 immune cells (CD45+) from each sampling MN (**Figure 3-4A**). Of these, 20% were T cells (CD3e+), about 15% were B cells (CD19+) and more than 60% of these were non-B&T cells (**Figure 3-4B**). One third of these non-B&T cells, which were about a fifth of the total immune cells, were APCs. This was interesting as it corroborated with our expectation and hypothesis that APCs came in to the alginate coating to interact with the ICMVs. However, what was most encouraging was that more than 80% of these APCs were also fluorescent in the DiD channel, indicating that the APCs had endo-cytosed the ICMVs. The fluorescent signal from the OVA was, however, only found in about 15% of these APCs indicating that, possibly, the APCs had processed the antigen and were cross-presenting the antigen on their MHC complexes or that the fluorescent OVA signal was too weak.

These findings were also evidenced by micrographs of individual nanowells containing the single cells (**Figure 3-4C**). We observed live APCs (Sytox-CD45+CD3-CD19-CD11c+) that showed bright fluorescent signal in the ICMV (DiD) channel and a weak signal in the OVA

channel. All of these fluorescent signals were co-localized which proved that the ICMVs were indeed inside the APCs.

3.3.2 Delayed Type Hypersensitivity Test Based Sampling

Our initial tests of the complete cell sampling MN patches were based on classic DTH tests (e.g., the Tuberculin 'Mantoux' test or allergen tests) in which an antigen is injected into the skin and the site is monitored for 2-3 days. If an individual has previously been exposed to the antigen, a palpable induration will develop within ~72 hours[35].

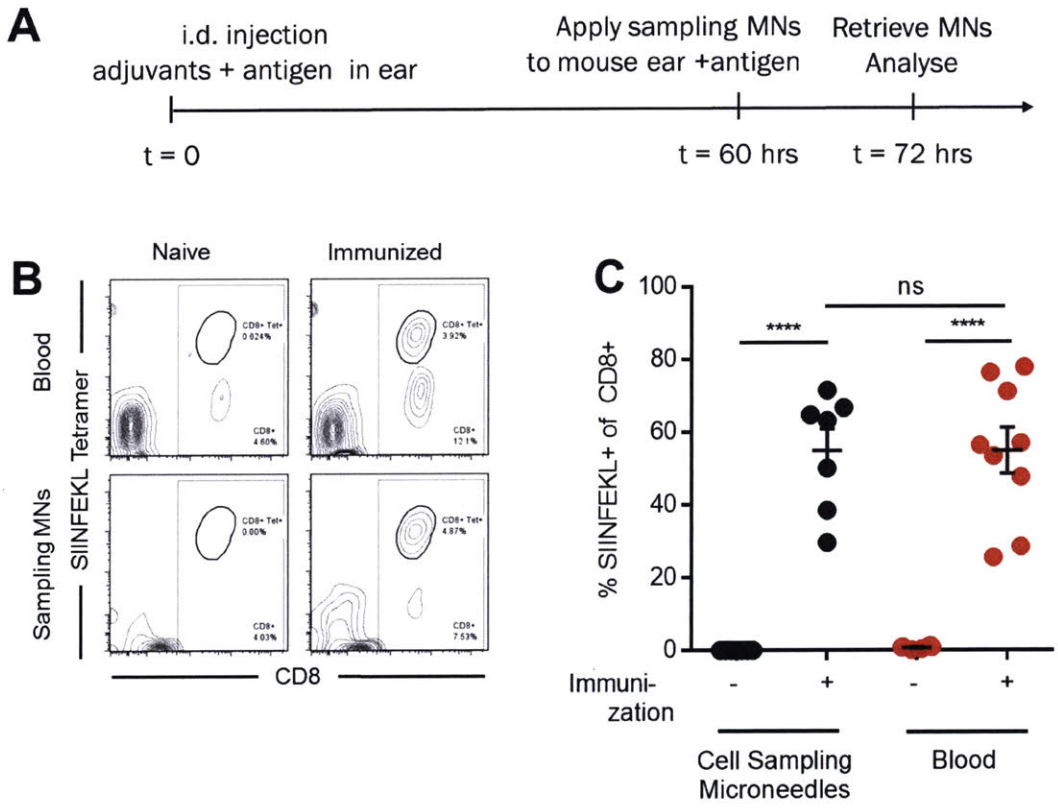

Figure 3-5: Cell sampling MNs allow detection of cellular immune responses. Groups of OVA-immunized or naïve C57Bl/6 mice (n=8/group) were injected intradermally in the ear at time zero with 2 μg OVA and 5 μg each of polyI:C and Pam3Cys. 60 hours later, sampling MN were applied to the same site for 12 hr, followed by retrieval for flow cytometry analysis. (A) Timeline of immunization and sampling. (B) Flow cytometry plots showing OVA-specific $CD8^+$ cells in naïve and immunized mice, as sampled from blood or with cell-sampling MNs, staining for CD8 and OVA-specific cells (using OVA peptide-MHC streptavidin tetramers). (C) OVA-specific (SIINFEKL+) cells as a percentage of total $CD8^+$ cells quantified via flow cytometry. Shown are means ± s.e.m., ns, nonsignificant, ****, $p < 0.0001$, analyzed by one-way ANOVA, followed by Tukey's HSD.

Replicating the same setting, C57BL6 mice immunized with OVA protein (4 weeks prior to the assay) were injected in the ear, intra-dermally, with adjuvants and 2 μg of OVA (**Figure 3-5A**). After 60 hours, MNs coated with crosslinked alginate (carrying no adjuvants) were applied for 12 hours to the same skin site, after which they were retrieved and the alginate coating was dissolved by exposing the MNs to a solution of 100 mM EDTA in media for 30 mins at 37°C to retrieve cells for analysis. Blood was also collected from the same animal for comparison of the results from MNs. Flow cytometry plots showed that as expected, in the blood (**Figure 3-5B**) naïve mice lacked detectable OVA-specific $CD8^+$ T-cells, while OVA-specific cells were present at high levels in immunized mice. These high frequencies of antigen-specific cells present in blood were expected and consistent with previous similar OVA + lipo-CpG immunization studies in our research group,[141] especially in the period of 2-4 weeks post an immunization event (prime or boost). Similar results were seen in MN samples, although lower total numbers of cells were collected. Quantifying the results from groups of animals, the frequency of OVA-specific $CD8^+$ T-cells detected using the sampling MNs was the same as observed in the blood (**Figure 3-5C**). Thus, we established the sampling MNs were capable of detecting cellular immune responses and specifically, sampling for antigen-specific cells from tissue *in situ* at comparable levels to those found in blood following pre-exposure to antigen and adjuvants about 60 hours before sampling, during the effector phase of an immune response.

3.3.3 Cell Recruitment into MNs with Adjuvants and CXCL10

We subsequently tested if vaccine adjuvants could be used to recruit more cells into the skin at the MN application sites, allowing the entire "DTH" response to be stimulated from the MNs. We first compared the capacity of 3 different adjuvants to recruit cells into the skin: a TLR3 agonist polyI:C; the TLR 7/8 agonist R848; and the TLR2/TLR1 agonist Pam3Cys.

Each of these adjuvants, as well as the combination of polyI:C and Pam3Cys, were injected intradermally in the ears of mice. 48 hours after these injections, the skin site was digested using collagenase and analyzed via flow cytometry for infiltrating cell populations. We observed that the combination of polyI:C and Pam3Cys elicited significantly increased recruitment of various immune cell populations, including $CD11b^+CD11c^-$ myeloid cells and $CD8^+$ T-cells, into the application ear, as seen in **Figure 3-6A-B**.

Next, we utilized our subcutaneous gel-injection model to test if the adjuvants, like the chemoattractants (as discussed in **Section 2.3.2**), also increased cell recruitment into alginate gels. C57BL6 mice were injected subcutaneously, underneath the dorsal flank skin, with alginate gels, with and without the combination of polyI:C and Pam3Cys (5 μg each). The gels were harvested after 24 hours and the cell infiltrate was analyzed via flow cytometry. We observed that the presence of the adjuvant combination doubled the number of live cells that were recruited into the gels (**Figure 3-6C**).

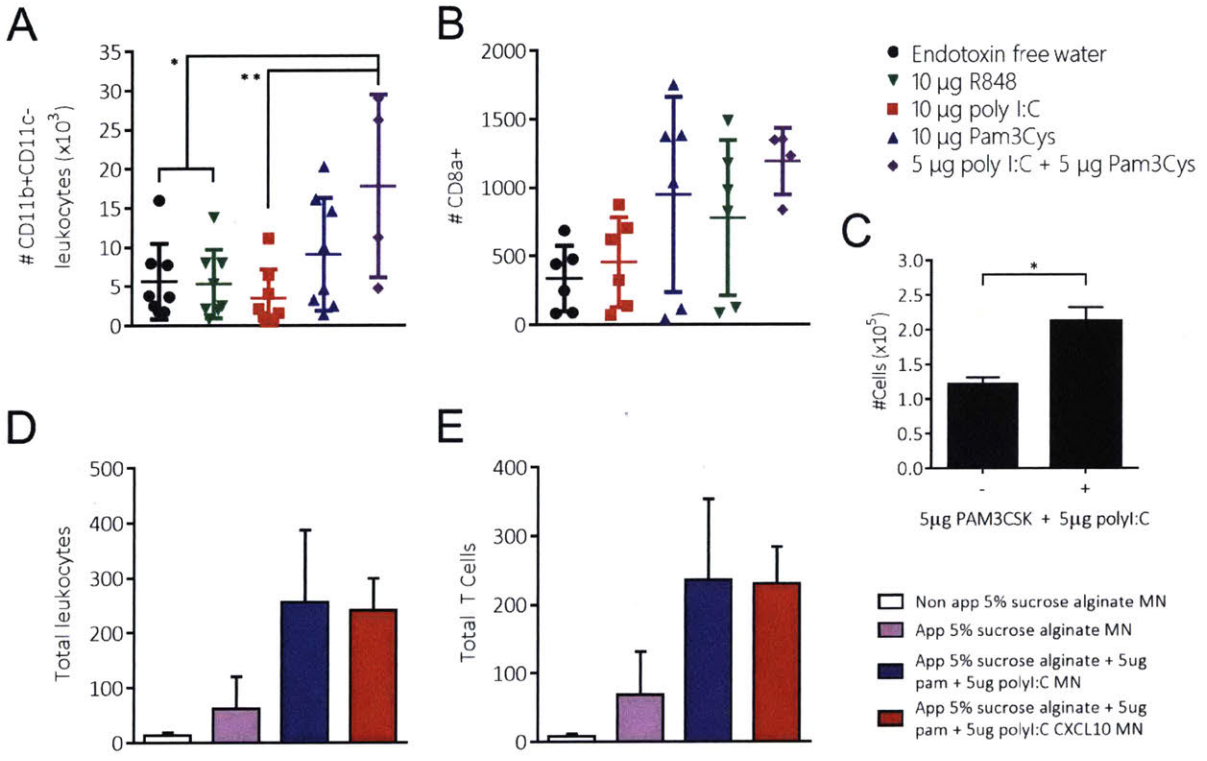

Figure 3-6: Cell recruitment into MNs with adjuvants and CXCL10. 7wk old C57BL/6 mice were injected intradermally in their ears with adjuvants. Mice were euthanized 48 hours later and ears were digested and analyzed using flow cytometry for infiltrating populations including $CD11b^{+}CD11c^{-}$ leukocytes (A) and $CD8\alpha^{+}$ leukocytes (B). Live cells recruited into subcutaneously injected gels under the dorsal flank of naïve C57BL6 mice for 24 hours, with and without presence of adjuvants Pam3Cys and polyI:C (C). Cell-sampling MNs, including adjuvants in the coating, were applied for 12 hours on the ears of naïve C57BL/6 mice. The alginate coatings on the MNs were digested and analyzed using flow cytometry for infiltrating cell populations including total leukocytes (CD45+) (D) and total T cells (CD3e+) (E). "Non app" is a control MN array that was not applied to the skin, and represents the background noise of the measurement. Data sets represent mean ± s.e.m., *, $p < 0.05$ and **, $p < 0.01$, analyzed by one-way ANOVA, followed by Tukey's HSD.

Our next step was to investigate if the inclusion of these of agonists into the alginate coating of cell-sampling MNs could facilitate increased cell recruitment into the alginate coating itself. We fabricated sampling MNs as depicted in **Figure 2-2,** but also included adjuvants in the alginate coating, expecting they could diffuse into the neighboring tissue upon application to the skin. MNs were applied to the ear skin of groups of mice and retrieved 12 hours later. The alginate layers of each MN patch were dissolved using EDTA, and the recovered cells were stained with antibodies for flow cytometry analysis. As shown in (**Figure 3-6D-E**), even without added adjuvants, the gel-coated MNs elicited some level of cell recruitment, likely mediated by chemokines triggered in the surrounding tissue following the micro-damage caused by MN penetration into the epidermis.[142–144] Notably, the combination of Pam3Cys and polyI:C led to more cell recruitment than "empty" alginate MNs, but addition of CXCL10 did not further increase the number of captured cells (**Figure 3-6D-E**). Though small numbers of cells were recovered in the MNs in this short application time, this experiment demonstrated the proof of concept that a significant population of cells can be collected in just 12 hr of application time.

Mouse ears subjected to MNs that contained CXCL10 in the alginate coating showed increased redness and inflammation. For some animals, the ear tissue disintegrated and necrosed because of excessive inflammation and the periphery of the ear tissue showed scar tissue formation. We suspect that because CXCL10 (and CCL21) are both pro-inflammatory cytokines, the doses of these included in the sampling MNs to recruit cells for sampling are not healthy for the long-term recovery, healing and survival of the tissue. Thus, subsequently, we focused on including only the adjuvant combination of Pam3Cys and polyI:C (5 μg each) in the MNs to signal for cell infiltration.

3.3.4 Encapsulation of Adjuvant in ICMVs Elicits Increased Recruitment

The adjuvants included in the alginate coating in the previous results (**Section 3.3.3**) were in soluble form, being co-dissolved in the calcium crosslinking solution added on to the alginate coating during the preparation of these MNs. Our research group has previously shown that lipid nanocapsules (ICMVs) loaded with antigen and/or adjuvant compounds efficiently activate and promote antigen presentation by APCs.[135,137] Consequently we next explored if the encapsulation of adjuvants in ICMVs, embedded in the alginate coating of the sampling MNs, could further increase the number of cells recruited into them. ICMVs incorporating Pam3Cys were synthesized

and polyI:C was included in soluble form in the alginate coating. These sampling MNs, with adjuvants incorporated into ICMV particles, recruited ~8x more cells than those present in the coating in soluble form (**Figure 3-7A**).

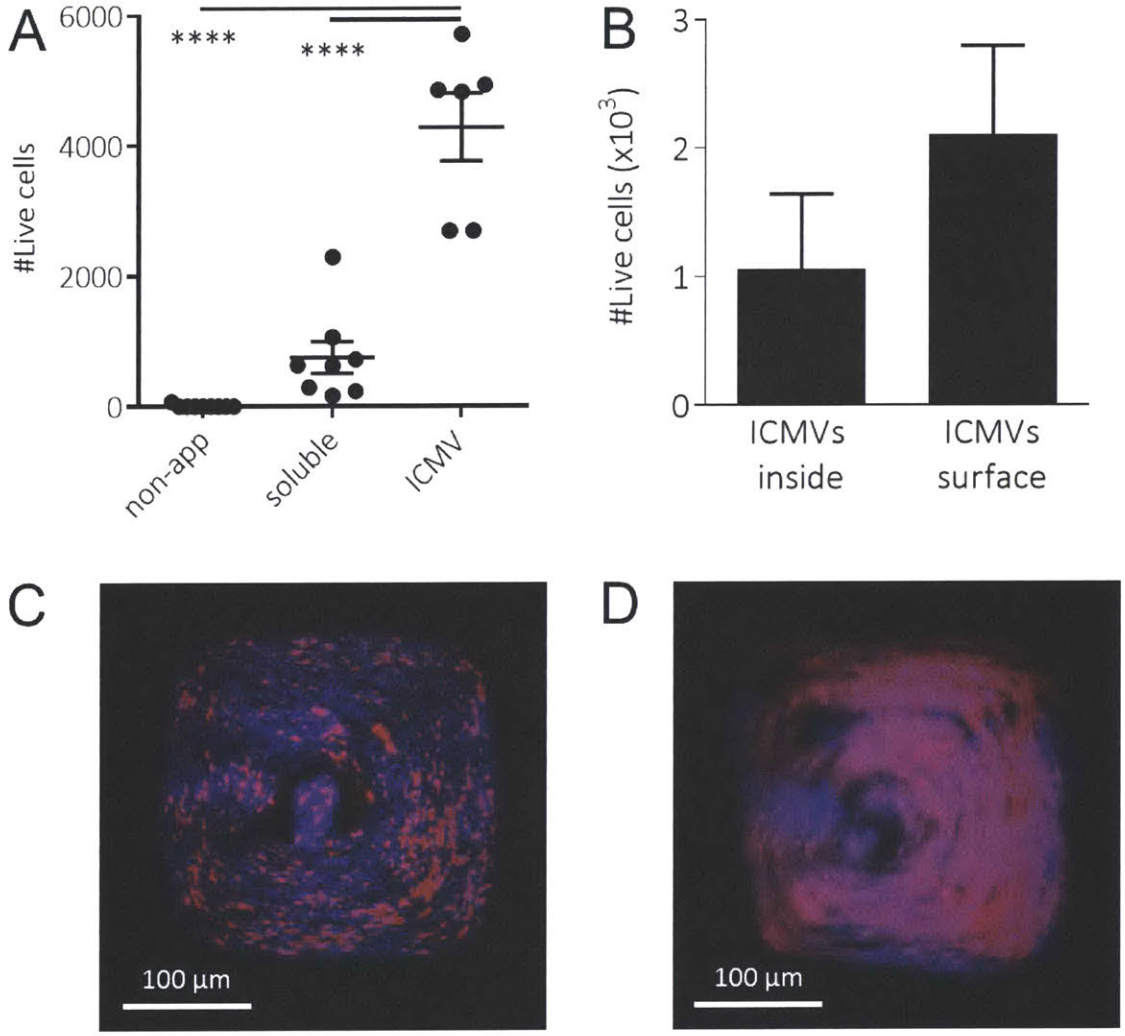

Figure 3-7: ICMVs encapsulating antigen and adjuvant, when embedded in the alginate layer of sampling MNs, elicit increased recruitment of cells into sampling MNs. Groups of 8-10 wk old naïve C57BL/6 mice (n=8/group) were sampled for 12 hours using sampling MNs containing adjuvant (5 µg Pam3Cys) in either soluble or ICMV encapsulated formats, with 5 µg poly I:C included in soluble form in the alginate coating. (A) Live cells retrieved, per MN array. "Non app" is a control MN array that was not applied to the skin, and represents that background noise of the measurement. (B) Live cells retrieved upon sampling C57BL/6 mice for 12 hours with sampling MNs containing ICMVs containing Pam3Cys incorporated in the crosslinking/outside/surface layer recruit more cells than those placed 'inside' in the alginate layer. (C) and (D): Confocal micrographs of ICMVs containing fluorescent OVA (red) encapsulated in ICMVs within in fluorescently tagged alginate (blue) as prepared by including the ICMVs in the

alginate solution, or in the calcium crosslinking solution, respectively. Data sets represent mean ± s.e.m., ***, $p < 0.001$, analyzed by one-way ANOVA, followed by Tukey's HSD.

We next investigated if the inclusion of the adjuvant-incorporating ICMVs ('inside') in the alginate solution during preparation of the sampling MNs versus their inclusion in the calcium crosslinking solution ('surface') elicited differing degrees of cell recruitment and infiltration. MNs with ICMVs incorporated in these ways were applied to C57BL6 mice for 12 hours (**Figure 3-7B**), and we found that ICMVs incorporated in the surface layer recruited almost twice as more cells into the alginate layer, presumably since the particles were more accessible to leukocytes entering the gel from the surrounding tissue, leading to more rapid/pronounced local stimulation. We investigated the morphological reason for these biological effects by encapsulating fluorescently labeled OVA inside ICMVs that were included either in the alginate layer (also fluorescently labeled) or in the calcium crosslinking solution during preparation of the sampling MNs. We observed that ICMVs, included 'inside' the alginate layer during preparation, showed aggregation (**Figure 3-7C**) whereas when ICMVs were included in the calcium crosslinking layer during preparation, they stayed dispered and were uniformly distributed in the alginate layer (**Figure 3-7D**). Since dispersed ICMVs can be understood to be more accessible for interactions with incoming cells much more than aggregated ones, we performed all following studies by including the ICMVs in calcium crosslinking solution during the preparation of the sampling MNs.

3.3.5 Confirmation of Resident Memory T Cells in Tissue

The experiments performed thus far suggested that our sampling MNs could recruit a diagnostically-significant number of T cells. We then wished to go one step further and check for the recruitment of antigen-specific T_{RM}s that are known to preferentially reside in peripheral tissue like the skin, and do not otherwise circulate systemically in the blood.[3,19,20,124,145]

To this end, we first sought to characterize the immune cell phenotypes in skin and specifically check for the existence of not just T_{RM}s, but in mice immunized with the OVA antigen, OVA-specific T_{RM}s. We first confirmed that our subcutaneous immunization protocol establishes a population of skin-resident memory cells: Blood and digested ear tissue were obtained from both naïve as well as immunized C57BL6 mice, at ~ 4 weeks post boosting. We noted that OVA-specific $CD8^+$ cells were present in the blood and ear tissue of only the immunized animals. As expected, when we gated forward on these antigen-specific cell populations for the T_{RM} markers

CD69 and CD103, only the ear tissue from the immunized animals showed the presence of cells which were positive for both of these cell-surface markers. This is exemplified by the flow cytometric plots in **Figure 3-8A**. If we consider the antigen-specific population for the blood sample from immunized mice ("Imm. Blood"), we see these cells express neither of the two skin-homing markers and, therefore, lie in the bottom left quadrant of the flow cytometric plot shown.

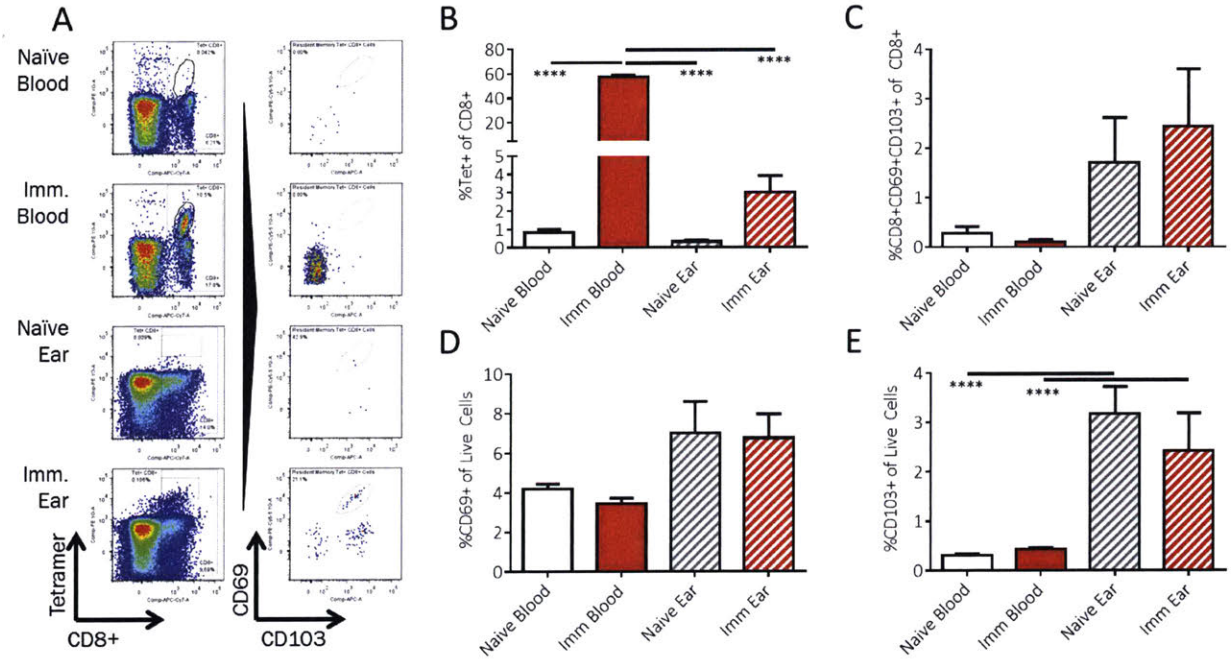

Figure 3-8: T_{RM} characterization in the blood and skin compartments in OVA-immunized mouse model. Groups of OVA-immunized mice (n=3/group) were bled, euthanized and their ears were digested and analyzed via flow cytometry. (A) Flow cytometric plots showing gating strategy for characterizing T_{RM}s in blood and digested ear tissue from C57BL6 mice that are naïve ("Naïve Blood", "Naïve Ear") or were immunized ("Imm. Blood", "Imm. Ear" with OVA. OVA tetramer (SIINFEKL) (B) and antigen-specific T_{RM} s (C) as a frequency of $CD8^+$ cells. (D) and (E) show $CD69^+$ and $CD103^+$ cells as a frequency of all live cells. Data sets represent mean ± s.e.m., ****, $p < 0.0001$, analyzed by one-way ANOVA, followed by Tukey's HSD.

When we considered the proportion of $CD8^+$ cells that were OVA-specific in the immunized animals, as expected from our understanding of previous similar studies and also from **Figure 3-5**, the blood of these immunized animals consisted of 60% of its $CD8^+$ being specific for the antigen (**Figure 3-8B**). The ear tissue in contrast, consisted only of about 3% $CD8^+$ that were specific for OVA. However, of the same total $CD8^+$ cell population, 2.5% of them were of the

T_{RM} phenotype ($CD8^+$ $CD69^+$ $CD103^+$) in the ear tissue from the immunized mice as compared to almost negligible levels in the blood from immunized mice (**Figure 3-8C**).The vast excess of other $CD8^+$ cells are presumably circulating cells from blood vessels and capillaries in the ear. Interestingly, about 1.8% of the CD8+ cells in the ear tissue from naïve mice were T_{RM}s, which are probably specific to other antigens that these animals have been exposed to environmentally.

CD69 is an early activation induced marker for T cells and CD69 is expressed on almost all these cells as they egress the blood compartment and make their way into secondary lymph organs and especially the skin, CD69 is expressed on almost all cells.[146] This trend is seen in **Figure 3-8D**, where the ear tissue cells are seen to have higher CD69 expression than live cells from blood, irrespective of whether the sample comes from naïve or immunized animals. The αE integrin CD103 (which binds e-cadherin on epithelial cells) is a specific feature of CD8+ T_{RM}. As a proportion of live cells, cell samples from blood show significantly lower levels of CD103 expression whereas for cells from digested ear tissue, about 2-3% of the live cells consist of cells expressing CD103 (**Figure 3-8E**).

These observations led us to the holy grail of our efforts — to test for the sampling of T_{RM}s that specifically reside in the skin and cannot be observed by peripheral blood draws, using our sampling MNs.

3.3.6 Optimized Sampling Conditions: Antigen Dose and Time of Application.

Having established the presence of T_{RM}s in our immunized animals, we next sought to determine whether sampling MNs could recover these cells, as illustrated in **Figure 3-9A**. Sampling MNs were applied to OVA-immunized C57BL6 mice, ~ 10 weeks after immunization, for 24 hours, including 2μg OVA and 5μg Pam3Cys in ICMVs, as well as 5μg polyI:C in the alginate coating. Similar to the results we obtained from digested tissue and blood (**Figure 3-8**), when considering $CD8^+$ T cells, and gating forward on CD69 and CD103, the sample from sampling MNs shows a population of T_{RM}s that does not exist in blood. After this, we investigated the effect of (i) MN application time and (ii) antigen dose included in the coating on cell sampling effectiveness in the absence of a pre-injection of antigen into the skin. To achieve this, we incorporated both antigen (OVA) and adjuvants (polyI:C and Pam3Cys) into ICMV nanoparticles, and encapsulated the ICMVs in the surface layer of the alginate gel coating on MNs.

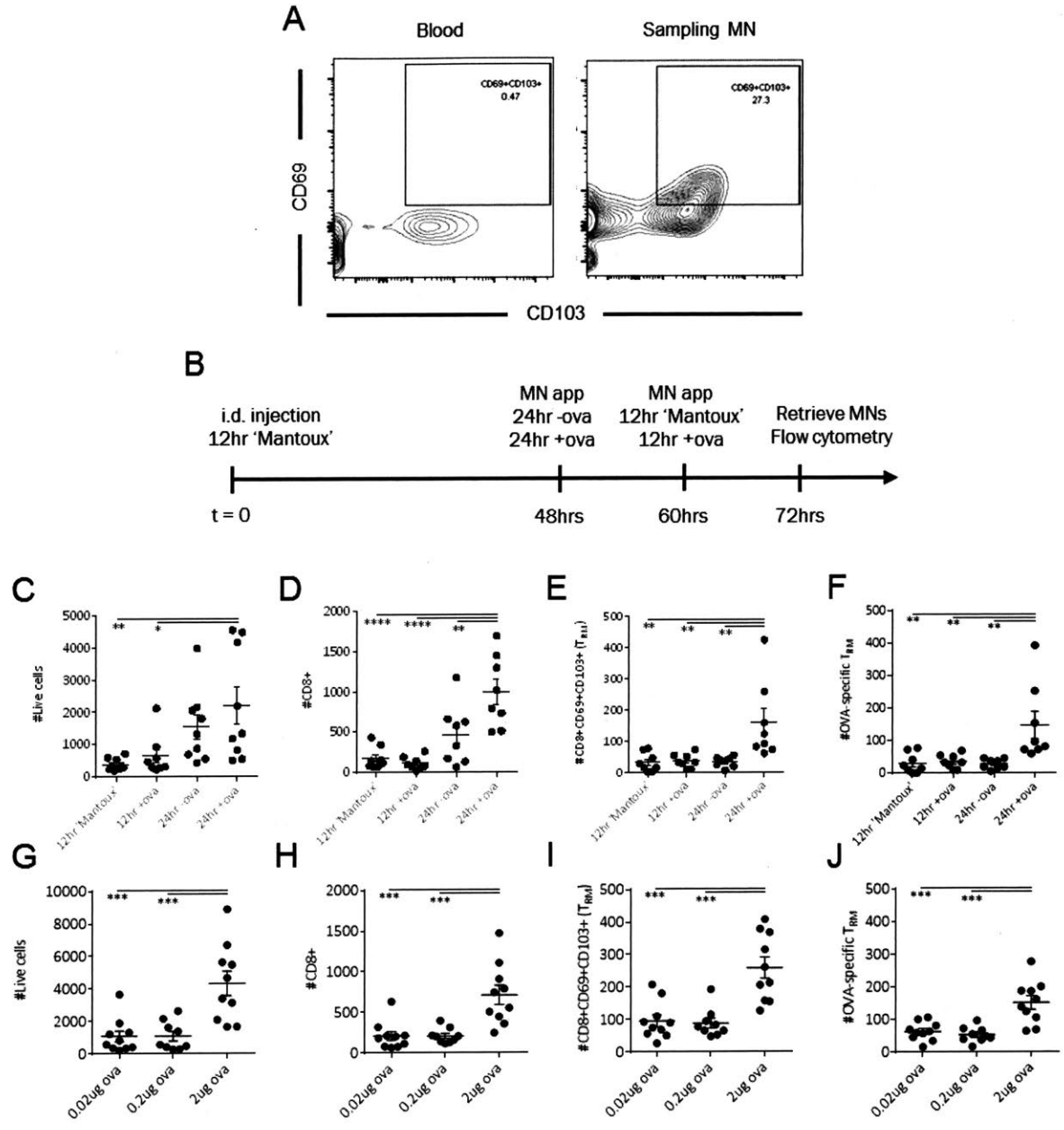

Figure 3-9: Optimal parameters for sampling of T_{RM}s. Groups of OVA-immunized mice (n=5/group) were sampled with sampling MNs with or without 0.02 μg, 0.2 μg or 2 μg OVA, applied to mouse ears for upto 24 hours to optimize the duration of application and dose of antigen for sampling. (A) Sample flow cytometry plots showing staining for CD69 and CD103 in blood and cell-sampling MN samples. (B) Timeline of timing optimization experiment. (C), (D), (E) and (F): Live cells, CD8+ cells, CD8+CD69+CD103+ T_{RM}s and OVA-specific CD8+ T_{RM}s, respectively, per sampling MN array, from sampling MNs applied to naïve or OVA-immunized C57BL/6 mice to study effect of duration of application on recruited cell numbers. (G), (H), (I) and (J): Live cells, CD8+ cells, CD8+CD69+CD103+ T_{RM}s and OVA-specific CD8+ T_{RM}s, respectively, per sampling MN array, from sampling MNs containing ICMVs encapsulating 0.02ug,

0.2ug and 2ug OVA to study dependence of recruited cell numbers on antigen level. Data sets represent mean ± s.e.m., *, $p<0.05$, **, $p<0.01$, ***, $p < 0.001$ and ****, $p < 0.0001$ analyzed by one-way ANOVA, followed by Tukey's HSD.

We first optimized the time of application of the sampling MNs. Since a two-step sampling strategy as in the Mantoux test (with an intradermal injection two days prior to sampling) discussed in **Section 3.3.1** may be difficult to employ, particularly in a front-line medical setting, we investigated if a one-time application of MNs loaded with antigen-containing ICMV nanoparticles could recruit enough cells into the hydrogel layer of the patch. Using ICMVs containing 2 μg of OVA, MNs were applied for either 12 or 24 hours (with no prior intradermal injection of adjuvant or antigen) onto the ears of C57BL6 mice that were previously immunized with OVA (**Figure 3-9B**). MNs with ICMVs applied for 24 hours showed a higher recruitment of cells of interest (**Figure 3-9C-E**) for all relevant phenotypes of cells (CD8+, T_{RM}s and OVA-specific (SIINFEKL+) T_{RM}s). The latter are T-cell populations that enter the skin and permanently reside there following immunization, thereby providing local immunity.

These cells are of particular interest since, by definition, they cannot be measured by traditional blood draws. Based on these studies, we concluded that, for murine studies at least, 24 hours was the most useful timeframe over which to apply sampling MNs, as this give us the highest number of cells recruited. It is possible to imagine that in other larger animal models and humans, increasing the size of the MN array or patch can mimic the benefits of a larger sample size or cell suspension that is collected from the skin. However, in a mouse model, we have consistently seen that the 12 hour application time yields only, at most, half the number of cells of each type that can be obtained from the application of the same sampling MNs for 24 hours.

We also included a group of MNs that were applied to similar mice, which did not contain antigen in their alginate coating, and only contained the adjuvant combination. As can be seen in **Figure 3-9C-D**, the infiltration level at 24 hours, even without the presence of the antigen, is higher than those groups in which the sampling MNs containing both antigen and adjuvant were applied for 12 hours. However, these CD8+ cells were not of the T_{RM} phenotype (**Figure 3-9E-F**) and are probably CD8+ leukocytes of naïve or central memory lineage.

We next sought to titrate the OVA dose to identify the lowest dose of antigen that could be incorporated within the ICMVs and still trigger an enrichment of antigen-specific cells in the MNs. The initial usage of 2 μg of OVA was based on two approximations: (i) the chemokine doses, when

they were being used, were used at 2-4 μg so we chose to stay in the same concentration range and (ii) the mice were initially immunized with 10 μg of OVA, via an injection given at the tail-base subcutaneously. 20% of this dose seemed a high enough starting point to test for with the sampling MNs.

With this reasoning in mind, three doses of antigen were investigated: 0.02μg, 0.2μg and 2 μg of OVA. MNs containing these OVA-loaded ICMVs were applied for 24 hours to the skin of C57BL6 mice that had been immunized with OVA and boosted two weeks prior to the assay. We analyzed recovered cells by flow cytometry and stained the cells with antibodies to identify total CD8+ T-cells, T_{RM}s and OVA-specific tissue-resident (CD103+CD69+) CD8+ T-cells (**Figure 3-9G-J**). MNs with ICMVs containing 2 μg of OVA showed maximum recruitment of cells into the corresponding cell-sampling MNs for all relevant phenotypes of cells (live, CD8+, OVA-specific CD8+ T-cells and OVA-specific CD8+ T_{RM}s with decreasing numbers of cells recruited for each type of cell in the MNs that contained OVA equivalent to a tenth or a hundredth of that dose. While this behavior can be explained by the fact that a higher antigen stimulus recruits more antigen specific cells, we can also think of using a lower dose and a larger surface area of the MN array to combat the trade-off between dose and recruited number of cells. Thus, for our future murine studies, we chose the 2 μg dose of antigen.

Based on these studies, a 24 hour application of cell-sampling MNs incorporating ICMVs (containing 2 μg OVA and 5 μg Pam3Cys) as well as co-dissolved polyI:C (5 μg), in the crosslinking layer of the alginate coating, was designated as the finalized sampling strategy.

3.3.7 Antigen is Required to Signal for Recruitment of Antigen-Specific Cells

Next, we evaluated the ability of cell-sampling MNs to be used to monitor these tissue-resident cells at long times following vaccination. Continuing with our model of C57BL6 mice immunized with OVA, we looked at a time point 10 weeks post boost (i.e. exposure to antigen), as depicted in **Figure 3-10A**. We first compared MNs carrying ICMV nanoparticles either loaded with antigen together with adjuvants or loaded with adjuvants only, to test the effect of the antigen in recruitment of the cells of interest. We hypothesized that antigen would be required to signal for the retention of antigen-specific cells, though we were interested to see the phenotype of cells recruited into the MNs with only the presence of adjuvants since we knew that the resting 'naïve' ear population also consisted of other T_{RM}s, which weren't specific for OVA.

In each case, antigen-loaded MNs were more effective in recruiting/retaining leukocytes (live cells, CD8+ leukocytes, antigen-specific CD8+ cells, T_{RM}s and antigen-specific T_{RM}s, **Figure 3-10B-F**), especially antigen-specific T-cells (**Figure 3-10D** and **Figure 3-10F**). As expected, no $CD69^{+}CD103^{+}$ T_{RM} cells were detected in blood (**Figure 3-10E** and **Figure 3-10F**).

Combining this information with our previous inquiry into the effect of exclusion of antigen from the coating of sampling MNs in **Section 3.3.6**, we concluded that in the OVA-immunized mouse model, sampling MNs applied for 24 hours, containing ICMVs on their surface that encapsulate the OVA antigen as well as Pam3Cys, in addition to polyI:C that is co-dissolved in the coating as a co-adjuvant, was the most effective way to sample for cells, providing ~ 5-10k live cells which can be quantified reliably using flow cytometry.

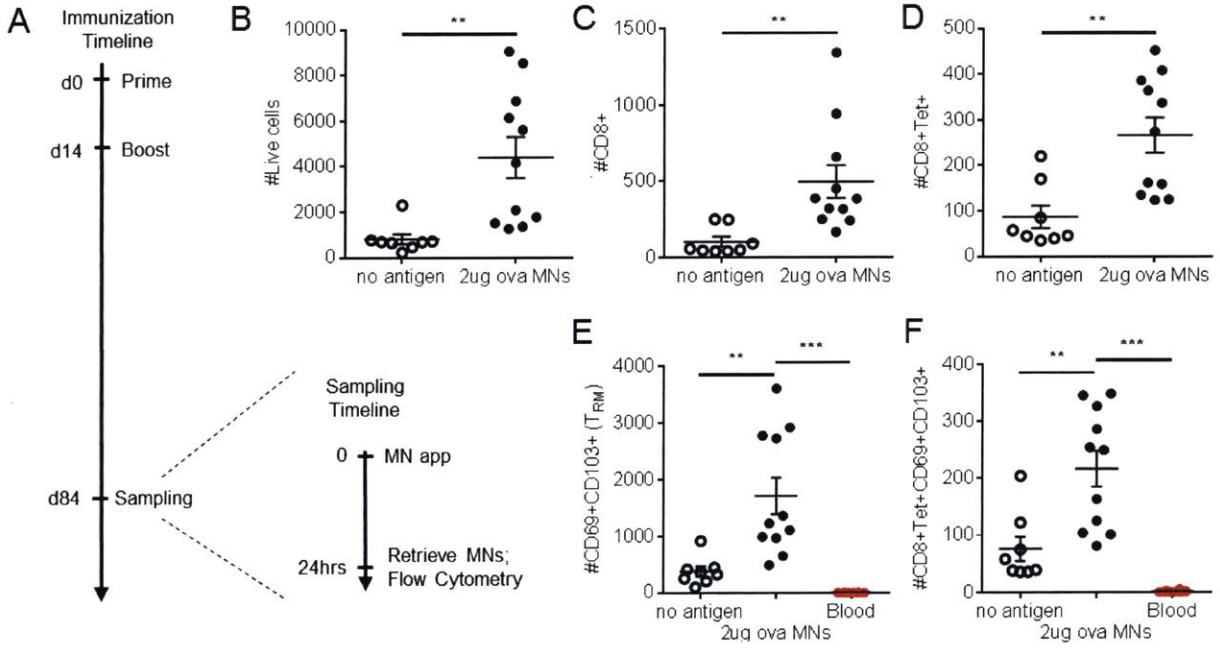

Figure 3-10: Antigen stimulus is required for the sampling and recruitment of antigen-specific cells via sampling MNs. Groups of OVA-immunized mice (n=5/group) were sampled 11 weeks post boost for the presence of T_{RM}s with sampling MNs containing no or 2 μg of OVA, applied for 24 hours, retrieved and analyzed via flow cytometry. (A) Timeline of immunization and sampling. (B), (C), (D), (E) and (F) Live cells, CD8+ cells, tetramer+CD8+ cells, T_{RM}s and OVA-specific CD8+ T_{RM}s, respectively, per sampling MN array, from cell-sampling MNs containing no antigen (open circles) and 2ug OVA encapsulated in ICMVs incorporated in MN coating (filled circles). Data sets represent mean ± s.e.m., **, $p<0.01$ and ***, $p < 0.001$, analyzed by one-way ANOVA, followed by Tukey's HSD.

We were, however, skeptical of the inclusion of this 'high' dose of antigen for purely a sampling need since, ideally, to gauge the status of a system, one should not perturb the system (even though, measuring the state of a system without any perturbation is an impossibility in itself).[147]

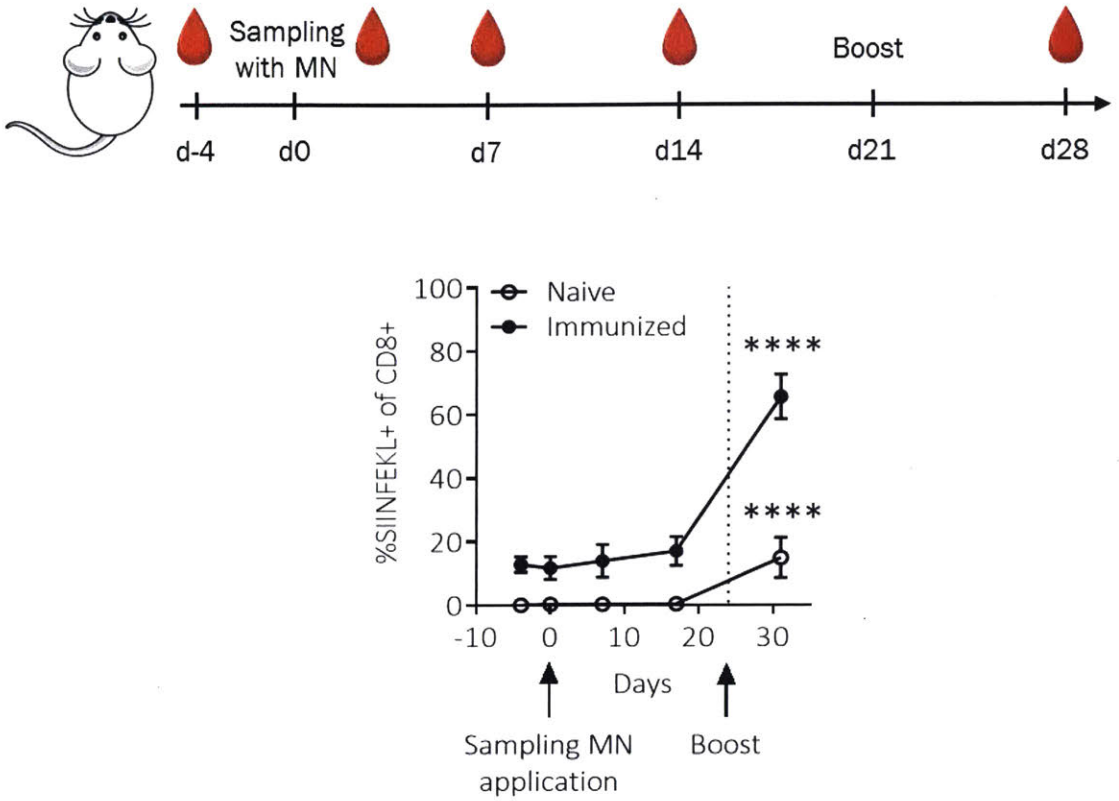

Figure 3-11: Sampling MNs do not change the immune status, as seen by monitoring levels of antigen-specific cells in blood post sampling. Groups of naïve or OVA-immunized mice (n=5/group) were sampled with sampling MNs containing 2 μg of OVA, applied for 24 hours, retrieved and analyzed via flow cytometry. Frequencies of OVA-specific CD8+ T cells from blood in naïve (open circles) and previously immunized (filled circles) C57BL/6 mice, post sampling MN application at day 0 and boost on day 24. Data sets represent mean ± s.e.m., ****, $p < 0.0001$ analyzed by two-way ANOVA,

3.3.8 Testing of Possible 'Immunization' via Sampling MNs

In order to test if the process of sampling itself constituted a 'mini-immunization,' we used C57BL6 mice that had previously been immunized (prime + boost) with OVA and lipo-CpG 36-77 weeks prior to these studies. The OVA-specific CD8+ cells were monitored via retro-orbital blood draws pre- and post- sampling MN application at day 0 for age-matched naïve and

immunized mice. The sampling MN protocol used was the one finalized for the OVA-immunized mice, as described in Section **3.3.6**. Mice were bled 4 days prior to the sampling MN application to allow for a baseline assessment of the antigen-specific cells present at 'steady state' and were bled on the day of sampling and then, every week for 3 weeks after the sampling. We observed that for both naïve and immunized mice the levels of OVA-specific (SIINFEKL+) cells, as a frequency of CD8+ cells, had no statistically significant change with the sampling MN application event (**Figure 3-11**).

To compare the effect in a 'real' immunization event, we boosted the mice again with 10 μg of OVA and 1.24nmol of lipo-CpG (the same cocktail was used for the initial prime-boost regimen) at day 21. As expected, for the immunized mice, this resulted in OVA-specific cells proliferating to become more than 60% of the CD8+ cell compartment, while, for the naïve mice, these numbers were lower (~ 15%). This is in line with the behavior of naïve mice when they are exposed to this vaccine combination for the first time, from our previous studies in the research group.[141] Based on these results, we concluded that the process of sampling with the inclusion of antigen (2 μg OVA) in the sampling device itself did not cause a significant change in the cellular immune response of both naive mice as well as mice that were previously exposed to the antigen itself.

3.3.9 T_{RM} Sampling in Vaccinia-SIVgag Infection Model

Thus far, we proved the ability of sampling MNs to recruit antigen-specific cells and antigen-specific T_{RM}s in an animal model in which mice were immunized with OVA, which is a model antigen. To test the ability of the sampling MNs to recruit T_{RM}s established by a live pathogen, we chose a vaccinia virus infection model.

Vaccinia virus is used for immunization against small-pox, and is a well-studied model in the laboratory for biology of poxvirus. We specifically chose skin-scarification as the infection route as it is known that scarification as a method of vaccinia-virus vaccination is superior to subcutaneous and intramuscular injection in the induction of vaccinia-virus-specific immune responses.[148] In the tail-skin scarification studies we referenced[126,149], mice either succumbed to the infection or were sacrificed within 3-4 weeks of the scarification procedure. Since we intended to test for T_{RM} sampling at long times (>10 weeks) post infection, we first wished to find the

highest dose of virus to be used for the infection that the mice would be able to recover from and for which the scarified skin lesion would eventually disappear.

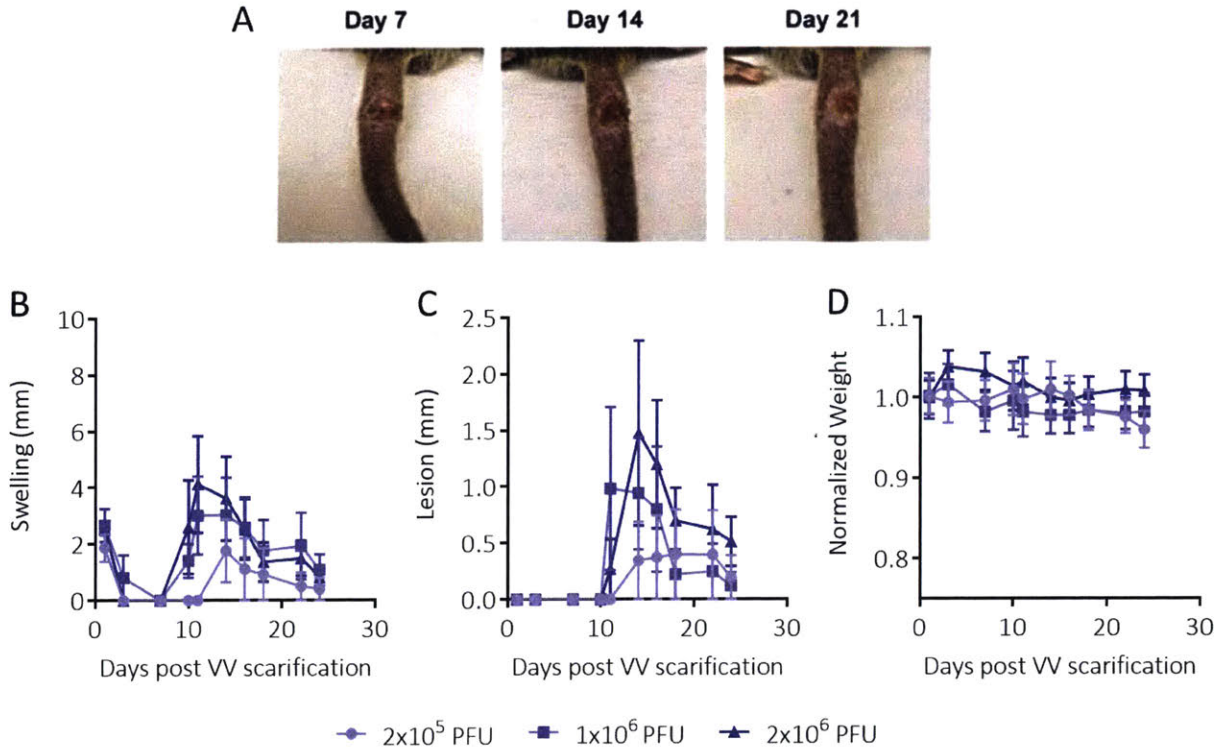

Figure 3-12: Dose titration studies in a vaccinia-SIVgag virus tail-skin scarification infection mouse model. Groups of C57BL/6 mice (n=5/group) were infected via tail-skin scarification with vaccinia-SIVgag virus and monitored. (A) Photographs of skin lesions and swelling region post tail-skin scarification of C57BL6 mice Adapted from [149]. (B) Swelling, (C) lesion size and (D) body weight (normalized to average weight of group on day 0) post tail-skin scarification with $2x10^5$, $1x10^6$ and $2x10^6$ PFU of vaccinia-SIVgag virus.

To this end, we explored three doses of vaccinia-virus expressing SIVgag[150] – $2x10^5$, $1x10^6$ and $2x10^6$ PFU that was used to scarify three groups of 10-12 week old C57BL6 mice. Most mice developed skin lesions and swollen regions around the scarification site, as shown in **Figure 3-12A**. The lesion (broken, exposed skin), the swelling (red, swollen region around the scarification site) and body weight of these mice was measured (**Figure 3-12B-D**). Based on this dose titration study, even though there was no statistical difference between any of the groups, we chose to proceed with the highest viral load ($2x10^6$ PFU) since the animals from this group did not

succumb to the infection and maintained body weight and good health up to 80 days post infection (data not shown).

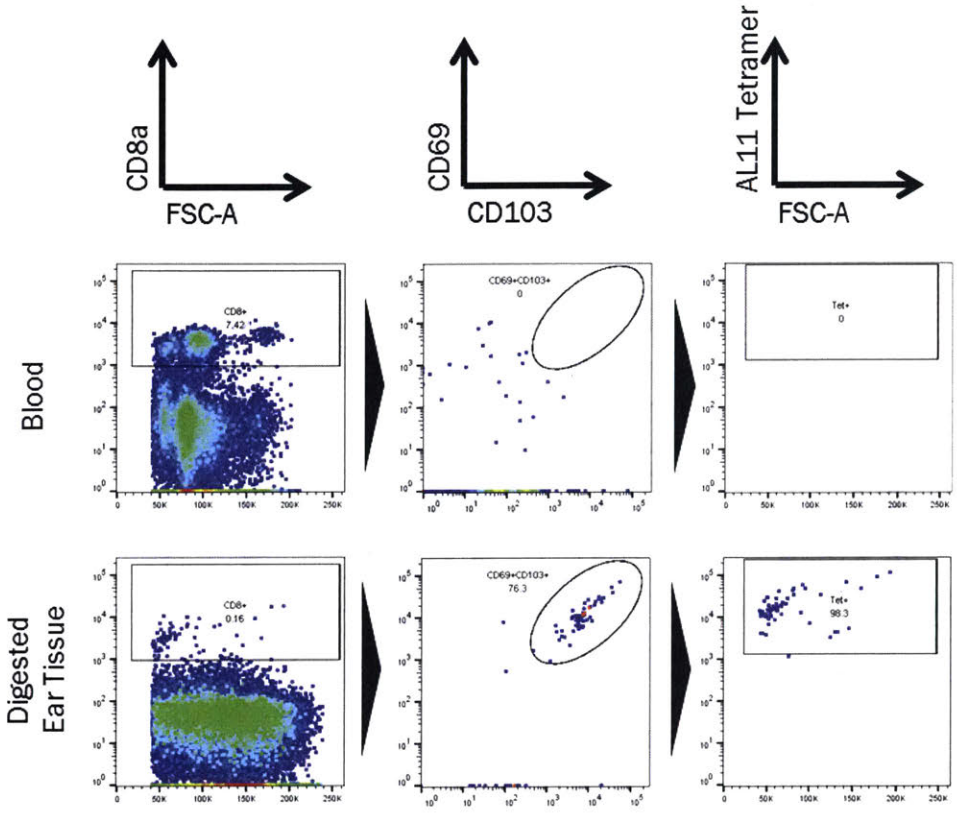

Figure 3-13: T_{RM} characterization in the blood and skin compartments in vaccinia-SIVgag virus tail-skin scarification mouse model. Groups of C57BL6 mice infected with $2x10^6$ PFU of vaccinia-SIVgag virus via tail skin scarification (n=5/group) were bled, euthanzied and ear tissue was resected and digested to confirm presence of antigen-specific T_{RM}s. Flow cytometric plots showing gating strategy for characterizing T_{RM}s in blood and digested ear tissue.

Similar to our efforts for T_{RM} sampling in the OVA-immunized mouse model, in the vaccinia-SIVgag virus tail-skin scarification model we first sought to prove that (i) vaccinia-SIVgag virus specific T_{RM}s existed in the skin that (ii) could be sampled using sampling MNs. We first obtained blood and ear tissue from mice that were infected, 8 weeks prior to euthanization, via tail-skin scarification with $2x10^6$ PFU of vaccinia virus expressing SIVgag and process these compartments by antibody staining for analysis via flow cytometry. As expected, we were able to serially look for markers expressed on T_{RM}s (CD8, CD69 and CD103) and these cells were only

found in digested ear tissue and not in blood (**Figure 3-13**). It was also interesting to note that almost all the T_{RM}s in the digested ear tissue from the infected mice were specific for the SIVgag antigen (tested by their ability to bind to the AL11-MHC tetramer.

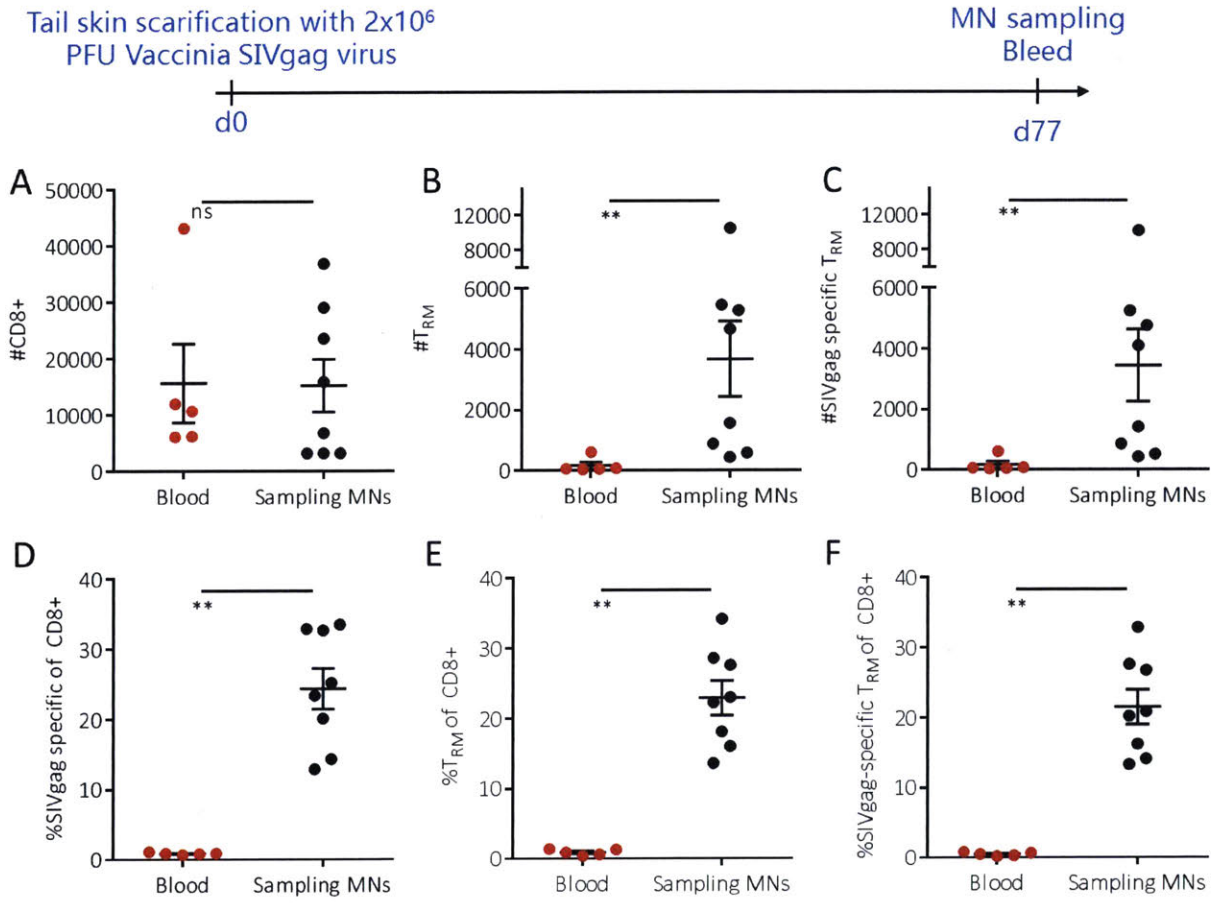

Figure 3-14: T_{RM} sampling in vaccinia-SIVgag tail-skin scarification infection mouse model. Groups of C57BL6 mice infected with $2x10^6$ PFU of vaccinia-SIVgag virus via tail skin scarification (n=5/group) were sampled 11 weeks post infection with sampling MNs containing 2 μg AL11 peptide, and 5 μg each of polyI:C and Pam3Cys, applied to mouse ears for 24 hours, retreived and analyzed via flow ctyometry. (A) CD8+ cells, (B) T_{RM} (CD8+ CD69+ CD103+) cells and (C) SIVgag-specific (SIVgag Tetramer+) T_{RM} sampled from 100μL blood (red circles) and sampling MNs (black circles) (D) SIVgag-specific (SIVgag Tetramer+) cells, (E) T_{RM} and (F) SIVgag-specific (SIVgag Tetramer+) T_{RM}s as a frequency of CD8+ cells. Data sets represent mean ± s.e.m., ns, nonsignificant, **, $p<0.01$, analyzed by one-way ANOVA, followed by Tukey's HSD.

Having proved that the cell phenotype of interest was preferentially found in the skin, we next applied sampling MNs containing our pre-established adjuvant combination (5μg each of

Pam3Cys and polyI:C) along with AL11 peptide as the antigen. The AL11 antigen and Pam3Cys were co-encapsulated within ICMVs, which along with the polyI:C were included in the alginate coating of the sampling MNs. MNs were applied on the ears of C57BL6 mice infected via tail-skin scarification with $2x10^6$ PFU of vaccinia-SIVgag virus 11 weeks post infection. Sample flow cytometric plots are presented in the **Appendix Section 6.9.**

We largely observed the same trends in the vaccinia-SIVgag virus infected mice as we obtained from our studies for T_{RM} sampling in OVA-immunized mice. While the number of CD8+ cells collected from the sampling MNs was not significantly different from that collected from ~100μL of peripheral blood (**Figure 3-14A**), T_{RM}s and SIV-gag specific (AL11 tetramer+) T_{RM}s were only found in sampling MNs which were applied to dorsal skin surface of the mouse ear (**Figure 3-14B-C**). SIVgag-specific cells, T_{RM}s and SIVgag-specific T_{RM}s as a frequency of CD8+ cells (**Figure 3-14D-F**) were numerically almost the equal, indicating that almost all T_{RM}s were, in fact, SIVgag specific T_{RM}s which is consistent with our digested ear tissue phenotyping studies (**Figure 3-13**).

Upon any (re)exposure to antigen, the immune system mounts an immune response which contracts over time[151,152], and thus we see the proportion of tetramer+ (OVA-specific) CD8+ T-cells in blood decay with time following the vaccine boost (**Figure 3-13A**). In the vaccinia-SIVgag virus tail-skin scarification model, we can see that at long times (>10 weeks), post infection, the frequency of SIVgag specific cells is also negligible in the blood (**Figure 3-13B**). This is understandable because the infection model is a much weaker exposure to antigen (due to exposure via scarification of the skin surface) as compared the OVA model (which involves a subcutaneous injection at the tail-base for the mouse, and hence, direct drainage via lymph and exposure to the lymph nodes, resulting in a more robust immune response). The weakness of the infection model via skin-scarification is also comprehensible since the levels of SIVgag-specific cells in the peripheral blood, even two weeks after the immunization were about 1-2%.

3.3.10 Antigen-Specific Cell Recruitment at Long Times

In contrast, as predicted by basic biology studies of T_{RM}s, the tissue-resident population of T-cells primed by the vaccine (and the infection event) remain constant over time, reflecting their stable engraftment into the skin tissue. For both mouse models, sampling MNs were able to

consistently sample for antigen-specific cells at higher levels than that seen in blood. In the OVA-immunized mouse model, while the steady state proportion of CD8+ cells in blood that were OVA-specific was about 15%, in the sampling MNs, this level was at least 40% or more. In the vaccinia-SIVgag virus infection model, though proportion of CD8+ in the blood that were SIVgag specific was near zero, in the skin, as demonstrated by sampling MNs, this proportion was at least about 25%.

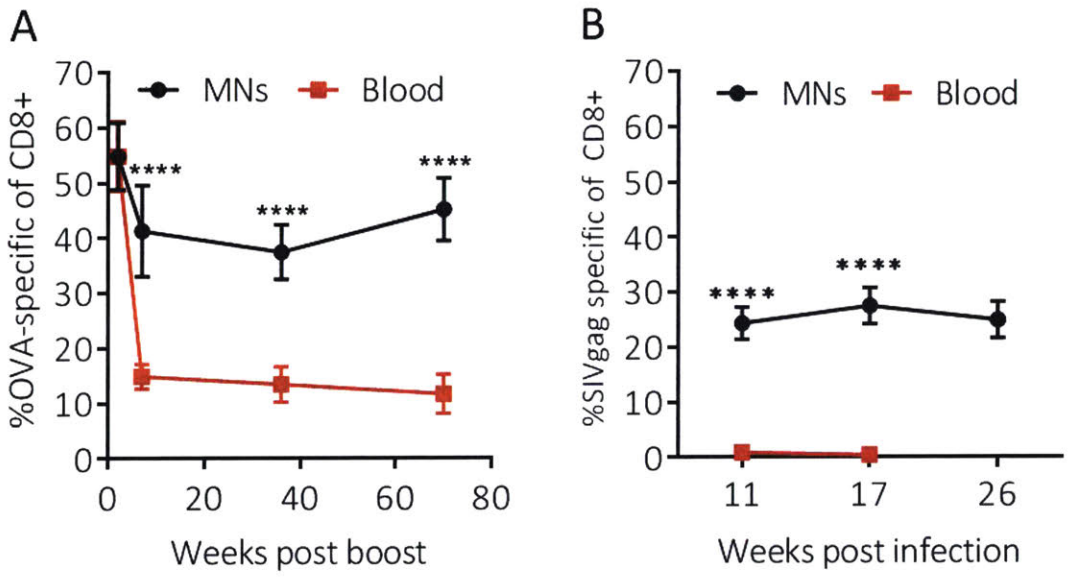

Figure 3-15: Sampling MNs consistently recruit higher proportion of antigen specific cells as compared to peripheral blood draws. Antigen-specific cells as a frequency of CD8+ leukocytes as queried by sampling MNs (black circles) and from peripheral blood (red squares) over long times (A) post immunization in an OVA-immunized mouse model and (B) post infection in a tail-skin scarification with vaccinia-SIVgag virus mouse model. Data sets represent mean ± s.e.m., ****, $p < 0.0001$ analyzed by two-way ANOVA,

These results highlight the ability of cell-sampling MNs to quantify tissue-specific immunity in a manner completely distinct from traditional sampling of peripheral blood.

3.4 Conclusions

In this chapter, we demonstrated the ability of sampling MNs to not only sample for cells and effectively perform a 'micro-biopsy' when applied to skin, but also to provide access to immune cell populations that reside only in the skin and do not circulate in the blood

Building on the sampling MN array preparation method we described in Chapter 2, with the help of a deep-phenotyping method from Love and coworkers at MIT, we were able to confirm our hypothesis that antigen-presenting cells were present in the sampling MNs, making up almost a fifth of the cell infiltrate, and that these APCs internalized the ICMVs that were embedded in the alginate coating of the sampling MNs.

We then established that alginate coated MNs, without any attractants, when applied for 12 hours in a DTH test scenario, in an OVA-immunized mouse model, were able to sample for antigen specific cells, at comparable frequencies to those found in blood. Since chemoattractants (CXCL10 and CCL21) caused irritation, inflammation and scar-tissue formation at the local area of MN application, we included TLR agonists as adjuvants, encapsulated within ICMVs as cell-recruiting factors, embedded in the alginate coating of the sampling MNs. We showed that these ICMV encapsulated adjuvants were more effective at recruiting cells of interest into the sampling MNs, as compared to the soluble form of the adjuvant.

To prove that sampling MNs could indeed query for cell populations preferentially are present only in peripheral tissues like skin and are absent from blood, we utilized two mouse models: (i) a model in which mice were immunized via subcutaneous injections of OVA and (ii) a model in which mice were infected via tail-skin scarification with vaccinia virus expressing SIVgag. In both models, we first proved the existence of T_{RM}s in the digested ear tissue. We then showed that sampling MNs were capable of antigen-specific T_{RM}s, which provide lasting immunity at barrier tissues like skin and also, that consistently, over many weeks and months post immunization/infection, sampling MNs consistently recruited for higher proportions of antigen-specific cells than those present in blood, in both mouse models.

We showed that while 12 hours of continuous application of the sampling MNs showed recruitment of cells, a 24 hour application provided us with 4-5x more cells which allowed for more confident processing and handling of samples, without worrying about losses due to processing of samples. We also titrated the dose of antigen included in the ICMVs and found that included 2μg of antigen gave us the best results in terms of highest numbers of cells recruited. Note that the presence of antigen was required in 'effector-phase' experiments (after 4-6 weeks post boost), in case of a single extended sampling MN application

We also examined whether the process of inclusion of antigen in the sampling MNs caused an immunization event by itself, and learnt that there was no significant change in the frequencies

of antigen specific cells present in the blood before and after the application of sampling MNs on both naïve and OVA-immunized mice.

In conclusion, in this chapter we have shown that sampling MNs can be used to painlessly sample for immune cell populations, specifically the cell populations found in the skin, in a one-step process. The ability to sample for important immune cell populations like T_{RM}s not only enables the design of vaccines in different animal models, but also allows for the possibility of long-term immune monitoring without the need to do end-point studies to look at skin-resident immune cell populations. In a translational context, sampling MNs can be utilized in human patients with diseases of auto-immune background, in which the state and function of skin-resident cells play important roles in the immune status of the patient.

Chapter Four

SAMPLING MICRONEEDLES FOR BIOMARKER EVALUATION

4.1 Introduction

Interstitial fluid (ISF) [153–155] is the clear, colorless solution that bathes and surrounds tissues and organs in the body. It constitutes the environment of the cells and is regulated by homeostasis. Plasma and ISF are very similar[156–158] because water, ions and small solutes are continuously exchanged between plasma and ISF, across the walls of capillaries through pores and clefts in capillary endothelium. ISF, when collected in lymphatic vessels, forms lymph.

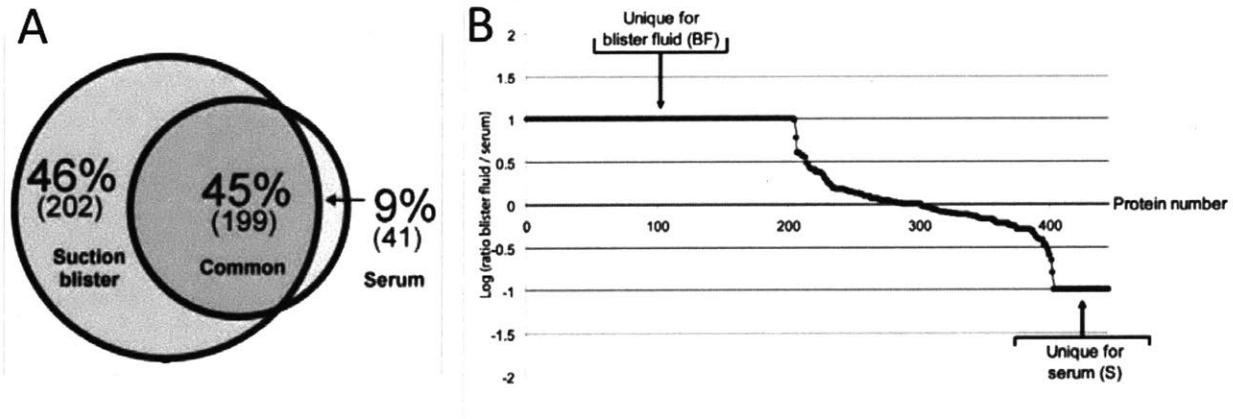

Figure 4-1: Distribution of proteins found in suction blister fluid and serum. (A) Venn-diagram of overlapping proteins found (percentages and numbers) both in suction blister fluid and serum and proteins uniquely found in one of the two matrices. Data obtained from 2-D-HPLC MS/MS. Numbers of proteins detected are given between parenthesis and as a percentage. (Minimal protein ID probability: 99%, number of uniquely detected pep- tides: at least 2,minimal peptide ID probability: 95%.) (B) Logarithm of the ratios between the uniquely detected peptides per protein found in suction blister fluid and serum. Higher ratios than 10 or lower than 0.1 were set at 10 and 0.1, respectively. Adapted from [40].

ISF is of interest to pharmacodynamic and pharmacokinetic studies since concentrations of drugs in ISF often accurately reflect free (unbound and pharmacologically active) concentrations of drugs in plasma. In fact, total (free + bound) plasma concentrations are often less predictive of clinical outcome than tissue concentrations.[159,160] In addition, ISF is also rich in biomarkers — proteins, ions and other analytes which are present, albeit in different concentrations as compared to serum (**Figure 4-1**). Proteomic analysis of ISF[40,161] obtained via the suction blister method shows that it not only contains almost half of the proteins present in serum, but in fact, about 200 proteins exist solely in ISF and cannot be found (or detected by assays currently available) in serum. The interstitium of the tumor microenvironment has also recently been of interest for the same reasons — the ability to quantify unique proteins that may be found only in the vicinity of the tumor in the tumor ISF and shed light upon the workings of immunotherapy methods or the cancer itself.[162–164] For these reasons, there is a strong need in the community to design routes for the facile access to ISF and the rich pool of immunological biomarkers it contains.

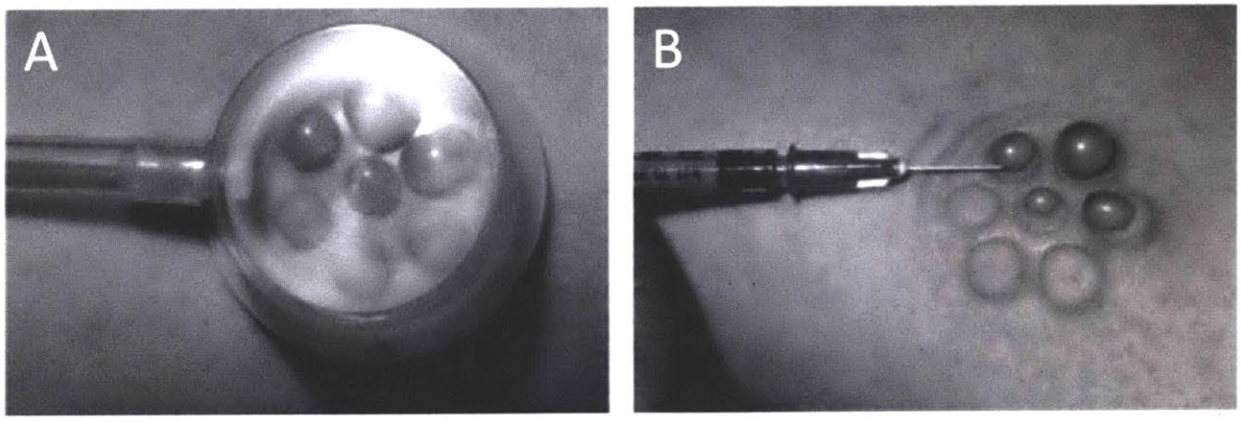

Figure 4-2: Accessing suction blister fluid. (A) Suction chamber during the development of blisters; (B) puncture of blisters and collection of suction blister fluid. Adapted from [40]

However, accessing ISF has always been a challenge. Because the skin is the largest organ and presents maximum surface area for access, dermal ISF is the most acessible form. Methods such as the wick method[155,165], reverse iontophoresis[159,166,167], clinical microdialysis[160], and Lorentz force actuated injectors[168] are invasive, painful, cumbersome to use with bulky apparati, and/or often require the use of trained personnel to extract samples. The suction blister method[40,169] (**Figure 4-2**), which enlists the use of vacuum pump to create a suction chamber for the creation

of blisters, from which ISF is extracted via a syringe, is one of a few minimally invasive methods, and is currently the most prevalent method of extracting ISF.[40,161,169–173]

MNs, since their invention, have predominantly been used to bypass the challenges associated with oral delivery routes and deliver drugs, vaccines, and other bioactive molecules transdermally.[57,107,109] In recent years, MNs have also been used for the purpose of sampling ISF and enumerating its consituents. Swellable hydrogel MNs[64,174] and hollow MNs[76,175,176] have been used to measure analytes such as glucose[62,63,72,166,177–181] and lactate[180,182], to monitor neurochemicals such as choline,[180] acetylcholine[183], glutamate[184], nitric oxide,[185] and biological analytes like antibodies for dengue fever virus NS1.[65–67] While some of these applications leverage polymer based MNs that are designed for sample extraction, others are a product of innovations in the bioMEMS[180,184,186–188] field, in which MNs are fashioned into micro-electrodes which are used to detect analytes based on fluorescence, polarimetry, spectroscopy methods, ultrasound, electromagnetic sensing or reflectance methods.[189]

The sampling MNs used in this work, described in Chapters 2 and 3, are primarlily designed to sample for immune cells, found in the viable dermis of the skin. By virtue of reaching these immune cells, sampling MNs also access dermal ISF, when applied to skin. In this chapter we explore the possibility of sampling for ISF, and hence the biomarkers present in ISF, via application of these sampling MNs to skin. We also show that with a single application, these sampling MNs can monitor both the cellular and humoral components of the immune response.

4.2 Materials and Methods

4.2.1 Materials

PDMS molds (Sylgard 184, Dow Corning) were fabricated by laser ablation using a Clark-MXR, CPA-2010 micromachining system. Poly-L-lactide (Resomer L207S) was purchased from Evonik Industries AG (Essen, Germany). SLM20 (MW 75-150 kDa, > 50% manuronic acid content, apparent viscosity 20-99 mPa·s, < 100 EU/g endotoxin, pH 5.5-8.5) and SLG100 (MW 200-300 kDa, > 60% manuronic acid content, apparent viscosity 100-300 mPa·s, < 100 EU/g endotoxin, pH 5.5-8.5) sterile ultrapure alginates were purchased from Pronova (FMC Biopolymer/Novamatrix, Sandvika, Norway). Calcium chloride dehydrate and sucrose were purchased from Sigma-Aldrich. Chromatographically purified OVA, purchased from Worthington

(Lakewood, NJ), was processed through Detoxi-Gels (Pierce, Rockford, IL) to remove any residual endotoxin. Lipo-CpG was synthesized as described previously.[133,141]

For ELISAs, the following regents were used: 96-well flat bottomed assay plates, NUNC maxisorp (Thermo Fisher), goat α-mouse Igκ (Southern Biotech, #1050-01) unlabeled (UNLB), goat α-mouse Igλ (Southern Biotech, #1060-01) unlabeled (UNLB), goat α-mouse IgG-HRP (Southern Biotech, #1030-05) TMB peroxidase EIA substrate kit (Bio-Rad). Tween 20, bovine serum albumin and 2N H_2SO_4 were purchased from Sigma Alrich.

4.2.2 Animals and Immunizations

All animal experiments were conducted under an IUCAC-approved protocol in accordance with local, state, and NIH animal care and use guidelines. C57BL/6 mice and balb/c mice were purchased from Jackson Labs. Groups of 8-12 week old C57BL6 female mice were immunized using a prime-boost regimen: animals were primed on day 0 and boosted on day 14 with 10 μg OVA and 1.24 nmol lipo-CpG suspended in PBS, via injections administered subcutaneously at the base of the tail.

4.2.3 ISF Sample Collection from Sampling MNs

Sampling MNs were prepared as described in Chapter 3, Briefly, poly-L-lactide was melt molded into PDMS molds. MN surface was coated with poly-L-lysine and with solution containing alginate and sucrose, dried under vacuum at room temperature. Calcium chloride solution was pipetted onto these MNs and MNs dried under vacuum. MNs were stored under vacuum until further use. No additional chemoattractants and adjuvants were included in the coating of the MNs for the purpose of sampling ISF.

Sampling MNs were applied to the dorsal surface of the C57BL6 mouse ears for times ranging from 5 minutes to 24 hours, as indicated in text, and secured using a combination of waterproof tapes. MNs were retrieved from anesthetized mice and a cell suspension was retrieved via immersion in 200μL of PBS containing 1% BSA and 100mM EDTA for 30 minutes at 37°C while shaking at 150rpm and pelleting via centrifugation. Supernatant was stored for -20°C until further quantification. .

4.2.4 ISF Volume Determination

Ears of 8-12 week old balb/c mice were resected from euthanized mice, weighed and placed on double-sided adhesive tape, affixed onto glass slides. Pre-weighed blank or alginate coated

MNs were immediately applied to these dissected ears and secured with paper-based lab tape. These were placed in a covered petri-dish containing a reservoir of water (to create an environment saturated with water vapor) for 5–30 minutes. After removal of the MN arrays, the weight of the MNs and the ears were noted, to calculate the change in weight pre- and post- MN application.

4.2.5 Total IgG and OVA-specific IgG Titer ELISA

Serum total IgG titers were measured using ELISA. Capture antibody was adsorbed on to flat-bottom transparent 96-well Nunc Maxisorp plates (ThermoFisher) by adding anti-mouse Igκ and anti-mouse Igλ, diluted in PBS to each well at room temperature overnight. Plates were washed with 0.05% Tween 20 in PBS, incubated for 1 hour with PBS containing 1% w/v bovine serum albumin for blocking and washed again. Serially diluted serum and ISF samples (starting from a minimum dilution of 300x and 200x, respectively) were then added and incubated at room temperature for an hour. Following another washing step, the plates were incubated for one hour with anti-mouse IgG-HRP, washed, developed with TMB substrate, and read on a Tecan Infinite M200 Pro (Männedorf, Switzerland) optical absorbance plate reader at 450 nm. Antibody titer is reported as reciprocal serum dilution at an absorbance of 0.3.

Serum ova-specific IgG titers were determined as previously described.[136] Briefly, 96-well plates were coated with OVA and blocked with bovine serum albumin, then incubated with serially diluted serum and ISF samples and detected with HRP-labeled anti-mouse IgG, followed by development and measurement of optical absorbance.

Detailed protocols are provided in the Appendix.

4.3 Results and Discussion

4.3.1 ISF Collection via Sampling MNs

Upon application of sampling MNs to skin, in addition to the cells that are recruited into the alginate matrix of the MNs, ISF from surrounding tissue also infiltrates the alginate matrix, carrying with it biomarkers, cytokines and other cell products. We first quantified the amount of ISF collected in the sampling MNs and then, as a preliminary test of sampling ISF from our gel-coated MNs, an ELISA was used to detect IgG antibodies present in collected ISF and compared with serum antibody titers.

MNs with and without alginate coatings were applied to dissected mouse ears from balb/c mice kept in humid conditions. Control mouse ears, which were not penetrated with MNs, and the MNs themselves, did not show any change in weight (data not shown). Change in weight of mouse ears on which 'blank MNs' (MNs without alginate coating) was about 0.4mg (white, **Figure 4-3A**), promoted by the loss of water from the epidermis.[102,190,191] Ears that were applied with alginate-coated MNs for 5 minutes and 30 minutes lost 1 mg and 2 mg in weight, respectively (blue, **Figure 4-3A**). Notably, this was more than the weight lost from the ears penetrated with uncoated MNs. We hypothesized that this was due to the uptake of ISF by the alginate coating of the MNs. When we measured the weight these MNs, they showed an average increase (orange, **Figure 4-3A**) of 1 mg in weight. Considering the density of to be the same as water (1 g/mL), we concluded that about 1 μL of ISF could be collected from mouse ears upon application of these sampling MNs (comprised of 77 individual MNs arrayed in a 1 cm^2 area).

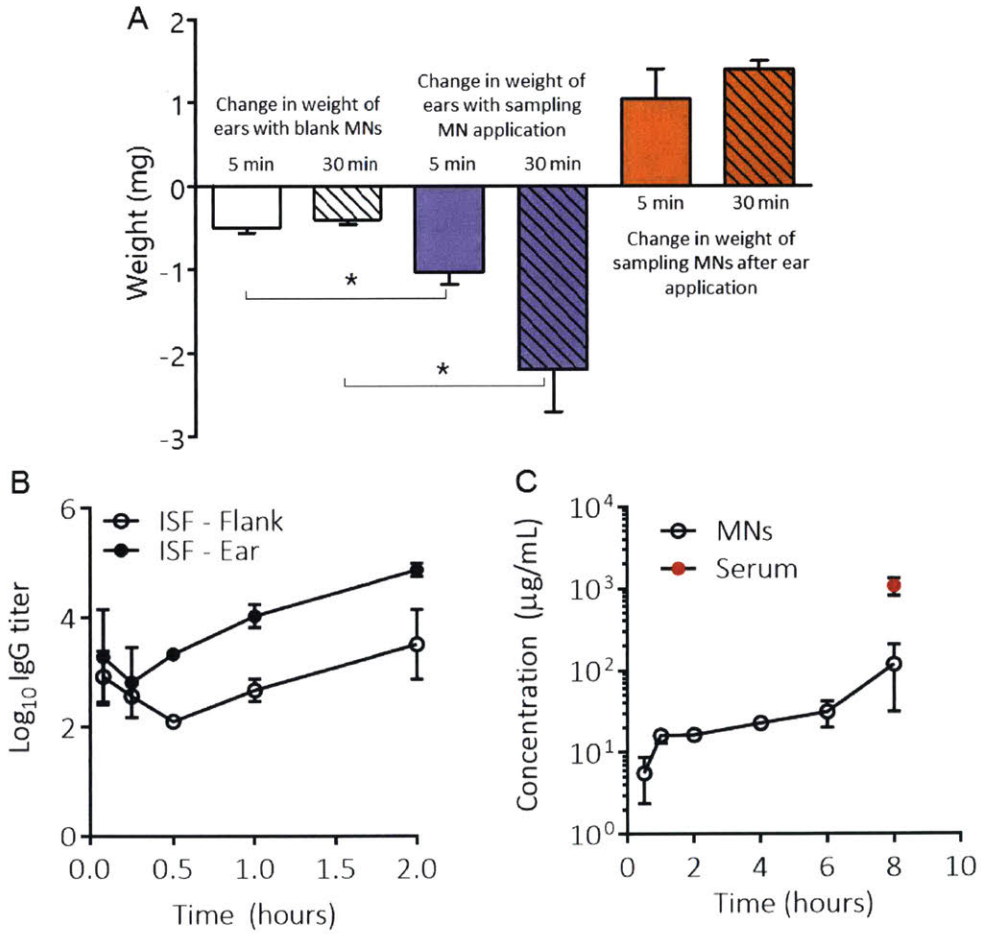

Figure 4-3: Quantification of ISF. (A) Quantification of collection of ISF by comparison of weights of dissected ears (blank and blue bars) and alginate layer weight (orange bar). MNs were applied to the ear tissues for 5 mins or 30 mins (solid and diagonally hatched bars respectively). (B) Quantification of total IgG titer measured by ELISA obtained from digested sampling MNs used to collect ISF from mouse ears and flanks. (C) Concentration of total IgG protein in ISF obtained from mouse flanks and from serum. *$p < 0.05$, analyzed by one-way ANOVA, followed by Tukey's HSD for multiple comparisons.

The next step was to quantify a possible biomarker from ISF and compare results to serum—the standard fluid for analysis. We chose immunoglobulin G (IgG) which is one of the most abundant proteins in serum.[192] It represents approximately 75% of serum antibodies in humans and is the most common antibody in circulation.[193] Alginate-coated MN arrays were applied to the flank skin of naive balb/c mice for varying amounts of time, then the MN patches were removed, the alginate layer was digested using EDTA, and the supernatant was analyzed by ELISA for total serum IgG. Sampling MNs applied for less than 30 minutes gave variable results so for future studies, for ISF collection, we applied sampling MNs for at least 30 minutes (**Figure 4-3B**). After 30 minutes, the total IgG titer from ISF obtained from the ear was observed to be about one order of magnitude higher than that obtained from flanks. This can be attributed to the high density of capillaries and perfusion in the ear, as compared to other areas of skin on the body of the mouse, such as the flank. We also observed that, overall, as we increased the time of application of the MNs, the amount of IgG collected via ISF increased with time (**Figure 4-3C**).

Based on these results, we concluded that sampling MNs could sample approximately 1 μL of ISF, per MN array and that sampling MNs applied for at least 30 minutes provided reliable samples for quantification.

4.3.2 Quantification of Antigen-Specific IgG

To explore the applicability of MNs to quantify not just the cellular immune response, but also humoral immunity, we compared OVA-specific IgG titers measured by ELISA for fluid recovered from MN patches, and compared to the same analysis on a traditional serum sample.

Sampling MNs were applied to the ears of mice immunized with OVA and lipo-CpG for 24 hours. Upon retrieval, MNs were immersed in a solution containing EDTA to chelate out the calcium from the alginate layer, freeing entrapped cells for downstream analysis. This solution was centrifuged to collect the cell pellet and the resulting supernatant was analysed via ELISA for OVA-specific IgG titers. Titers from ISF were ~10-fold lower than measured in serum, consistent

with estimates of the dilution of serum antibodies from blood to tissues[194]. However, the measurement from ISF, like serum, has a very high signal-to-noise ratio (comparing to the controls of serum and ISF obtained via sampling MNs, from naïve mice).

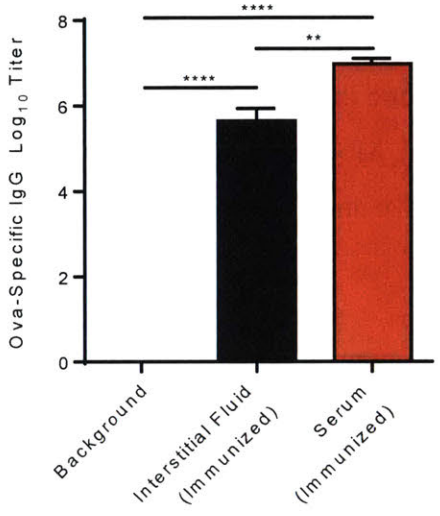

Figure 4-4: Quantification of OVA-specific IgG obtained from ISF via sampling MNs. Ova-specific IgG can be quantified from ISF collected from sampling MNs, applied for 24 hours on ear skin of C57BL6 mice immunized with ovalbumin. **$p < 0.01$, ****, $p < 0.0001$, analyzed by one-way ANOVA, followed by Tukey's HSD for multiple comparisons.

These experiments suggested that, going forward, ISF is a promising body-fluid compartment that, since it can be accessed painlessly with minimally invasive MN application, can be used for long-term monitoring of diseases, especially incurable chronic auto-immune diseases like lupus, ulcerative colitis, etc.

4.4 Conclusions

In this chapter, we explored the ability of using sampling MNs to quantify meaningful biomarkers from dermal ISF. We quantified that the amount of ISF that could be collected on sampling MNs, per MN array was about 1 μL, in between 5-30 minutes of application, based on the swelling of the dried alginate layer on the MN surface. We showed that it was possible to quantify proteins and biomarkers from dermal ISF collected via sampling MNs by assaying for total IgG in naïve mice and OVA-specific IgG in OVA-immunized mice. The lack of false

positives and false negatives encourages the exploration of this body fluid compartment for quantification and detection of other proteins. Though these proteins may be present in differing or lower concentrations than blood, they can be quantified based on a standard curve made specifically for dermal ISF samples.

Sampling MNs also provide a way to quantify both the cellular and the humoral response, since the cell suspension obtained can be analyzed via flow cytometry or other phenotyping methods for the cellular response and the supernatant can be analyzed for biomarkers. This proves the universality of the sampling MNs as a sampling device to access cell and biomarker populations, in a minimally invasive and painless manner.

Chapter Five

CONCLUSIONS AND FUTURE DIRECTIONS

5.1 Summary of Key Results in this Thesis

This thesis has focused on the development of a novel sampling and diagnostic platform to enable the collection of skin-resident, non-recirculating cell populations and dermal ISF, in a minimally invasive and painless manner. These compartments are currently either accessible only via invasive methods such as biopsies in human or larger animal models and necropsies in smaller animal models, or via DTH tests which are qualitative and do not provide a phenotypic, quantitative, or functional readout. To address these issues, we developed a MN-based device, containing a matrix capable of retaining sampled cells and ISF, upon the application of the device to the skin. This goal was accomplished by coating a dried hydrogel (containing immunostimulatory agents to signal for the recruitment of cells from the vicinity of the region of device application) on the surface of MNs that swells to retain dermal ISF. The primary findings of each chapter are summarized below.

In Chapter 2, we first explored the possibility of fabricating porous MNs, which was unsuccessful because of their compromised mechanical integrity and inconsistent penetration of murine ear skin. We then discussed the specifics of the hydrogel-coated sampling MN platform. Based on atomic force microscopy and subcutaneously injected alginate gel-based studies, we optimized for the molecular weight, density and composition of the alginate and sucrose based hydrogel coating. We explored the use of two pro-inflammatory chemoattractants – CCL21 and CXCL10 – in the subcutaneously injected gels, as well as inside the gels on the MN surface, while studying the effect of dosing of the chemoattractants and duration of sampling on the number and phenotype of cells recruited into the gels or in the MN coatings. We ensured that the hydrogel-coated MNs satisfied our intended design goals of: (i) mechanical integrity and robustness, (ii) reproducible fabrication, (iii) effective skin penetration, (iv) a compartment within platform to contain cell-recruiting signals, (v) a fabrication process amenable to the inclusion of bio-active

molecules, and, (vi) a compartment within the sampling platform for cells and ISF to be collected, and retained upon collection.

In Chapter 3, we demonstrated the ability of sampling MNs to not only sample for cells and effectively perform a 'micro-biopsy' when applied to skin, but also provide access to resident memory T cells (T_{RM}s). We established that alginate coated MNs, without any attractants, when applied for 12 hours in a DTH test scenario, in an OVA-immunized mouse model, were able to sample for antigen specific cells at comparable frequencies to those found in blood. Since chemoattractants (CXCL10 and CCL21) were observed to cause irritation, inflammation and scar-tissue formation at the local area of MN application, we included TLR agonists as adjuvants, encapsulated within ICMVs as cell-recruiting factors, embedded in the alginate coating of the sampling MNs. We showed that these ICMV encapsulated adjuvants were more effective at recruiting cells of interest into the sampling MNs, as compared to the soluble form of the adjuvant. We utilized two mouse models: (i) a model in which mice were immunized via subcutaneous injections of OVA and (ii) a model in which mice were infected via tail-skin scarification with vaccinia virus expressing SIVgag. We showed that sampling MNs, when applied for 24 hours, were capable of sampling for antigen-specific T_{RM}s, and that over many weeks and months post immunization/infection, sampling MNs consistently recruited for higher proportions of antigen-specific cells than those present in blood, in both mouse models. We also showed that the presence of antigen in the sampling device is necessary for the collection of antigen-specific cells and the process of sampling with sampling MNs does not alter the immune status of the animal.

In Chapter 4, we considered the possibility of quantifying biomarkers sampled from the dermal ISF collected in the sampling MNs. We calculated that each MN array, when applied to murine ear for 5-30 minutes, retained about 1 μL of dermal ISF. We were able to reliably detect and quantify immunoglobulin G (IgG), one of the most abundant proteins in serum and ISF, from ISF sampled from MNs. We also demonstrated the ability to detect OVA-specific IgG in mice immunized with OVA, with a good signal to noise ratio and a lack of false positives and false negatives.

In summary, sampling MNs are a universal sample collection platform capable of performing a 'micro-biopsy' in a minimially-invasive and painless manner. Furthermore, they can collect skin-resident, non-recirculating cells as well as biomarkers present in dermal ISF. Consequently, these sampling MNs provide a way to quantify both the cellular and humoral

components of the immune response, especially in a long-term immune monitoring context, without the need for invasive biopsies (in humans and larger animal models) or end-point based studies (in smaller animal models).

5.2 Future Directions

The sampling MNs platform developed in this thesis constitute a generic platform for accessing tissue and fluid compartments that have been previously been accessible only in an invasive fashion. In this Section we discuss possible future directions for this work in both the diagnostic capacity of these MNs as well as their sample collection capacity.

In this thesis, sampling MNs were considered only as a sample collection device, with collected tissue and fluid compartments analyzed downstream via various phenotyping and quantification methods. However, it is also possible to adapt these sampling MNs into a diagnostic platform – including a coupled colorimetric test (similar to a pH indicator) to indicate the presence or absence of an analyte of interest. MNs in a similar vein have been developed by Kendall and co-workers[65–67,195] to facilitate circulating biomarker detection via an on-MN-array ELISA-based assay. Coupling a colorimetric agent, either on the surface of the sampling MNs themselves, or as a solution into which the MN array can be immersed after removal from skin, can have potential utility as quick diagnostic assays for use in the field, where expensive equipment and expertise may not be available. Such analyte-detection based diagnostic tests, predominantly in the form of lateral flow assays[196], are typically immunoassays that require short incubation times after sample is added to the test strip. The sample is generally blood, urine or saliva.[32,197] However, as we discussed in Chapter 4, there are many proteins present in the ISF milieu, which are unique and not detectable in blood[40,198]. For such biomarkers, specifically in diseases that present with dermatological complications, being able to access dermal ISF, especially for biomarkers that enable the monitoring of the disease, would be potentially very valuable to the management of the disease itself.

For example, in the case of systemic lupus erythematosus (known as SLE, or lupus), patients experience sudden onsets of heightened states of the disease, known as flares, which are managed by the regulation of their drug regimens. Being able to prophylactically predict the onset of these flares can enable these patients to have a better quality of life, by possibly delaying,

suppressing, or even avoiding the onset of the flare. While there has been preliminary work[51] to find biomarkers that predict the onset of these flares, all of these works have been confined to the analysis of blood. Phlebotomy is not only painful and invasive, it requires trained personnel to perform blood draws and it is resource and time intensive, both from the hospital side as well as the patient side. It would be beneficial to evaluate the utility of sampling MNs for the detection of flare-prediction related biomarkers via dermal ISF. However, it should be noted, that since the ISF extracted is about 1 μL per MN array, (~1 cm^2 surface area, containing 77 MNs), using conventional assays may pose limit-of-detection related challenges. Note, that for humans, increasing the size of the MN array can also enable the collection of higher volumes of ISF and larger numbers of cells. However, this will probably be limited to an increase of one, or at most, two orders of magnitude. This is because while going up to 10 cm^2 in surface area for the sampling patch may be feasible, 100 cm^2 of skin area, for humans, would be difficult to sample for in an efficient manner (due to issues with tight adherence of the MNs to the skin surface due to curvature of the skin around limbs, etc.)

It may also be possible to study the microenvironment of tumors[163,164] or dermatological diseases, particularly those that present with findings near the skin or dermis. Examples include atopic and contact dermatitis, cutaneous T cell lymphoma, psoriasis etc.

For the specific process of vaccine design,[199,200] currently the assessment of vaccine candidates in small animal models is done on the basis of either antibody based titers from peripheral blood (as a continuing measurement) or from whole organ digestion studies (as an end-point measurement). Since the formation of antigen-specific T_{RM}s, resident in tissues that form the first line of defense, constitutes the final check point for a vaccination regimen, the ability to sample for these cells and monitor the immune status in peripheral tissues *in situ* could provide a way to perform long-term studies to assess the efficacy of a vaccine candidate without the need to sacrifice animals at different time points.

In this thesis, we have not characterized the phenotypical change in MN infiltrate composition when MNs are applied for varying amounts of time on the skin surface. We expect that, similar to an immune response during a DTH test, APCs should be the first and the most abundant cell type on site, followed by T cells, which should peak around the 48-hour mark. The composition of the infiltrate will also differ depending on the immune status of the animal or human. For example, sampling MNs applied to lupus-inflicted mice might have differing

composition of cell infiltrate collected via sampling MNs depending on whether the mice are undergoing a state of flare or not. Pre-, during- and post- flare scenarios may indicate different states of disease specific cell populations – upregulation, activation, proliferation, homing, etc. These insights may potentially inform the treatment and management of these disease conditions.

Finally, in this thesis, we have worked with applying sampling MNs to murine ears and dorsal flank tissue. In theory, as long as the MN surface can remain in close contact with the tissue being sampled, the sampling mechanism should work. Thus, the smaller the surface area, the easier it is maintain the close contact. Since MNs offer a unique ability to access tissue compartments that are difficult to biopsy, in addition to skin, sampling MNs may also find use in sampling other peripheral tissue, such as mucosal linings.

APPENDIX

6.1 Protocol for Fabrication of Sampling Microneedles

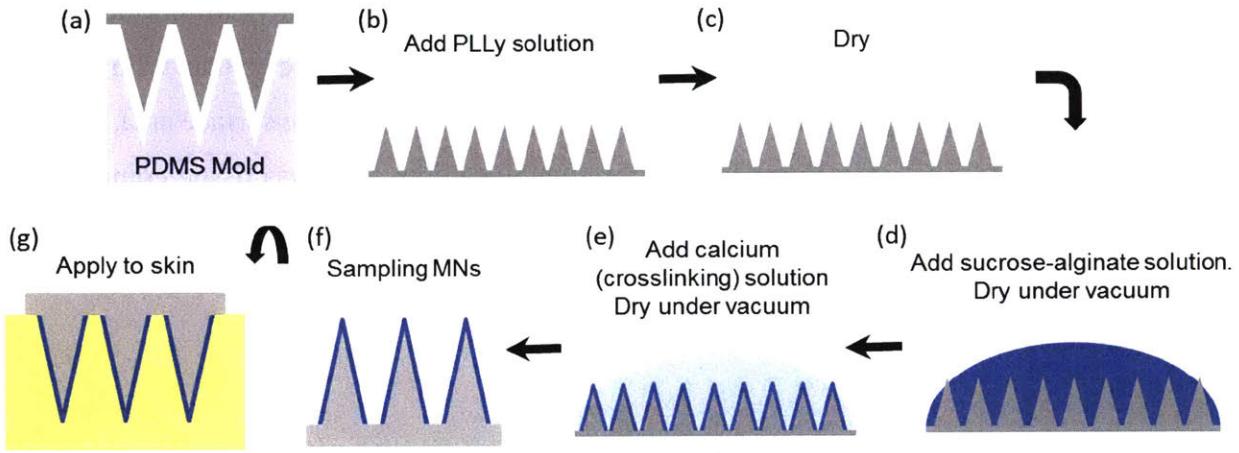

Figure 6-1: Schematic of method of fabrication of sampling (alginate coated) MNs. (a) MNs are fabricated by melt-molding poly-L-Lactide into PDMS molds (b) PLLy is added for 30 minutes, removed and (c) dried. (d) Sucrose-alginate solution is added and dri ried under vacuum. (f) Resulting sampling MNs are stored under vacuum before (g) aplication to skin.

Poly-L-lactide (PLLA) MNs were melt-molded into PDMS #4 molds (square cross section, pyramidal, ~600μm height and 250μm base) by adding 150mg of PLLA (Resomer L-207S) to the PDMS molds, incubating at 150°C for 30 minutes under vacuum (-25mm Hg) and then melting at 200°C for one hour until melted and free of internal bubbles. Molds were kept at -20°C for at least 30 minutes, prior to careful demolding.

To coat the MNs with alginate:

(i) MNs were exposed to poly-L-lysine (PLLy, Sigma P4832) by pipetting 100μL of PLLy solution on each MN array and incubating at room temperature for 30 minutes. PLLy solution was removed and MNs were allowed to dry at room temperature for 2 hours.

(ii) The 'Alginate Layer' was fabricated by pipetting 60μL of sucrose-alginate solution (35μL SLG100 from Pronova 0.01g/L dissolved in milliQ water + 25μL of 5.625% sucrose from Sigma dissolved in milliQ water) onto each MN array and drying the array under vacuum (-25mm Hg) for >2 hours at room temperature. To include 'cargo' in the alginate layer, co-dissolve the cargo with sucrose-alginate mix and make sure volume does not exceed 75μL.

(iii) The 'Crosslinking Layer' was fabricated by adding 20μL of 0.5 wt% CaCl2 in milliQ water, made up to 50μL (for ease of pipetting and covering entire MN array with solution) with milliQ water on top of MN array with dried alginate. To include 'cargo' in the crosslinking layer, co-dissolve the cargo with 20μL of 0.5 wt% calcium and dilute with milliQ water up to 50μL.

6.2 Protocol for ICMV Synthesis

Description: Synthesis of INT-ICMVs multilamellar ("stapled") liposomes containing antigen (OVA or AL11)

Materials: DOPC (Avantilipids #850375), MPB (Avantilipids #870012), PEG-thiol lipid (http://laysanbio.com/ Item# MPEG-SH-2000), OVA protein, PAM3CSK4 (tlrl-pms, Invitrogen), AL11 peptide (AAVKNWMTQTL, GenScript), DTT (Sigma), $CaCl_2$ (Sigma), bis-tris-propane (Sigma), Ultrasonicator (Misonix)

Typical dose: Each batch yields 10 doses, to be encapsulated into the crosslinking layer of sampling MNs

PROCEDURE

Preparation

1. Add appropriate volumes DOPC, MPB, to glass scintillation vial
    a. Keep moles fixed at 1.26 μmoles of lipid when varying composition (1.26 umoles with this recipe)
2. Basic composition: 50% DOPC (95 uL of 5.29 mg/ml) and 50% MPB (65uL of 10 mg/ml)
3. When storing the lipids, purge lipids required for formulation under nitrogen stream for 30 seconds
4. Dry lipids overnight (2 hour minimum) in 7 ml glass scintillation vial.

Liposome preparation

5. Prepare 10X bis-tris-propane (200 mM in H2O, adjust pH to 7.0 w/ HCl). Sterilize filter.
6. For each sample, prepare 200 uL of solution.
    a. For blank ICMVs, use 200uL BTP solution at WC.
    b. For pam ICMVs, use 50uL of pam solution at 1mg/mL and 150uL of BTP solution at WC.
    c. For pam-ova ICMVs, use 4ul of ova stock solution at 5mg/mL, 50uL of pam solution at 1mg/mL and 146uL of BTP solution at WC
    d. For AL11 ICMVs, use 6.2uL of AL11 peptide stock solution at 3.25mg/mL, 50uL of pam solution at 1mg/mL and 143.8uL of BTP solution at WC.
7. Add 200 μL of the above solutions to the dried lipid film (containing 1.26 μmoles of lipid) and vortex for 1 minute, stopping every 10 seconds, every 10 minutes for 1 hour (solution will be cloudy).
8. Sonicate each sample in an eppendorf tube on ice for 5 minutes, alternating between a duty setting of "4" and "1" every 30 seconds to prevent excessive sample heating (solution will be clear)

Fusing and cross-linking of liposomes (i.e., "stapling")

9. Prepare stock solutions of 200 mM CaCl2 and 150 mM DTT (freeze aliquots in H2O, make fresh is ideal). Final [working] are 40 mM CaCl2 and 3 mM DTT

10. To each sample (200 µL) add 40 µL CaCl2 and mix). Solution should become immediately cloudy upon addition of CaCl2.
11. Add 4 µL DTT and mix. These amounts yield a 1:1 ratio of maleimide to DTT (i.e., with maleimide:thiol = 1:2).
12. Incubate 1 hr at 37 °C (max 2-3 hrs).
13. Centrifuge and wash at 18000g for 4 minutes.
14. Resuspend in 200µL H2O, and perform one additional wash (pellet will completely resuspend by end of wash steps).
15. Add 100 uL 20 mg/ml PEG-thiol in H2O (2 mgs) (make fresh).
16. Incubate for 30 minutes at 37 °C.
17. Wash twice with H2O as in steps 6 and 7.
18. Resuspend in 100uL MQ water. (10 doses of 10uL each).

For quantification

1. Dilute 10 uL of solution from step 18 to 100 uL using H2O (10x dilution) into a 96 well flat-bottom plate.
2. Read the encapsulated protein amount using an ELISA for ova.

Alternatively, make ICMVs with fluorescent ova (OVA, Alexa-Fluor 555 Conjugate from Thermo Fisher Scientific) and quantify by making a calibration curve.

6.3 Protocol for Sampling Microneedle Application and Processing

6.3.1 MN Application onto Ear

19. Sampling MNs, after fabrication, are stored under vacuum until application to mouse ear (or dorsal flank).
20. For MN application to ear, anesthetize C57BL/6 mice using insofluorane (~ 3% for 5 mins and 1.5-2% for up to 10 minutes after) in the cage. Move the mice to nose-cone for MN application purposes.
21. Cut out ~ 1 inch x ½ inch pieces of 3M® Nexcare Absolute Waterproof tape and ~ 1.5 inch x ¾ inch pieces of standard electrical tape. The Nexcare tape, designed for sensitive skin, is the only tape that will be in contact with the mouse skin. The electrical tape has two purposes:
    a. Strong adhesive that cannot be easily interfered with by the mice,
    b. Waterproofing nature that prevents any water from getting into the MN array applied region.
22. Spread the ear of the mouse flat onto the Nexcare tape which is laid, sticky side up, on a 'slide stack' (10-12 microscope slides taped together, to allow the ear to rest on the stack). Using tweezers, ensure that the ear is flat (no folds of skin should be present as this causes non-uniform application of the MN array).
23. Brush away any hair from the base of the ear/base of the head of the mouse away from the ear.

24. Place the MN array (needles pointing down) onto the ear skin. Press down with thumb of one hand, applying only vertically downward pressure (else MNs can break) while using tweezers with other hand to tightly secure Nexcare tape around applied MN array. Press MN array again to secure application.
25. Using tweezers, lift Nexcare and MN array bound mouse ear and now place inside piece of electrical tape. Proceed to envelope and tightly press and seal joints and corners (use tweezers to create a tighter seal) so that Nexcare tape and MN array is completely covered by electrical tape.
26. Make sure no whiskers of the mouse are caught inside the tape while taping as this causes discomfort to the mouse upon awakening.
27. Press the MN array onto the ear again from the outside to ensure a tight application.
28. Leave MN on mice for up to 24 hours.

6.3.2 MN application onto Dorsal Flank

1. At least 12-18 hours before application, shave the region using clippers and remove hair by using hair removal product like Nair. Anesthetize the mice as above in cage. Shave dorsal flank area with clippers (MNs will be applied roughly directly opposite to the 3rd and 4th nipples on the ventral side) from base of neck to tail base, and till base of each limb.
2. Cut out ~ 1 inch x 2 inch pieces of 3M® Absolute Waterproof Nexcare tape, ~ 4 inch x ¾ inch pieces of electrical tape and ~ ½ inch x 1 inch pieces of Scotch® Permanent Heavy Duty Mounting Tape (double sided foam tape).
3. Transfer mouse onto nose cone and lay on side. Stick the Scotch® double sided foam tape onto the slide stack and line the slide stack the body of the mouse. Pinch skin on the back of the mouse and stick the shaved dorsal skin onto the double sided tape.
4. Place MNs face/needles down as above. Holding Necxcare tape, press MNs onto the dorsal skin, roll off the double sided tape and press the Nexcare onto the body of the mouse to firmly adhere to shaved skin.
5. Apply electrical tape, around the abdomen of the mouse to keep MNs in place and ensure no water can get into the MN applied region.
    a. Make cuts on the electrical tape for the limbs of the mice, especially legs, to ensure the movement of the mouse is not restricted.
    b. Do not bandage electrical tape too tightly, but just tight enough to ensure waterproofing.
    c. Ensure no Nexcare tape is visible from the outside.
6. Leave MN on mice for up to 24 hours.

6.3.3 MN Retrieval and Extraction of Cell & ISF Sample

1. To remove the MN array, anesthetize mice as above. Transfer to nose cone.
2. Use tweezers to remove electrical tape and Nexcare tape.
3. Ensure MNs do not break in the process of removal.

4. Immerse in 200 µL of PBS containing 1% BSA with 100mM of K_2EDTA, on ice, in 48 well plate.
5. Shake at 150 rpm on bench top mini incubating shaker at 37°C for 30 minutes.
6. Retrieve MN array from wells and keep aside. Transfer cell suspension to 96 well plate. Using 50 µL of 1% BSA in PBS, pipette up and down on the MN array surface to retrieve loosely adhered cells and add to relevant well in 96 well plate.
7. Spin down in centrifuge (1500rpm or 700g, 5 mins) and collect cell pellet.
8. Store supernatant at < -20°C to quantify biomarkers using other assays.

6.4 Tail-skin Scarification using Vaccinia-SIVgag virus

1. In a biosafety cabinet, disinfect area and all relevant instruments (pipette, tweezers, etc) with bleach wipes and 70% ethanol before starting
2. Anesthetize mouse and transfer to nose cone
3. Clean area to be scarified, tail skin area about 1cm from the base of the tail, with 70% ethanol in water.
4. Take 5µL of diluted virus with pipette and apply to cleaned tail skin area. Scratch 25 times with 27 1/2 G needle. Discard pipette tip in a beaker filled with bleach.
5. Leave mouse on nose cone for five minutes, making sure scarified area does not touch other surfaces.
6. Take Kimwipe and dab scarified surface to clean excess viral solution to avoid contamination on cage and other surfaces.
7. After scarifying all animals, clean and disinfect area with bleach wipes and discard all bio-waste in biohazard bin. After letting beaker with bleach with discarded pipette tips stand for 10-15 minutes, discard solution in the sink.

6.5 Staining for Flow Cytometry

1. After obtaining cell pellet as above, re-suspend in 50 µL of FACS buffer containing FcBlock (Purified anti-mouse CD16/32 Antibody, from eBioscience, 14-0161-86) at 1:100 dilution.
    a. For tetramer staining include either ova tetramer (iTAg Tetramer/PE - H-2 Kb OVA (SIINFEKL), from MBL) at 1:100 dilution or SIVgag tetramer (iTAg Tetramer/PE - H-2 Db SIV GAG (AAVKNWMTQTL)) at 1µg per sample). Incubate for 15 minutes in the dark, at room temperature.
    b. For tetramer staining, use tetramer stain FACS buffer (50nM dasatinib, 1mM EDTA in 1%BSA in PBS).
2. Add rest of the antibodies and incubate at 4°C for 1 hour.
    a. Anti-mouse antibodies were obtained from BioLegend or eBioscience. The following is a list of antibodies that were used for experiments:
        i. Anti-mouse CD3e PerCP, BioLegend, cat#100326
        ii. Anti-mouse CD8a APCCy7, BioLegend, cat#100714
        iii. Anti-mouse CD103 BV421, BioLegend, cat#121421
        iv. Anti-mouse CD11b BV650, BioLegend, cat#101239

v. Anti-mouse CD69 PECy5, eBioscience, 15-0691-82

b. This is especially required for ear tissue samples – whether they are from digested ear tissue or from sampling MNs.

c. For blood or spleen samples, staining for 15-20 minutes at room temperature or at 37°C will suffice.

3. For CFSE staining:
   a. Add 50μL DMSO to each vial of Cell Trace CFSE to create 1.8mM of stock solution. Store stock solution at -20°C.
   b. For each staining, use 5mL of PBS and add 1μL of CFSE stock solution in a reservoir.
   c. Add 100μL of this diluted CFSE solution in PBS to each cell pellet. Stain for 5 minutes at room temperature, in the dark.
   d. Add 150μL of RPMI + 10% FBS to each well and incubate for 15 minutes at room temperature, in the dark.
   e. Pellet using centrifuge (1500rpm or 700g, 5 minutes).
4. For fixing with PFA (for samples from vaccinia-SIVgag virus infected mice):
   a. Add 100μL of 1% PFA in PBS and incubate in ice for 15 minutes, in the dark.
   b. Pellet using centrifuge (1500rpm or 700g, 5 minutes).
5. Wash 1x with PBS containing 1% BSA and pellet.
6. Re-suspend in 90μL of FACS buffer and add 10μL of counting beads (note beads/μL for the counting beads for analysis) and keep on ice until running on flow cytometry machine.

6.6 Protocol for Total IgG Measurement via ELISA

Materials:

96-well flat bottomed assay plates, NUNC maxisorp (Thermo Fisher)
Capture Antibody (for measurement of total IgG or IgM - use both):
Goat α-mouse Igκ (Southern Biotech, #1050-01) unlabeled (UNLB)
Goat α-mouse Igλ (Southern Biotech, #1060-01) unlabeled (UNLB)
Detection Antibody:
Goat α-mouse IgG-HRP (Southern Biotech, #1030-05)
Goat α-mouse IgM-HRP (Southern Biotech, #1020-05)
Developing Reagent: TMB peroxidase EIA substrate kit (Bio-Rad)
Wash Buffer (WB): PBS/0.05% Tween 20
Blocking Buffer (BB): PBS/1% BSA
Stop Solution: 2N H_2SO_4
Serum samples
ISF samples
For dilution plate - 96-well V-bottomed plate
Tecan plate reader (M200 Pro, Mannedorf, Switzerland)

Protocol:

* Bring All Reagents to Room Temperature

* During wash steps, incubate for 30s between washes

1. Coat 96-well assay plates with capture antibody: add 50 uL of solution containing 2ug/mL of α-mouse Igκ and α-mouse Igλ each, diluted in PBS. Make 5mL per plate.
2. Seal and incubate overnight at 4°C.
3. In the morning wash 2x and fill wells with 200 uL of blocking buffer. Cover and incubate at room temperature for 1 hour.
4. For Dilution Plate:
   a. In the 96-well V-bottomed plates, mark out which wells correspond to serum dilutions and which correspond to ISF dilutions
   b. For serum columns, start with 1:300 dilution in blocking buffer and carry out a 4x serial dilution ahead. Add 90 uL of BB to wells below and from top sample row, transfer down 30uL, mixing well by pipetting up and down, leaving 120 uL in the final row.
   c. For ISF, add original sample to top row (original sample is at 200x). And carry out a 2x serial dilution: add 55uL of blocking buffer to wells below and transfer down 55uL, mixing well by pipetting up and down, leaving 110 uL in the final row.
5. Wash assay plate 4x and transfer 50uL/well of prepped solutions. Cover and incubate for 1 hour at room temperature.
6. Wash assay plate 4x, add 50uL of goat α-mouse IgG-HRP (when assaying for IgG) or goat α-mouse IgM-HRP (when assaying for IgM) diluted to 1:5000 in BB to each well. Cover and incubate for 1 hour at room temperature.
7. Wash 4x and 50 uL of TMB substrate to each well (protecting from light). Incubate for 20 mins.
8. Stop reaction by adding 50 uL of 2N H_2SO_4. Immediately cover plates with aluminum foil. Longer light exposure may increase background or reduce OD (compressing the OD value range).
9. Read OD450 on plate reader.

6.7 Protocol for Ova-Specific IgG Measurement via ELISA

Materials:

96-well flat bottomed assay plates, NUNC Maxisorp (Thermo Fisher)
Capture Antibody: OVA Egg White (Worthington 3048 P0K12101)
Detection Antibody: Goat α-mouse IgG-HRP (Southern Biotech, #1030-05)
Developing Reagent: TMB peroxidase EIA substrate kit (Bio-Rad)
Wash Buffer (WB): PBS/0.05% Tween 20
Blocking Buffer (BB): PBS + 5% milk + 1% FBS + 0.2% Tween20
Dilution Buffer (DB): PBS + 1% FBS + 0.2% Tween20
Stop Solution: 2N H_2SO_4
Serum samples
ISF samples
For dilution plate - 96-well V-bottomed plate
Tecan plate reader (M200 Pro, Mannedorf, Switzerland)

Protocol:

* Bring All Reagents to Room Temperature

1. Coat 96-well assay plates with capture antibody with 100 µL/well of OVA at 1mg/ml in PBS. Rotate for 4 hrs at RT.
2. Empty plates, add 200µl/well of Blocking Buffer. Incubate overnight @ 4°C. Now these plates can be stored. Wrap until use.
3. Meanwhile set up serum dilutions in 96-well V bottom plates.. The base volume needs to be enough for 100µL*number of plates + 20µL for extra volume. Use dilution buffer for doing these. Start at 1:50 dilution of the collected serum and 4x serial dilutions.
4. Wash assay plate 4x and transfer 100µL/well of serum dilutions to each plate. Incubate 1.5 hrs @ RT. Don't rotate.
5. Wash assay plate 4x, add 100µL/well of goat α-mouse IgG-HRP (when assaying for IgG) diluted to 1:5000 in DB. Cover and incubate for 1 hour at room temperature.
6. Wash 4x and 100 µL of TMB substrate to each well (protecting from light). Incubate for 20 mins.
7. Stop reaction by adding 50µL/well of 2N H_2SO_4. Immediately cover plates with aluminum foil. Longer light exposure may increase background or reduce OD (compressing the OD value range).
8. Read OD_{450} on plate reader. Use OD_{540} as reference.

6.8 Protocol for Fluorescent Labeling of Alginate

Materials:

SLG100 - Pronova FMC Biopolymers, Norway
EDC (1-Ethyl-3-[3-dimethylaminopropyl]carbodiimide hydrochloride) - Sigma E1769
Sulfo-NHS (N-hydroxysulfo succinimide) - Sigma 56485
PBS - KI Core
Alexa Fluor® 647 Cadaverine (Thermo Fisher Scientific)

Based on protocol from Strand, B. L., Morch, Y. A., Espevik, T. & Skjak-Braek, G. (2003) Biotechnol Bioeng 82, 386-94 (and modified from Yuki Hori's thesis)

Protocol:

For in vivo use, keep the whole process sterile. Use sterile PBS for dissolving reagents and for dialysis. Perform as much of the procedure as possible in the TC hood. Protect from light after all steps involving fluorophore.

1. Prepare 1.6 w/v % alginate solution dissolved in PBS and let it dissolve overnight at 4°C.
2. Take 4mL of this 1.6% solution in a 20mL glass vial. Add 172.5mg of EDC and 195mg of sulfo-NHS to the alginate and react via stirring with magnetic stir bar, at room temperature, for two hours.
3. Add the sulfo-NHS solution to alginate solution containing EDC. Vortex.

4. *Steps 3 and 4 can be done consecutively, i.e. without incubating with EDC for a while.
5. Shake for 2 hrs at room temperature.
6. Add 2 μL of β-mercaptoethanol to quench the reaction.
7. Add 60μL of 10mg/mL AF647 cadaverine into this mix.
8. Incubate and let the dye and alginate react at room temperature for 18 hrs while stirring. Protect from light.
9. Dialyze the alginate/dye solution with (using 7 kDa MWCO dialysis cassette from Pierce) against large volumes of MQ water (~3.5 L) at RT. Change water at 2hr, 4hr, 6hr and 8hr and change roughly every 12 hours after. Choose the size of cassette such that not much PBS can diffuse into it to dilute out the final alginate concentration.
10. Run a TLC to confirm that there is no free dye.
    i. To run TLC, cut TLC plate ~ 1.5 inches x 3 inches.
    ii. Make TLC mobile phase (2 mL ethyl acetate, 2 mL methanol, 1mL MQ water, 1-2 drops of acetic acid).
    iii. Add mobile phase to small glass jar, with filter paper running up to the top, so that it forms a liquid layer ~ 1cm high.
    iv. On the TLC plate, mark a base-line in pencil ~1.5 cm above the bottom surface of the plate. Take 0.5μL – 1μL of each solution and spot on baseline. Compare against pure polymer (alginate) and pure dye.
    v. Dry either by air (5 minutes) or with vacuum. View under UV lamp.
    vi. Place spotted TLC plate in jar and cover the top. Protect from light.
    vii. Run for ~ 15 minutes.
    viii. Dry for ~ 5 minutes in air in the dark.
    ix. View under UV lamp. For dye conjugated with polymer, fluorescent polymer should stay at baseline while free dye separates and runs up the plate.
    x. Optional: Dip TLC plate into $KMnO_4$ stain solution and dry using blow gun. Pure polymer will oxidize and leave behind yellow spot at the baseline where it was initially. Labeled polymer should also show the same property, in addition to being fluorescent when viewed under UV lamp prior to exposing to oxidizing stain. (To prepare this stain, dissolve 1.5 g $KMnO_4$, 10 g K_2CO_3, and 1.25 mL 10% NaOH in 200 mL water).
11. If no free dye is visible, proceed to lyophilization.
12. Transfer the dialyzed to pre-weighed 15 mL conical tubes. Freeze in liquid nitrogen for > 30 minutes. Check every ten minutes and re-fill the canister if needed.
13. Lyophilize for > 2 days.
14. Adjust the final volume of the alginate so the alginate concentration will be 0.01 g/mL (1 % alginate in MQ water).
15. Sterile-filter the alginate solution with Sterile Acrodisc Syringe Filters (Pall Corporation) with 0.45 μm pore size.
16. Store at 4 °C in dark, covered with foil, till use.

Notes: This protocol uses a 25x equivalents for EDC and sulfo-NHS, based on the number of equivalents of COOH groups in the original polymer (alginate). Based on different stoichiometries we tried, we suspect it will be even better to use up to 100x equivalents of EDC and sulfo-NHS, increase the EDC-sulfo-NHS reaction time to greater than 2 hours and using

higher equivalents of the dye than currently used. Sulfo-NHS is used here since it is more stable and reaction does not occur if NHS is used.

6.9 Gating Strategy for Flow Cytometric Analyses

Shown below are sample flow cytometry gates for blood and sampling MN samples from C57BL/6 mice infected via tail-skin scarification with Vaccinia-SIVgag virus. This specific (sample) experiment and analysis was done 11 weeks post infection. Similar gates are used for other time points as well as, for the ova-immunized mouse model.

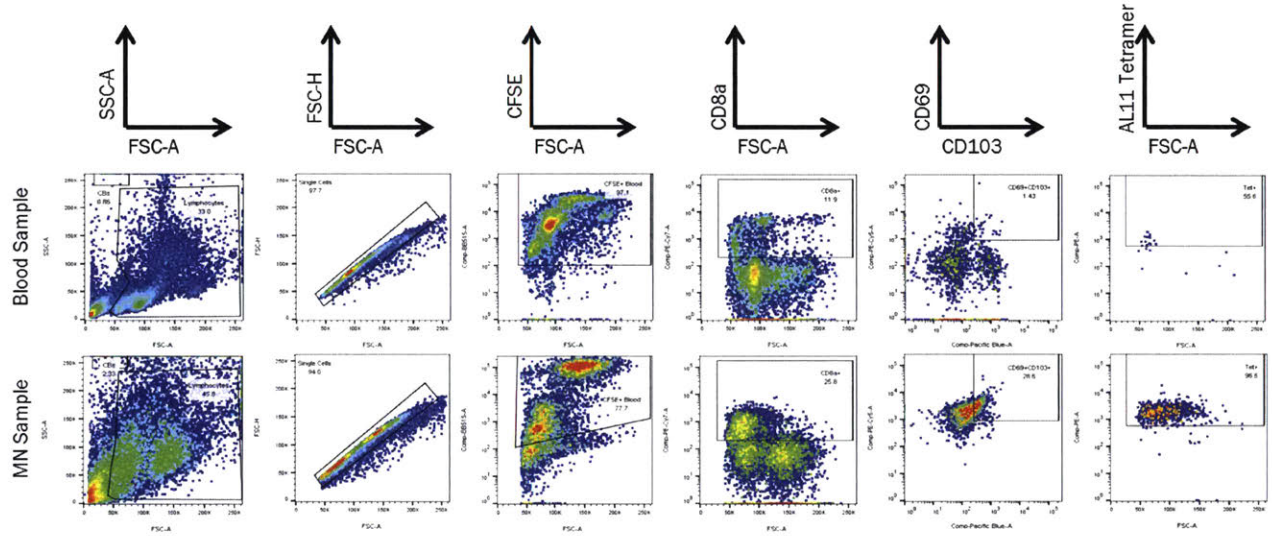

Figure 6-2: Sample serial flow cytometry gates for blood and MN samples (Gates are sequential)

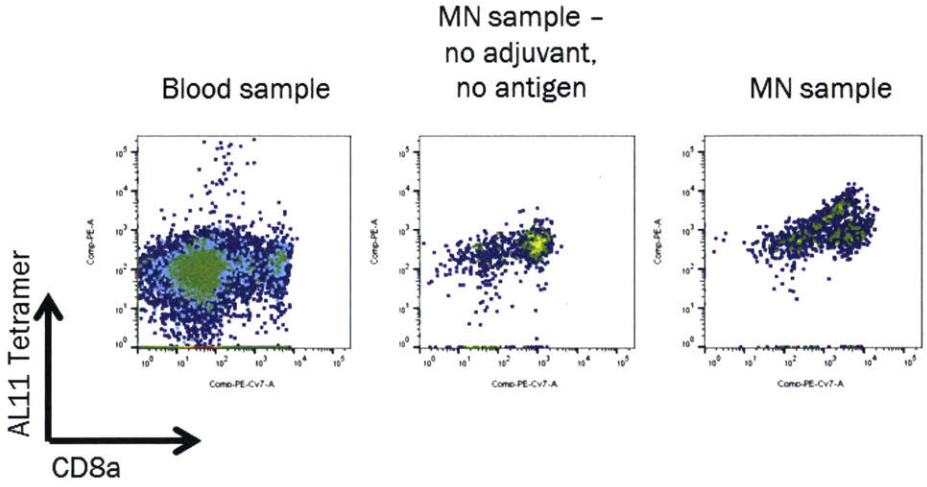

Figure 6-3: Flow cytometric plots showing skewing of antigen specific (AL11 Tetramer+ CD8+) population in samples obtained vis sampling MNs, as compared to blood and sampling MNs containing no adjuvant and no antigen.

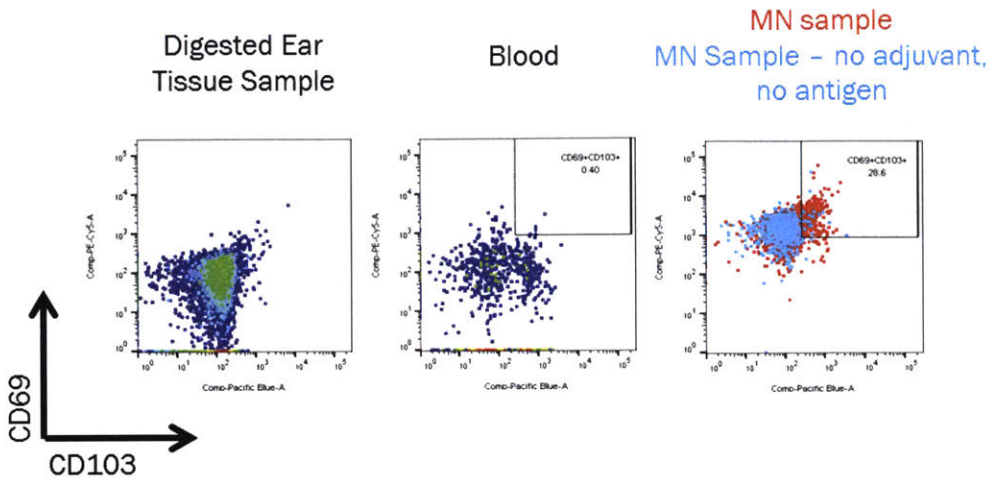

Figure 6-4: Flow cytometric plots showing skewing of resident memory T cells (CD69+CD103+) population in samples obtained vis sampling MNs, as compared to digested ear tissue and blood.

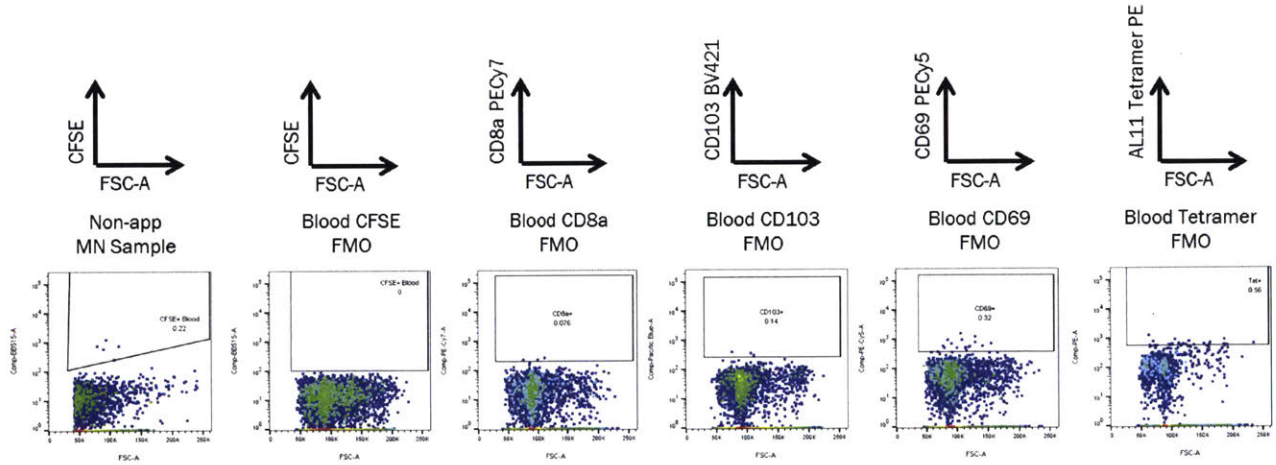

Figure 6-5: Non-applied sampling MN control for live cell gate and fluorescence Minus One (FMO) Controls based on blood samples.

BIBLIOGRAPHY

1. Masopust, D. *et al.* Activated primary and memory CD8 T cells migrate to nonlymphoid tissues regardless of site of activation or tissue of origin. *J. Immunol.* **172,** 4875–82 (2004).
2. Masopust, D., Vezys, V., Marzo, A. L. & Lefrançois, L. Preferential localization of effector memory cells in nonlymphoid tissue. *Science* **291,** 2413–7 (2001).
3. Gebhardt, T. *et al.* Memory T cells in nonlymphoid tissue that provide enhanced local immunity during infection with herpes simplex virus. *Nat. Immunol.* **10,** 524–30 (2009).
4. Mackay, L. K. *et al.* The developmental pathway for CD103+CD8+ tissue-resident memory T cells of skin. *Nat. Publ. Gr.* **14,** (2013).
5. Inoue, S.-I., Niikura, M., Mineo, S. & Kobayashi, F. Roles of IFN-γ and γδ T Cells in Protective Immunity Against Blood-Stage Malaria. *Front. Immunol.* **4,** 258 (2013).
6. Beura, L. K. & Masopust, D. SnapShot: Resident Memory T Cells. *Cell* **157,** 1488–1488.e1 (2014).
7. Takeda, K., Kaisho, T. & Akira, S. Toll-like Receptors. *Annu. Rev. Immunol.* **21,** 335–376 (2003).
8. Dowling, J. K. & Mansell, A. Toll-like receptors: the swiss army knife of immunity and vaccine development. *Clin. Transl. Immunol.* **5,** e85 (2016).
9. Kägi, D., Ledermann, B., Bürki, K., Zinkernagel, R. M. & Hengartner, H. Molecular mechanisms of lymphocyte-mediated cytotoxicity and their role in immunological protection and pathogenesis in vivo. *Annu. Rev. Immunol.* **14,** 207–232 (1996).
10. Harty, J. T., Tvinnereim, A. R. & White, D. W. CD8+ T Cell Effector Mechanisms in Resistance to Infection. *Annu. Rev. Immunol.* **18,** 275–308 (2000).
11. Dobber, R., Hertogh-Huijbregts, A., Rozing, J., Bottomly, K. & Nagelkerken, L. The Involvement of the Intestinal Microflora in the Expansion of CD4+ T Cells with a-Naive Phenotype in the Periphery. *Dev. Immunol.* **2,** 141–150 (1992).
12. Zimmerman, C., Brduscha-Riem, K., Blaser, C., Zinkernagel, R. M. & Pircher, H. Visualization, characterization, and turnover of CD8+ memory T cells in virus-infected hosts. *J. Exp. Med.* **183,** (1996).
13. Butz, E. A. & Bevan, M. J. Massive Expansion of Antigen-Specific CD8+ T Cells during an Acute Virus Infection. *Immunity* **8,** 167–175 (1998).
14. Murali-Krishna, K. *et al.* Counting Antigen-Specific CD8 T Cells: A Reevaluation of

Bystander Activation during Viral Infection. *Immunity* **8,** 177–187 (1998).

15. Busch, D. H., Pilip, I. M., Vijh, S. & Pamer, E. G. Coordinate Regulation of Complex T Cell Populations Responding to Bacterial Infection. *Immunity* **8,** 353–362 (1998).
16. Kim, S.-K., Schluns, K. S. & Lefrançois, L. Induction and Visualization of Mucosal Memory CD8 T Cells Following Systemic Virus Infection. *J. Immunol.* **163,** (1999).
17. Flynn, K. J. *et al.* Virus-Specific CD8+ T Cells in Primary and Secondary Influenza Pneumonia. *Immunity* **8,** 683–691 (1998).
18. Cauley, L. S. & Lefrançois, L. Guarding the perimeter: protection of the mucosa by tissue-resident memory T cells. *Mucosal Immunol.* **6,** 14–23 (2013).
19. Clark, R. A. *et al.* The Vast Majority of CLA + T Cells Are Resident in Normal Skin. (2013).
20. Clark, R. A. Skin-Resident T Cells: The Ups and Downs of On Site Immunity. *J. Invest. Dermatol.* **130,** 362–370 (2010).
21. Kupper, T. S. & Fuhlbrigge, R. C. Immune Surveillance in the Skin: Mechanisms and Clinical Consequences. *Nat. Rev. Immunol.* **4,** (2004).
22. Nestle, F. O., Meglio, P. Di, Qin, J. Z. & Nickoloff, B. J. Skin immune sentinels in health and disease. *Nat. Rev. Immunol.* **9,** 679–691 (2009).
23. Proksch, E., Brandner, J. M. & Jensen, J. M. The skin: an indispensable barrier. *Exp. Dermatol.* **17,** 1063–1072 (2008).
24. Sandby-Møller, J., Poulsen, T. & Wulf, H. C. Epidermal Thickness at Different Body Sites: Relationship to Age, Gender, Pigmentation, Blood Content, Skin Type and Smoking Habits. *Acta Derm. Venereol.* **83,** 410–413 (2003).
25. Babiuk, S., Baca-Estrada, M., Babiuk, L. A., Ewen, C. & Foldvari, M. Cutaneous vaccination: the skin as an immunologically active tissue and the challenge of antigen delivery. *J. Control. Release* **66,** 199–214 (2000).
26. Demuth, P. C., Moon, J. J., Suh, H., Hammond, P. T. & Irvine, D. J. Releasable Layer-by-Layer Assembly of Stabilized Lipid Nanocapsules on Microneedles for Enhanced Transcutaneous Vaccine Delivery. *ACS Nano* 8041–8051 (2012).
27. Demuth, P. C. *et al.* Polymer multilayer tattooing for enhanced DNA vaccination. *Nat. Mater.* **12,** 367–376 (2013).
28. Lugo-Janer, G., Sánchez, J. L. & Santiago-Delpin, E. Prevalence and clinical spectrum of skin diseases in kidney transplant recipients. *J. Am. Acad. Dermatol.* **24,** 410–414 (1991).

29. Uthayakumar, S., Nandwani, R., Drinkwater, T., Nayagam, A. T. & Darley, C. R. The prevalence of skin disease in HIV infection and its relationship to the degree of immunosuppression. *Br. J. Dermatol.* **137,** 595–598 (1997).

30. Parapia, L. A. History of bloodletting by phlebotomy. *Br. J. Haematol.* **143,** 490–495 (2008).

31. Streitz, M. *et al.* Standardization of whole blood immune phenotype monitoring for clinical trials: panels and methods from the ONE study. *Transplant. Res.* **2,** 17 (2013).

32. Srinivasan, V., Pamula, V., Pollack, M. & Fair, R. Clinical diagnostics on human whole blood, plasma, serum, urine, saliva, sweat, and tears on a digital microfluidic platform. *Proc. μTAS* 1287–1290 (2003). at <http://www.rsc.org/binaries/loc/2003/Volume2/104-412.pdf>

33. Black, C. A. P. Delayed type hypersensitivity: Current theories with a historic perspective. *Dermatol. Online J.* **5,** (1999).

34. Ahmed, A. R. Delayed-Type Hypersensitivity Skin Testing. *Arch. Dermatol.* **119,** 934 (1983).

35. Vukmanovic-Stejic, M., Reed, J. R., Lacy, K. E., Rustin, M. H. a. & Akbar, A. N. Mantoux Test as a model for a secondary immune response in humans. *Immunol. Lett.* **107,** 93–101 (2006).

36. Spergel, J. M. & Brown-Whitehorn, T. The use of patch testing in the diagnosis of food allergy. *Curr. Allergy Asthma Rep.* **5,** 86–90 (2005).

37. Spiewak, R. Patch Testing for Contact Allergy and Allergic Contact Dermatitis§. *Open Allergy J.* **1,** 42–51 (2008).

38. Akbar, A. N. *et al.* Investigation of the cutaneous response to recall antigen in humans in vivo. *Clin. Exp. Immunol.* **173,** 163–172 (2013).

39. Tatovic, D. *et al.* Fine-Needle Aspiration Biopsy of the Lymph Node: A Novel Tool for the Monitoring of Immune Responses after Skin Antigen Delivery. *J. Immunol.* **195,** 386–392 (2015).

40. Kool, J. *et al.* Suction blister fluid as potential body fluid for biomarker proteins. *Proteomics* **7,** 3638–3650 (2007).

41. Fernández-Ruiz, M., Kumar, D. & Humar, A. Clinical immune-monitoring strategies for predicting infection risk in solid organ transplantation. *Clin. Transl. Immunol.* **3,** e12 (2014).

42. Cendales, L. C., Kanitakis, J. & Burns, C. in *Pathology of Solid Organ Transplantation*

393–399 (Springer Berlin Heidelberg, 2009). doi:10.1007/978-3-540-79343-4_12

43. Otterburn, D. & Cendales, L. C. in *Tissue and Cell Clinical Use* 302–311 (Wiley-Blackwell, 2012). doi:10.1002/9781118498453.ch14

44. Bueno, E. M. *et al.* Vascularized Composite Allotransplantation and Tissue Engineering. *J. Craniofac. Surg.* **24,** 256–263 (2013).

45. Pomahac, B. *et al.* Three Patients with Full Facial Transplantation. *N. Engl. J. Med.* **366,** 715–722 (2012).

46. Lian, C. G. *et al.* Biomarker evaluation of face transplant rejection: association of donor T cells with target cell injury. *Mod. Pathol.* **27,** 788–99 (2014).

47. Kueckelhaus, M. *et al.* Noninvasive Monitoring of Immune Rejection in Face Transplant Recipients. *Plast Reconstr Surg* **136,** 1082–1089 (2015).

48. Cervera, R., Khamashta, M. A., Font, J. & et al. Systemic Lupus Erythematosus: Clinical and Immunologic Patterns of Disease Expression in a Cohort of 1,000 Patients. *Medicine (Baltimore).* **72,** 113–124 (1993).

49. Smith, P. P. & Gordon, C. Systemic lupus erythematosus: Clinical presentations. *Autoimmun. Rev.* **10,** 43–45 (2010).

50. Fernando, M. M. a & Isenberg, D. a. How to monitor SLE in routine clinical practice. *Ann. Rheum. Dis.* **64,** 524–527 (2005).

51. Ahearn, J. M., Liu, C.-C., Kao, A. H. & Manzi, S. Biomarkers for systemic lupus erythematosus. *Transl. Res.* **159,** 326–42 (2012).

52. Matrat, A. *et al.* Simultaneous detection of anti-C1q and anti-double stranded DNA autoantibodies in lupus nephritis: predictive value for renal flares. *Lupus* **20,** 28–34 (2011).

53. Liu, C.-C. & Ahearn, J. M. The search for lupus biomarkers. *Best Pract. Res. Clin. Rheumatol.* **23,** 507–23 (2009).

54. Illei, G. G., Tackey, E., Lapteva, L. & Lipsky, P. E. Biomarkers in systemic lupus erythematosus: II. Markers of disease activity. *Arthritis Rheum.* **50,** 2048–65 (2004).

55. Franz, B. *et al.* Low number of regulatory T cells in skin lesions of patients with cutaneous lupus erythematosus. *Arthritis Rheum.* **56,** 1910–1920 (2007).

56. Prausnitz, M. R. Microneedles for transdermal drug delivery. *Adv. Drug Deliv. Rev.* **56,** 581–587 (2004).

57. Cheung, K. & Das, D. B. Microneedles for drug delivery: trends and progress. *Drug Deliv*

7544, 1–17 (2015).

58. Mooney, K., McElnay, J. C. & Donnelly, R. F. Children's views on microneedle use as an alternative to blood sampling for patient monitoring. *Int. J. Pharm. Pract.* (2013). doi:10.1111/ijpp.12081
59. Gill, H. S., Denson, D. D., Burris, B. A. & Prausnitz, M. R. Effect of microneedle design on pain in human volunteers. *Clin. J. Pain* **24,** 585–94 (2008).
60. Gerstel, M. S. & Place, V. . Drug delivery device. *US Pat. No. 3,964,482* (1976). at <https://www.google.com/patents/US3964482>
61. Mitragotri, S. Immunization without needles. *Nat. Rev. Immunol.* **5,** 905–916 (2005).
62. Wang, P. M., Cornwell, M. & Prausnitz, M. R. Minimally invasive extraction of dermal interstitial fluid for glucose monitoring using microneedles. *Diabetes Technol. Ther.* **7,** 131–41 (2005).
63. Ito, Y. *et al.* Application of dissolving microneedles to glucose monitoring through dermal interstitial fluid. *Biol. Pharm. Bull.* **37,** 1776–81 (2014).
64. Romanyuk, A. V. *et al.* Collection of analytes from microneedle patches. *Anal. Chem.* **86,** 10520–10523 (2014).
65. Corrie, S. R. *et al.* Surface-modified microprojection arrays for intradermal biomarker capture, with low non-specific protein binding. *Lab Chip* **10,** 2655 (2010).
66. Coffey, J. W., Corrie, S. R. & Kendall, M. A. F. Biomaterials Early circulating biomarker detection using a wearable microprojection array skin patch. *Biomaterials* 1–12 (2013). doi:10.1016/j.biomaterials.2013.08.078
67. Bhargav, A., Muller, D. A., Kendall, M. A. F. & Corrie, S. R. Surface Modifications of Microprojection Arrays for Improved Biomarker Capture in the Skin of Live Mice. (2012).
68. Chen, X. *et al.* Site-Selectively Coated, Densely-Packed Microprojection Array Patches for Targeted Delivery of Vaccines to Skin. *Adv. Funct. Mater.* **21,** 464–473 (2011).
69. Caffarel-Salvador, E. *et al.* Hydrogel-Forming Microneedle Arrays Allow Detection of Drugs and Glucose In Vivo: Potential for Use in Diagnosis and Therapeutic Drug Monitoring. *PLoS One* **10,** e0145644 (2015).
70. Henry, S., McAllister, D. V., Allen, M. G. & Prausnitz, M. R. Microfabricated Microneedles: A Novel Approach to Transdermal Drug Delivery. *J. Pharm. Sci.* **87,** 922–925 (1998).

71. Demuth, B. P. C., Su, X., Samuel, R. E., Hammond, P. T. & Irvine, D. J. Nano-Layered Microneedles for Transcutaneous Delivery of Polymer Nanoparticles and Plasmid DNA. **2139,** 4851–4856 (2010).

72. Ito, Y., Hagiwara, E., Saeki, A., Sugioka, N. & Takada, K. Feasibility of microneedles for percutaneous absorption of insulin. *Eur. J. Pharm. Sci.* **29,** 82–8 (2006).

73. Martanto, W. *et al.* Transdermal delivery of insulin using microneedles in vivo. *Pharm. Res.* **21,** 947–52 (2004).

74. Lee, J. W., Park, J.-H. & Prausnitz, M. R. Dissolving microneedles for transdermal drug delivery. *Biomaterials* **29,** 2113–24 (2008).

75. Sherman, F. F., Yuzhakov, V. V., Gartstein, V. & Owens, G. D. US Patent No. 6,312,612 B1.

76. Sherman, F. F. *et al.* Portable interstitial fluid monitoring system US Patent. No. US6591124 B2. (2001). at <https://www.google.com/patents/US6591124>

77. Gupta, J., Gill, H. S., Andrews, S. N. & Prausnitz, M. R. Kinetics of skin resealing after insertion of microneedles in human subjects. *J. Control. Release* **154,** 148–155 (2011).

78. Gardeniers, H. J. G. E. *et al.* Silicon micromachined hollow microneedles for transdermal liquid transport. *J. Microelectromechanical Syst.* **12,** 855–862 (2003).

79. Demuth, P. C., Moon, J. J., Suh, H., Hammond, P. T. & Irvine, D. J. Releasable Layer-by-Layer Assembly of Stabilized Lipid Nanocapsules on Microneedles for Enhanced Transcutaneous Vaccine Delivery. 8041–8051 (2012).

80. Kuo, C. K. & Ma, P. X. Ionically crosslinked alginate hydrogels as scaffolds for tissue engineering: part 1. Structure, gelation rate and mechanical properties. *Biomaterials* **22,** 511–21 (2001).

81. Sun, J. & Tan, H. Alginate-Based Biomaterials for Regenerative Medicine Applications. *Materials (Basel).* **6,** 1285–1309 (2013).

82. SMIDSROD, O. & SKJAKBRK, G. Alginate as immobilization matrix for cells. *Trends Biotechnol.* **8,** 71–78 (1990).

83. Andersen, T., Strand, B. L., Formo, K., Alsberg ', E. & Christensen ', B. E. Alginates as biomaterials in tissue engineering. doi:10.103919781849732765-00227

84. Donnelly, R. F. *et al.* Hydrogel-Forming Microneedle Arrays for Enhanced Transdermal Drug Delivery. 1–12 (2012). doi:10.1002/adfm.201200864

85. Rossi, D. & Zlotnik, a. The biology of chemokines and their receptors. *Annu. Rev. Immunol.* **18,** 217–42 (2000).

86. Tufet, M. Chemokines: Dictating migration. *Nat. Rev. Immunol.* **7,** 663–663 (2007).

87. Weber, M. *et al.* Interstitial dendritic cell guidance by haptotactic chemokine gradients. *Science* **339,** 328–32 (2013).

88. Sallusto, F. The role of chemokine receptors in primary, effector and memory immune response. *Exp. Dermatol.* **11,** 476–478 (2002).

89. Sturm, E. M., Dyer, K. D., Percopo, C. M., Heinemann, A. & Rosenberg, H. F. Chemotaxis of bone marrow derived eosinophils in vivo: a novel method to explore receptor-dependent trafficking in the mouse. *Eur. J. Immunol.* **43,** 2217–28 (2013).

90. Hori, Y., Winans, A. M. & Irvine, D. J. Modular injectable matrices based on alginate solution / microsphere mixtures that gel in situ and co-deliver immunomodulatory factors. *Acta Biomater.* **5,** 969–982 (2009).

91. Wang, Y. & Irvine, D. J. Engineering chemoattractant gradients using chemokine-releasing polysaccharide microspheres. *Biomaterials* **32,** 4903–13 (2011).

92. Hori, Y., Winans, A. M., Huang, C. C., Horrigan, E. M. & Irvine, D. J. Injectable dendritic cell-carrying alginate gels for immunization and immunotherapy. *Biomaterials* **29,** 3671–82 (2008).

93. Lee, K. Y. & Mooney, D. J. Alginate: Properties and biomedical applications. *Prog. Polym. Sci.* **37,** 106–126 (2012).

94. Hori, Y., Stern, P. J., Hynes, R. O. & Irvine, D. J. Engulfing tumors with synthetic extracellular matrices for cancer immunotherapy. *Biomaterials* **30,** 6757–67 (2009).

95. DRAGET, K., SKJAKBRAK, G. & SMIDSROD, O. Alginic acid gels: the effect of alginate chemical composition and molecular weight. *Carbohydr. Polym.* **25,** 31–38 (1994).

96. Lee, K. Y. *et al.* Controlling the Mechanical and Swelling Properties of Alginate Hydrogels Independently by Cross-Linker Type and Cross-Linking Density. *Macromolecules* **33,** 4291–4294 (2000).

97. Li, J., Illeperuma, W. R. K., Suo, Z. & Vlassak, J. J. Hybrid Hydrogels with Extremely High Sti ff ness and Toughness. *ACS Macro Lett.* **3,** 520–523 (2014).

98. Ashour, A. E., Turnquist, H. R., Singh, R. K., Talmadge, J. E. & Solheim, J. C. CCL21-induced immune cell infiltration. *Int. Immunopharmacol.* **7,** 272–6 (2007).

99. Weninger, W. *et al.* Naive T cell recruitment to nonlymphoid tissues: a role for endothelium-expressed CC chemokine ligand 21 in autoimmune disease and lymphoid neogenesis. *J. Immunol.* **170,** 4638–48 (2003).

100. Anderson, J. M., Rodriguez, A. & Chang, D. T. Foreign body reaction to biomaterials. *Semin. Immunol.* **20,** 86–100 (2008).

101. Bariya, S. H., Gohel, M. C., Mehta, T. A. & Sharma, O. P. Microneedles : an emerging transdermal drug. 11–29 (2012). doi:10.1111/j.2042-7158.2011.01369.x

102. Gomaa, Y. A. *et al.* Effects of microneedle length, density, insertion time and multiple applications on human skin barrier function: Assessments by transepidermal water loss. *Toxicol. Vitr.* **24,** 1971–1978 (2010).

103. Andrews, S. N., Jeong, E. & Prausnitz, M. R. Transdermal delivery of molecules is limited by full epidermis, not just stratum corneum. *Pharm. Res.* **30,** 1099–1109 (2013).

104. Martanto, W. *et al.* Transdermal Delivery of Insulin Using Microneedles in Vivo. *Pharm. Res.* **21,** 947–952 (2004).

105. Chandrasekhar, S., Iyer, L. K. & Panchal, J. P. Microarrays and microneedle arrays for delivery of peptides , proteins , vaccines and other applications. 1–16 (2013).

106. Fukushima, K. *et al.* Two-layered dissolving microneedles for percutaneous delivery of peptide/protein drugs in rats. *Pharm. Res.* **28,** 7–21 (2011).

107. Prausnitz, M. R. Engineering Microneedle Patches for Vaccination and Drug Delivery to Skin. 1–24 (2017).

108. Prausnitz, M. R. & Langer, R. Transdermal drug delivery. **26,** 1261–1268 (2008).

109. Quinn, H. L., Kearney, M.-C., Courtenay, A. J., McCrudden, M. T. C. & Donnelly, R. F. The role of microneedles for drug and vaccine delivery. *Expert Opin. Drug Deliv.* **11,** 1769–1780 (2014).

110. Kim, Y., Park, J. & Prausnitz, M. R. Microneedles for drug and vaccine delivery ☆. *Adv. Drug Deliv. Rev.* **64,** 1547–1568 (2012).

111. Naito, S. *et al.* Antigen-loaded dissolving microneedle array as a novel tool for percutaneous vaccination. *Vaccine* **30,** 1191–7 (2012).

112. Vrdoljak, A. Review of recent literature on microneedle vaccine delivery technologies. *Vaccine Dev. Ther.* 47–55 (2013).

113. Maaden, K. Van Der, Jiskoot, W. & Bouwstra, J. Microneedle technologies for (trans)

dermal drug and vaccine delivery. *J. Control. Release* (2012). doi:10.1016/j.jconrel.2012.01.042

114. Lee, K., Lee, C. Y. & Jung, H. Dissolving microneedles for transdermal drug administration prepared by stepwise controlled drawing of maltose. *Biomaterials* **32,** 3134–3140 (2011).
115. Reed, S. G., Orr, M. T. & Fox, C. B. Key roles of adjuvants in modern vaccines. *Nat. Med.* **19,** 1597–608 (2013).
116. Cox, J. C. & Coulter, A. R. Adjuvants—a classification and review of their modes of action. *Vaccine* **15,** 248–256 (1997).
117. Ramon, G. Sur la toxine et sur l'anatoxine diphtheriques. *Ann. Inst. Pasteur* **38,** 1–10 (1924).
118. Kalali, B. N. *et al.* Double-stranded RNA induces an antiviral defense status in epidermal keratinocytes through TLR3-, PKR-, and MDA5/RIG-I-mediated differential signaling. *J. Immunol.* **181,** 2694–704 (2008).
119. Stahl-Hennig, C. *et al.* Synthetic Double-Stranded RNAs Are Adjuvants for the Induction of T Helper 1 and Humoral Immune Responses to Human Papillomavirus in Rhesus Macaques. *PLoS Pathog.* **5,** e1000373 (2009).
120. Nalla, N. *et al.* Design, synthesis and immunological evaluation of 1,2,3-triazole-tethered carbohydrate–Pam3Cys conjugates as TLR2 agonists. *Bioorg. Med. Chem.* **23,** 5846–5855 (2015).
121. Poulter, L. W., Seymour, G. J., Duke, O., Janossy, G. & Panayi, G. Immunohistological analysis of delayed-type hypersensitivity in man. *Cell. Immunol.* **74,** 358–369 (1982).
122. Najarian, J. S. & Feldman, J. D. Specificity of Passively Transferred Delayed Hypersensitivity. *J. Exp. Med.* **118,** 341–52 (1963).
123. Thome, J. J. C. & Farber, D. L. Emerging concepts in tissue-resident T cells: lessons from humans. *Trends Immunol.* **36,** 428–435 (2015).
124. Mackay, L. K. *et al.* Long-lived epithelial immunity by tissue-resident memory T (T RM) cells in the absence of persisting local antigen presentation. **109,** (2012).
125. Clark, R. A. *et al.* Skin Effector Memory T Cells Do Not Recirculate and Provide Immune Protection in Alemtuzumab-Treated CTCL Patients. **7,** (2012).
126. Liu, L., Fuhlbrigge, R. C., Karibian, K., Tian, T. & Kupper, T. S. Dynamic Programing of CD8+ T Cell Trafficking after Live Viral Immunization. *Immunity* **25,** 511–520 (2006).

127. Jiang, X. *et al.* Skin infection generates non-migratory memory CD8+ TRM cells providing global skin immunity. *Nature* **483,** 227–231 (2012).

128. Mueller, S. N. & Mackay, L. K. Tissue-resident memory T cells: local specialists in immune defence. *Nat. Rev. Immunol.* **16,** 1–11 (2015).

129. Turner, D. L., Gordon, C. L. & Farber, D. L. Tissue-resident T cells, in situ immunity and transplantation. *Immunol. Rev.* **258,** 150–166 (2014).

130. Thome, J. J. C. *et al.* Spatial map of human t cell compartmentalization and maintenance over decades of life. *Cell* **159,** 814–828 (2014).

131. Purwar, R. *et al.* Resident Memory T Cells (TRM) Are Abundant in Human Lung: Diversity, Function, and Antigen Specificity. *PLoS One* **6,** e16245 (2011).

132. Sathaliyawala, T. *et al.* Distribution and Compartmentalization of Human Circulating and Tissue-Resident Memory T Cell Subsets. *Immunity* **38,** 187–197 (2013).

133. Liu, H., Kwong, B. & Irvine, D. J. Membrane Anchored Immunostimulatory Oligonucleotides for In Vivo Cell Modification and Localized Immunotherapy. *Angew. Chemie Int. Ed.* **50,** 7052–7055 (2011).

134. Riol-Blanco, L. *et al.* Nociceptive sensory neurons drive interleukin-23- mediated psoriasiform skin inflammation. *Nature* **510,** (2014).

135. Moon, J. J. *et al.* Interbilayer-crosslinked multilamellar vesicles as synthetic vaccines for potent humoral and cellular immune responses. *Nat. Mater.* **10,** 243–51 (2011).

136. Bershteyn, A. *et al.* Robust IgG responses to nanograms of antigen using a biomimetic lipid-coated particle vaccine. *J. Control. Release* **157,** 354–365 (2012).

137. Moon, J. J. *et al.* Enhancing humoral responses to a malaria antigen with nanoparticle vaccines that expand Tfh cells and promote germinal center induction. *Proc. Natl. Acad. Sci.* **109,** 1080–1085 (2012).

138. Alvarez, D. F., Helm, K., Degregori, J., Roederer, M. & Majka, S. Publishing flow cytometry data. *Am. J. Physiol. Lung Cell. Mol. Physiol.* **298,** L127-30 (2010).

139. Roederer, M. How many events is enough? Are you positive? *Cytom. Part A* **73A,** 384–385 (2008).

140. Gierahn, T. M., Yalcin, A., Loginov, D. & Love, J. C. Deep phenotypic profiling of small clinical samples through MultiSpectral Imaging Cytometry (MuSIC) in nanowell arrays. *J. Immunol.* **196,** (2016).

141. Liu, H. *et al.* Structure-based programming of lymph-node targeting in molecular vaccines. *Nature* **507,** 519–22 (2014).

142. Depelsenaire, A. C. I. *et al.* Colocalization of Cell Death with Antigen Deposition in Skin Enhances Vaccine Immunogenicity. *J. Invest. Dermatol.* **134,** 2361–2370 (2014).

143. Verbaan, F. J. *et al.* Improved piercing of microneedle arrays in dermatomed human skin by an impact insertion method. *J. Control. Release* **128,** 80–88 (2008).

144. Park, J.-H., Allen, M. G. & Prausnitz, M. R. Biodegradable polymer microneedles: Fabrication, mechanics and transdermal drug delivery. *J. Control. Release* **104,** 51–66 (2005).

145. Bevan, M. J. Memory T cells as an occupying force. *Eur. J. Immunol.* **41,** 1192–1195 (2011).

146. Teijaro, J. R., Turner, D., Pham, Q., Wherry, E. J. & Farber, D. L. Cutting Edge: Tissue-Retentive Lung Memory CD4 T Cells Mediate Optimal Protection to Respiratory Virus Infection. **83022,** (2011).

147. Heisenberg, W. Über den anschaulichen Inhalt der quantentheoretischen Kinematik und Mechanik. *Zeitschrift für Phys.* **43,** 172–198 (1927).

148. Mcclain, D. J. *et al.* Immunologic Responses to Vaccinia Vaccines Administered by Different Parenteral Routes. *J. Infect. Dis.* **175,** 756–763 (1997).

149. Tian, T. *et al.* Disruption of TNF-α/TNFR1 Function in Resident Skin Cells Impairs Host Immune Response against Cutaneous Vaccinia Virus Infection. *J. Invest. Dermatol.* **132,** 1425–1434 (2012).

150. Liu, J. *et al.* Modulation of DNA vaccine-elicited CD8+ T-lymphocyte epitope immunodominance hierarchies. *J. Virol.* **80,** 11991–7 (2006).

151. Sprent, J. & Surh, C. D. T Cell Memory. *Annu. Rev. Immunol.* **20,** 551–579 (2002).

152. Badovinac, V. P., Porter, B. B. & Harty, J. T. Programmed contraction of CD8(+) T cells after infection. *Nat. Immunol.* **3,** 619–626 (2002).

153. Fogh-Andersen, N., Altura, B. M., Altura, B. T. & Siggaard-Andersen, O. Composition of interstitial fluid. *Clin. Chem.* **41,** 1522–1525 (1995).

154. Janle, E. M., Cregor, M. & Lafayette, W. Interstitial Fluid Calcium , Magnesium and Phosphorus Concentrations in Bone , Muscle and Subcutaneous Tissue Sampled with Ultrafiltration Probes. **3,** 81–85 (2001).

155. Aukland, K. & Fadnes, H. O. Protein Concentration of Interstitial Fluid Collected from Rat Skin by a Wick Method. *Acta Physiol. Scand.* **88,** 350–358 (1973).

156. Bantle, J. P. & Thomas, W. Glucose measurement in patients with diabetes mellitus with dermal interstitial fluid. *J. Lab. Clin. Med.* **130,** 436–41 (1997).

157. Wiig, H. & Swartz, M. a. Interstitial Fluid and Lymph Formation and Transport: Physiological Regulation and Roles in Inflammation and Cancer. *Physiol. Rev.* **92,** 1005–1060 (2012).

158. Worm, A.-M. Exchange of Macromolecules between Plasma and Skin Interstitium in Extensive Skin Disease. *J. Invest. Dermatol.* **76,** 489–492 (1981).

159. Leboulanger, B., Guy, R. H. & Delgado-Charro, M. B. Reverse iontophoresis for non-invasive transdermal monitoring. *Physiol. Meas.* **25,** R35-50 (2004).

160. Brunner, M. & Derendorf, H. Clinical microdialysis: Current applications and potential use in drug development. *TrAC Trends Anal. Chem.* **25,** 674–680 (2006).

161. Macdonald, N. *et al.* Proteomic analysis of suction blister fluid isolated from human skin. *Clin. Exp. Dermatol.* **31,** 445–448 (2006).

162. Haslene-Hox, H., Tenstad, O. & Wiig, H. Interstitial fluid-a reflection of the tumor cell microenvironment and secretome. *Biochim. Biophys. Acta* **1834,** 2336–46 (2013).

163. Gromov, P. *et al.* Tumor interstitial fluid — A treasure trove of cancer biomarkers. *Biochim. Biophys. Acta - Proteins Proteomics* **1834,** 2259–2270 (2013).

164. Wiig, H., Tenstad, O., Iversen, P. O., Kalluri, R. & Bjerkvig, R. Interstitial fluid: the overlooked component of the tumor microenvironment? *Fibrogenesis Tissue Repair* **3,** 12 (2010).

165. Fadnes, H. O. & Aukland, K. Protein concentration and colloid osmotic pressure of interstitial fluid collected by the wick technique: Analysis and evaluation of the method. *Microvasc. Res.* **14,** 11–25 (1977).

166. Mccormick, C., Heath, D. & Connolly, P. Sensors and Actuators B : Chemical Towards blood free measurement of glucose and potassium in humans using reverse iontophoresis. *Sensors Actuators B. Chem.* **166–167,** 593–600 (2012).

167. Garland, M. J., Caffarel-Salvador, E., Migalska, K., Woolfson, a D. & Donnelly, R. F. Dissolving polymeric microneedle arrays for electrically assisted transdermal drug delivery. *J. Control. Release* **159,** 52–9 (2012).

168. Chang, J. H., Hogan, N. C. & Hunter, I. W. A needle-free technique for interstitial fluid sample acquisition using a lorentz-force actuated jet injector. *J. Control. Release* **211,** 37–43 (2015).

169. Thennadil, S. N. *et al.* Comparison of glucose concentration in interstitial fluid, and capillary and venous blood during rapid changes in blood glucose levels. *Diabetes Technol. Ther.* **3,** 357–65 (2001).

170. BJERKE, J. R., LIVDEN, J. K., DEGRE, M. & MATRE, R. Interferon in suction blister fluid from psoriatic lesions. *Br. J. Dermatol.* **108,** 295–299 (1983).

171. Smith, T. J., Wilson, M. A., Young, A. J. & Montain, S. J. A suction blister model reliably assesses skin barrier restoration and immune response. *J. Immunol. Methods* **417,** 124–130 (2015).

172. Munnikes, R. J. M. *et al.* Intermediate stage complex regional pain syndrome type 1 is unrelated to proinflammatory cytokines. *Mediators Inflamm.* **2005,** 366–372 (2005).

173. Anbar, T., Zuel-Fakkar, N. M., Matta, M. F. & Arbab, M. M. I. Elevated homocysteine levels in suction-induced blister fluid of active vitiligo lesions. *doi.org* **26,** 64–67 (2016).

174. Donnelly, R. F. *et al.* Microneedle-Mediated Minimally Invasive Patient Monitoring. *Ther. Drug Monit.* **36,** 1 (2013).

175. Ronen Polsky, Philip Rocco Miller, J. T. B. US Patent US20160296149 In Vivo Extraction of Interstitial Fluid Using Hollow Microneedles. (2016). at <https://www.google.com/patents/US20160296149>

176. Miller, P. R. *et al.* Microneedle-Based Transdermal Sensor for On-Chip Potentiometric Determination of K,(+). *Adv. Healthc. Mater.* 1–6 (2013). doi:10.1002/adhm.201300541

177. Liu, Y., Yu, D., Zeng, C., Miao, Z. & Dai, L. Biocompatible graphene oxide-based glucose biosensors. *Langmuir* **26,** 6158–60 (2010).

178. Invernale, M. A. *et al.* Microneedle Electrodes Toward an Amperometric Glucose- Sensing Smart Patch. 1–5 (2013). doi:10.1002/adhm.201300142

179. Guy, R. Diagnostic devices: Managing diabetes through the skin. *Nat. Nanotechnol.* **11,** 1–2 (2016).

180. Vasylieva, N., Marinesco, S., Barbier, D. & Sabac, A. Silicon/SU8 multi-electrode micro-needle for in vivo neurochemical monitoring. *Biosens. Bioelectron.* **72,** 148–155 (2015).

181. Mukerjee, E. V.; Collins, S. D.; Isseroff, R. R.; Smith, R. L. Microneedle array for

transdermal biological fluid extraction and in situ analysis. *Sensors Actuators, A* **114,** 267–275 (2004).

182. Miller, P. R. *et al. Multiplexed microneedle-based biosensor array for characterization of metabolic acidosis. Talanta* **88,** (2012).

183. Burmeister, J. J. *et al.* Ceramic-based multisite microelectrode arrays for simultaneous measures of choline and acetylcholine in CNS. *Biosens. Bioelectron.* **23,** 1382–1389 (2008).

184. Frey, O. *et al.* Enzyme-based choline and l-glutamate biosensor electrodes on silicon microprobe arrays. *Biosens. Bioelectron.* **26,** 477–484 (2010).

185. Keum, D. H. *et al.* Cancer Detection: Microneedle Biosensor for Real-Time Electrical Detection of Nitric Oxide for In Situ Cancer Diagnosis During Endomicroscopy (Adv. Healthcare Mater. 8/2015). *Adv. Healthc. Mater.* **4,** 1152–1152 (2015).

186. Ngoepe, M. *et al.* Integration of Biosensors and Drug Delivery Technologies for Early Detection and Chronic Management of Illness. 7680–7713 (2013). doi:10.3390/s130607680

187. El-Laboudi, A., Oliver, N. S., Cass, A. & Johnston, D. Use of Microneedle Array Devices for Continuous Glucose Monitoring: A Review. *Diabetes Technol. Ther.* **15,** 101–115 (2013).

188. Yuen, C. & Liu, Q. Ag Coated Microneedle Based Surface Enhanced Raman Scattering Probe for Intradermal Measurements. **8798,** 6–9 (2013).

189. Vashist, S. K. Non-invasive glucose monitoring technology in diabetes management: A review. *Anal. Chim. Acta* **750,** 16–27 (2012).

190. Liu, S. *et al.* The development and characteristics of novel microneedle arrays fabricated from hyaluronic acid, and their application in the transdermal delivery of insulin. *J. Control. Release* **161,** 933–41 (2012).

191. Bal, S. M., Caussin, J., Pavel, S. & Bouwstra, J. A. In vivo assessment of safety of microneedle arrays in human skin. *Eur. J. Pharm. Sci.* **35,** 193–202 (2008).

192. Anderson, N. L. & Anderson, N. G. The human plasma proteome: history, character, and diagnostic prospects. *Mol. Cell. Proteomics* **1,** 845–67 (2002).

193. Junqueira, L. C. & Carneiro, J. *Basic Histology.* (McGraw-Hill, 2003).

194. Hedger, M. P. & Herriarachchi, S. Measurement of Immunoglobulin G Levels in Adult Rat Testicular Interstitial Fluid and Serum. *J. Androl.* **15,** 583–590 (1994).

195. Yeow, B. *et al.* Surface modification and characterization of polycarbonate microdevices for capture of circulating biomarkers, both in vitro and in vivo. *Anal. Chem.* **85,** 10196–10204 (2013).

196. Posthuma-Trumpie, G. A., Korf, J. & van Amerongen, A. Lateral flow (immuno)assay: its strengths, weaknesses, opportunities and threats. A literature survey. *Anal. Bioanal. Chem.* **393,** 569–582 (2009).

197. Corrie, S. R., Coffey, J. W., Islam, J., Markey, K. A. & Kendall, M. A. F. Blood, sweat, and tears: developing clinically relevant protein biosensors for integrated body fluid analysis. *Analyst* **140,** 4350–4364 (2015).

198. Huang, C. M. *et al.* Prospective highlights of functional skin proteomics. *Mass Spectrom. Rev.* **24,** 647–660 (2005).

199. Finco, O. & Rappuoli, R. Designing Vaccines for the Twenty-First Century Society. *Front. Immunol.* **5,** 12 (2014).

200. Nabel, G. J. Designing Tomorrow's Vaccines. *N. Engl. J. Med.* **368,** 551–560 (2013).